



**Q-SWITCHED AND MODE LOCKED SHORT PULSES FROM A DIODE
PUMPED, YB-DOPED FIBER LASER**

THESIS

Seth M. Swift, Captain, USAF

AFIT/GAP/ENP/09-M10

**DEPARTMENT OF THE AIR FORCE
AIR UNIVERSITY**

AIR FORCE INSTITUTE OF TECHNOLOGY

Wright-Patterson Air Force Base, Ohio

APPROVED FOR PUBLIC RELEASE; DISTRIBUTION UNLIMITED

The views expressed in this thesis are those of the author and do not reflect the official policy or position of the United States Air Force, Department of Defense, or the United States Government.

AFIT/GAP/ENP/09-M10

**Q-SWITCHED AND MODE LOCKED SHORT PULSES FROM A DIODE
PUMPED, YB-DOPED FIBER LASER**

THESIS

Presented to the Faculty

Department of Engineering Physics

Graduate School of Engineering and Management

Air Force Institute of Technology

Air University

Air Education and Training Command

In Partial Fulfillment of the Requirements for the

Degree of Master of Science in Applied Physics

Seth M. Swift, BS

Captain, USAF

March 2009

APPROVED FOR PUBLIC RELEASE; DISTRIBUTION UNLIMITED

**Q-SWITCHED AND MODE LOCKED SHORT PULSES FROM A DIODE
PUMPED, YB-DOPED FIBER LASER**


Seth M. Swift, BS

Captain, USAF

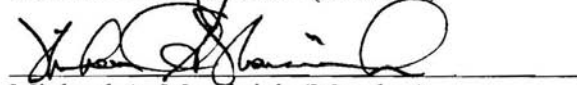
Approved:


Matthew J. Bohn (Chairman)

10 Mar 09
Date


Salvatore J. Cusumano (Member)

10 Mar 09
Date


Michael A. Marciniak (Member)

10 Mar 09
Date

Abstract

The development of fiber lasers as a possible replacement to high-cost, bulk solid-state lasers is of increasing interest to the Department of Defense (DOD), scientific research, and commercial industries. The objective of this experiment was to develop a diode-pumped, ytterbium (Yb)-doped fiber laser system, designed to operate in continuous wave (cw), passively Q-switched and passively mode locked operation.

The fiber laser designed for this experiment was the first fiber laser oscillator built at the Air Force Institute of Technology. A Cr^{4+} :YAG (Chromium: Ytterbium Aluminum Garnett) crystal was used as a saturable absorber to generate Q-switched pulses. Attempts to mode lock the laser were accomplished using a semiconductor saturable absorber mirror (SESAM) and through nonlinear polarization rotation (NPR).

Output power and spectra were measured in cw after testing two different Yb-fibers and three output couplers. The best output power result was 5 Watts (W) at an input power of 8.3 W, yielding an efficiency of 60%. Output spectral peaks were measured between 1087-1108 nm. Q-switched pulses using the Cr^{4+} :YAG crystal were 2.9 μs long with repetition rates between 60-150 kHz, pulse energies of 7-24 μJ , and peak powers twice as high as the average power. Q-switched and possible mode locked pulses were generated using NPR. Q-switched pulse widths ranged from 1.8-2.8 μs with repetition rates between 29-72 kHz. Mode locked pulse widths were 10.5 ns with a repetition rate of 17.2 MHz. Mode locking was not achieved using the SESAM, but the results that resemble mode beating are presented, and causes for error are analyzed.

Acknowledgments

I would like to thank my thesis advisor for the guidance he provided throughout this project, as well as the academic faculty, laboratory technical staff, and administrative staff at the Air Force Institute of Technology for this truly unique opportunity to pursue my degree, while at the same time continuing to serve in the United States Air Force. Last, I want to thank my family for their encouragement during those times of frustration. In particular, I'm so grateful to my wife for keeping the world in order while my head was buried in school work and in this thesis.

Seth M. Swift

Table of Contents

	Page
Abstract	iv
Acknowledgments.....	v
List of Figures	viii
List of Tables	xi
List of Acronyms.....	xii
 I. Introduction	 1
1.1 Background.....	1
1.2 Problem Statement.....	1
1.3 Thesis Overview	2
1.4 Research Focus	3
 II. Theory	 5
2.1 Chapter Overview.....	5
2.2 Previous Work	5
2.3 Propagation of a Pulse through a Fiber	9
2.4 Passive Q-Switching.....	14
2.4.1 Generating a Q-Switched Pulse.....	15
2.4.2 Utilizing the Cr ⁴⁺ :YAG Saturable Absorber	19
2.5 Passive Mode locking.....	20
2.5.1 Mode Locking with a Semiconductor Saturable Absorber Mirror (SESAM).....	21
2.5.2 Nonlinear Polarization Rotation	25
2.6 Compensation of Dispersion with a Grating Pair.....	29
2.7 Pulse Propagation	34
2.8 Summary.....	35
 III. Methodology	 37
3.1 Chapter Overview.....	37
3.2 Pump Power Calibration.....	37
3.3 Phase I – CW Operation	39
3.3.1 Ytterbium-doped fiber	40
3.3.2 Dichroic Mirrors in the Cavity Design.....	41
3.3.3 Beam Alignment in the Cavity	41
3.3.4 Diagnostics with the Output Couplers.....	42
3.4 Power and Spectrum Measurements	42
3.4.1 Diode Pump Temperature Optimization	43
3.4.2 Spectrum Characteristics	44

	Page
3.5 Phase II – Passive Q-Switched Operation with Cr ⁴⁺ :YAG Crystal.....	44
3.5.1 Q-switch Pulse Measurements	45
3.6 Phase III – Passive Mode Locked Operation with a SESAM	46
3.6.1 Measurement of Mode Locked Short Pulses	47
3.7 Phase IV – Passive Mode Locking with Nonlinear Polarization Rotation.....	48
3.7.1 Polarization State of the Beam through the Cavity	49
3.8 Summary.....	50
IV. Analysis and Results.....	52
4.1 Chapter Overview.....	52
4.2 Continuous Wave Operation	53
4.2.1 Output Power.....	53
4.2.2 Spectrum Measurements	60
4.3 Q-Switched Operation.....	64
4.4 Passive Mode Locking - Mode Beating	71
4.4.1 Gratings	74
4.4.2 Reasons Mode Locking was not Achieved	74
4.5 Nonlinear Polarization Rotation (NPR).....	75
4.6 Summary.....	81
V. Conclusions and Recommendations	84
5.1 Chapter Overview.....	84
5.2 Research Objectives and Results Obtained	84
5.3 Advantages and Disadvantages of Fiber Lasers	86
5.4 Recommendations for Future Research.....	90
5.5 Summary.....	92
Appendix A Component Specifics.....	95
Bibliography	96

List of Figures

Figure	Page
2.1 Evolution of power output for fiber lasers [15].....	6
2.2 Example of an Yb-doped double clad fiber [16].....	9
2.3 Acceptance angle of optical fibers [26].....	10
2.4 Time sequence depicting Q-switching [37].....	18
2.5 Profile of mode locked pulse in time and frequency domains [38,39].....	21
2.6 Diagram of a saturable absorber mirror [40].....	22
2.7 Spot size on saturable absorber mirror to achieve saturation fluence.....	24
2.8 Rotational mapping of cw and mode locked operation for NPR [43].....	28
2.9 Group Velocity Dispersion dependence on wavelength.....	30
2.10 Group Delay Dispersion dependence on fiber length.....	31
2.11 A grating pair showing separation distance and position angle [29].....	31
2.12 Reflected angle dependence between grating pair.....	33
2.13 Relationship between fiber length and grating separation.....	33
3.1. Calibration of diode pump corresponding to power in Watts.....	38
3.2 Laser setup for continuous wave operation.....	39
3.3 Surface area of polarization maintaining and non-PM fiber [46,48].....	40
3.4 Optimizing temperature of diode chiller to output power.....	43
3.5 Laser setup for passive Q-switch operation.....	45
3.6 Laser setup for passive mode locking operation.....	47
3.7 Laser setup for nonlinear polarization rotation operation.....	49

Figure	Page
4.1 Output power in continuous wave operation for different fibers.....	53
4.2 Output power efficiency in cw with different fibers.....	55
4.3 Diagram from figure 3.1 showing location of dichroic mirrors.....	56
4.4 Power measurements taken at dichroic mirrors.....	57
4.5 Output power in cw for different output couplers.....	58
4.6 Output power efficiency in cw for different output couplers.....	59
4.7 Laser output power compared to reflectance of output couplers.....	60
4.8 Spectral profile continuous wave operation.....	62
4.9 Spectrum measured with increased pump power.....	63
4.10 Spectrum measured as diode chiller temperature is varied.....	63
4.11 Comparison of output power in cw and Q-switched operation.....	64
4.12 Output power efficiency for Q-switched operation.....	65
4.13 Signal of Q-switched operation using Cr^{4+} :YAG.....	66
4.14 Measurements of Q-switched pulses and separation over power.....	67
4.15 Repetition rate for Q-switched pulses over power.....	68
4.16 Pulse energy for increased pump power in Q-switched operation.....	69
4.17 Pulse peak power and average power in Q-switched operation.....	70
4.18 Beat width, separation and repetition rate using SESAM.....	72
4.19 Signal of mode beating using SESAM.....	73
4.20 Fast Fourier Transform of mode beating in figure 4.19.....	73
4.21 Output power from polarized beam splitter using NPR.....	76

Figure	Page
4.22 Output power dependence on polarization rotation angle using NPR.....	77
4.23 Signal and FFT of possible mode locking using NPR.....	78
4.24 Q-switched signal using NPR at 2.4 W pump power.....	79
4.25 Q-switched signal using NPR at 3.5 W pump power.....	80

List of Tables

Table	Page
2.1 Damage Threshold for fused silica at 1064 nm [28].....	12
3.1 Summary of methodology, features of experiment, and objectives.....	51
4.1 Summary of spectrum results performed on the fiber laser.....	61
A.1 Component specifics for experiment setup.....	94

List of Acronyms

Acronym	Page
fs - Femtosecond.....	1
ns - Nanosecond.....	1
cw - Continuous Wave.....	1
Yb - Ytterbium.....	1
Cr ⁴⁺ :YAG - Chromium ⁴⁺ : Yttrium ₃ Aluminum ₅ Garnett ₁₂	1
QML - Quasi Mode Locked.....	1
SESAM - Semiconductor Saturable Absorber Mirror.....	2
NPR - Nonlinear Polarization Rotation.....	2
AFIT - Air Force Institute of Technology.....	2
GVD - Group Velocity Dispersion.....	3
TOD - Third Order Dispersion.....	3
ps - Picosecond.....	5
nJ - Nanojoule.....	5
kW - kilowatt.....	5
NDF - Ytterbium Doped Fiber.....	6
ASE - Amplified Stimulated Emission.....	7
CPA - Chirped Pulse Amplification.....	7
PCF - Photonic Crystal Fiber.....	9
MOPA - Master Oscillator/Power Amplifier.....	9
NA - Numerical Aperature.....	10

Acronym	Page
LIDT - Laser Induced Damage Threshold.....	12
SRS - Stimulated Raman Scattering.....	12
SBS - Stimulated Brillouin Scattering.....	12
FWHM - Full Width Half Maximum.....	20
SPM - Self Phase Modulation.....	26
XPM - Cross Phase Modulation.....	26
GDD - Group Delay Dispersion.....	29
HR - High Reflectance.....	39
HT - High Transmittance.....	39
LMA - Large Mode Area.....	40
PM - Polarization Maintaining.....	40
OC - Output Coupler.....	42
QWP - Quarter Wave Plate.....	48
HWP - Half Wave Plate.....	48
PBS - Polarized Beam Splitter.....	49
WDM - Wavelength Division Multiplexing.....	89

Q-SWITCHED AND MODE LOCKED SHORT PULSES FROM A DIODE PUMPED, YB-DOPED FIBER LASER

I. Introduction

1.1 Background

The development of fiber lasers as a possible replacement to high-cost, bulk solid-state lasers is of increasing interest to the Department of Defense (DOD), scientific research, and commercial industries. For high power applications, double-clad fiber lasers pumped by inexpensive diodes present simpler, more compact, and lower cost solutions, in the fields of communication, laser range finding, remote sensing, surgical marking, micro-machining, biomedical imaging and medical surgery [1]. Fiber lasers that operate in Q-switched or mode locked regimes, emitting short pulses and ultrashort pulses on the order of nanoseconds (ns) to femtoseconds (fs), at repetition rates of kHz to MHz, respectively, possess specific advantages over continuous wave (cw) operation, enabling cleaner ablation of materials in micro-machining and medical surgeries [2], higher efficiencies in laser communication, and precise measurement in remote sensing and laser range finding [3].

1.2 Problem Statement

The objective of this experiment and thesis was to develop a diode-pumped, ytterbium (Yb)-doped double-clad fiber laser system, designed to operate in the Q-switched, mode locked, and Q-switched mode locked (QML) regimes. A Cr^{4+} :YAG

(Chromium⁴⁺: Yttrium₃ Aluminum₅ Garnet₁₂) crystal was used as a saturable absorber to passively Q-switch the laser. In order to passively mode lock the laser, a semiconductor saturable-absorber mirror (SESAM) was placed in the cavity. A second technique to generate mode locked pulses implemented nonlinear polarization rotation (NPR). Data was collected and interpreted in order to compare measurements of the laser output power, efficiency, spectrum and short pulse characteristics. This includes pulse width, repetition rate, and pulse intensity, in order to further analyze the functionality, benefits, and disadvantages to Yb-doped fiber laser systems using a saturable-absorber as a simpler, compact, and less costly alternative to bulk solid-state laser systems for applications of short and ultrashort optics.

1.3 Thesis Overview

This thesis is a presentation of the research, experimental methods, data collection, and analysis conducted at the Air Force Institute of Technology (AFIT) from June 2008 through March 2009, with the primary experimental efforts taking place from September 2008 to January 2009. The remainder of the introduction section highlights the research objectives and the research focus of this experiment. Chapter II provides a summary of previous work conducted in the fields of fiber lasers and short pulse applications. This chapter will briefly cover the important aspects pertaining to the propagation of a pulse through a Yb-doped fiber, passive Q-switching, passive mode locking, nonlinear polarization rotation, and compensation of dispersion effects using a diffraction grating pair. Chapter III outlines the experimental setup, procedures, equipment and optics used, and the subsequent measurements taken. Chapter IV presents

the results acquired for the design concepts shown in chapter III, along with analysis of the data and explanation for error and complications of the experiment. The discussion and conclusion section in chapter V explores the advantages and disadvantages to the fiber laser pertaining to DOD interests and proposals for future research within AFIT.

1.4 Research Focus

While fiber lasers offer a broad array of challenges to multiple scientific disciplines, the focus of this experiment centers around the output power, pulse width, and spectral tuning of the system in cw, passively Q-switched, passively mode locked, and QML operation. There are significant linear and nonlinear effects that factor into the power output, temporal (time), and spectral characteristics of the laser. These issues are briefly addressed to the extent that they applied to the experiment, but not to the level of detail that they may deserve. This includes power losses inherent to the laser cavity design, damage thresholds of the fiber and optics, group velocity dispersion (GVD) and third order dispersion (TOD) contributions to the pulse width at higher input powers and intensities.

In the cw regime, laser output power compared to the pump power for each design provides experimental justification for the laser efficiency in comparison to the research conducted and current bulk solid-state lasers commercially available. Measurements of the pulse width in Q-switched and mode locked operation are compared to the theory developed in chapter II, and are based on the dimensions of the laser cavity. Additionally, fibers and other optical elements are a significant source of GVD and TOD that affect the group velocity of a pulse and significantly increase the pulse width. To

compensate for GVD, techniques for using a grating are presented in the next chapter. Passive mode locking was not achieved for experiments using the SESAM. Because of this, the inclusion of the gratings in chapter II serves more to support the theory of dispersion compensation, and was not used for comparison with the data collected in the experiment.

Spectral measurements were obtained for cw, Q-switch, mode locked and NPR design concepts, along with differing reflectance output couplers. The spectra of both the input and output beam for each design are presented and explained.

It was desired to keep the cavity length and design as consistent as possible in cw, Q-switched, and mode-locked operation in order to better compare the measurements described. However, this posed a significant challenge because the different operating regimes were better optimized at different cavity lengths or different positioning of lenses and mirrors in the cavity. Attempts to explore issues of optimization are presented as well.

II. Theory

2.1 Chapter Overview

This chapter begins by providing a brief historical development of fiber lasers and current advances in high power experiments. A comparison in performance between solid-state lasers and fiber lasers in cw and pulsed operations is summarized from literature searches, incorporating scientific reporting and a few examples of available commercial technology at the present time. This chapter also provides a brief summary of propagation of pulses through Yb-doped fibers, some of the important computational equations for passive Q-switching, passive mode locking, and compensation of dispersion within the cavity using a grating pair. The intent is to provide background directly applicable to the purpose of the experiment, and to highlight key relationships for taking power measurements of the output beam, measuring the pulse width, and collecting spectral data.

2.2 Previous Work

Fiber lasers are not a new technology. The first fiber lasers were developed in the early 1960's; they operated at wavelengths of about 1 μm , and provided just a few milliwatts (mW) of power [4, 5]. Techniques for mode locking and Q-switching lasers, generating picoseconds (ps) pulses were demonstrated in the mid-1960's using He-Ne and dye lasers [6,7]. Sub-picoseconds mode locked pulses in dye lasers with energies of 3 nJ and 4 kilowatts (kW) peak powers were reported in the mid-1970's [8]. Since the inception of fiber lasers, it seems they have continued to lag behind the industry standard

of the time, while continuing to show promise as the prudent alternative to bulky, expensive, and less efficient systems being marketed.

At present, the Ti:Sapphire solid-state laser is among the most popular sources for fs pulses and at the forefront of ultrafast technology for scientific research. Commercial versions typically supply 100 fs pulses at repetition rates of 80 MHz and pulse energies of 15 nanojoules (nJ) at average powers of 1-3 Watts. Generation of pulses shorter than 12 fs was demonstrated in the early 1990's [9, 10, 11]. However, Ti:Sapphire lasers are costly, some on the order of \$200,000. They require significant cooling and maintenance, and have output efficiencies of less than 20% [12, 13].

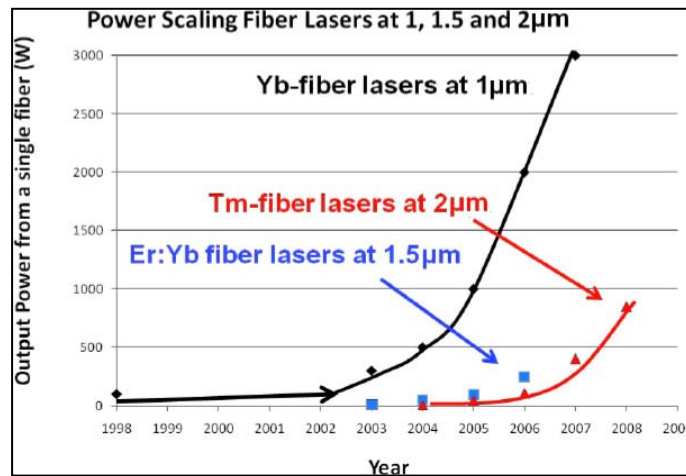


Figure 2.1. Evolution of power output for fiber lasers between 1998 and 2008 for rare-earth doped fibers [15].

Current research in fiber laser systems is attempting to resolve these issues of performance, cost, and simplicity. Ytterbium-doped glass fibers (YDF), with a quantum defect less than 10%, and power coupling efficiencies up to 80%, appear to be the gain medium of choice for high power output solutions [14]. Figure 2.1 [15], illustrates the power evolution achieved for cw output from rare-earth doped fibers between 1998 and

2008. What is significant from the graph is the relative slow progress in output power achieved during the late-1990's to a dramatic increase over the past seven years, particularly with Yb-doped fibers lasers. In 2005, IPG Photonics set a record for peak power at 17 kW by combining light from multiple Yb-doped fibers to produce a multimode beam. For single mode cw operation, powers up to 3 kW have been achieved since 2006 [15]. Leading groups in the area of power scaling fiber lasers include IPG, followed by a group at University of Southampton and Friedrich Schiller University Jena, who have produced 1 kW cw, single mode power outputs [16].

While significant advancements in high power have been achieved in the cw regime, the output power in Q-switched and mode locked operation is significantly restricted due to nonlinear processes playing a more dominant role in power and energy scaling [14]. Nonlinear processes such as amplified spontaneous emission (ASE) is significant in doped fibers due to the high gain of the fiber and continuous pumping, which in turn lowers the energy storage capacity of the fiber. This is an area where fiber lasers lag significantly behind their solid-state counter-parts. The high peak power of a Q-switched or mode locked pulse can quickly exceed the damage threshold of the fiber and destroy it. Work done thus far to achieve higher output power in ultrashort pulse fiber lasers is geared towards chirped-pulse amplification (CPA) techniques [17]. CPA methods involve first stretching the pulse prior to propagating through the fiber, and then compressing the stretched pulse that exits the gain medium, leading to higher output powers without damaging the fiber. In 2005, a group at Friedrich Schiller University demonstrated 131 W of average power for 220 fs pulses in a YDF CPA system [18]. For

Q-switched operation, output powers of 30 W by the same group were achieved using a rod-type photonic crystal fiber [14].

Commercial pulsed fiber laser systems currently offered by Polar Onyx range from 1-10 W, with pulse widths between 500-800 fs at wavelengths of 1030-1064 nm, and repetition rates of 10-1000 kHz with energies on the order of μJ [19]. In August 2008, the company SPI Lasers announced a commercial 30 W pulsed laser with pulse widths of 10-200 ns operating at 1065 nm [20, 21]. These are some of the highest power and pulse lasers available commercially.

In addition, the technique of nonlinear polarization rotation (NPR) is a relatively new method for achieving passive mode locked pulses on the order of 100's of femtoseconds. Rotating polarization wave plates in the optical cavity takes advantage of the nonlinear properties of the pulse propagating through the fiber, thereby allowing the intensity of the beam to be controlled to a point where mode locking and Q-switching can be self-started. This technique will be explained further in section 2.5.2 and in chapter III section 3.7. NPR was first demonstrated in 1992, and by the end of the year, cavity designs producing 452 fs pulses were demonstrated. By 1993, a ring design cavity using an erbium-doped fiber was capable of producing 76 fs pulses with peak powers of 1 kW and 90 pJ energies [22]. NPR methods are still being researched today. Utilizing both ring and linear cavities to produce short pulses on the order of 50 fs with nJ energies and 100's of kilowatt peak powers, NPR is certainly geared toward the objectives of generating pulsed laser systems that are cheaper, smaller, and more durable [23].

While getting around the deleterious nonlinear effects poses a challenge to current research, an emerging solution involves changing the fiber composition. Microstructured fibers, better known as photonic crystal fibers (PCFs), are making headways in the literature for resolving nonlinear effects such as ASE and self-phase modulation. In 2006, the company Aculight used a Yb-doped PCF and achieved ns pulses of 3 mJ energies, 3 MW peak power and 30 W average pulse power with a beam quality M^2 of 1.1 using a master-oscillator/power amplifier (MOPA) [24]. The proposed experiment in this thesis will not utilize photonic crystal fibers, so it will not be explored further in this section, but will be further discussed in section 5.4 with regards to future research recommendations.

2.3 Propagation of a Pulse through a Fiber

The Yb-doped double clad fiber (YDF) as shown in figure 2.2 [16] serves as the gain medium and encompasses the largest part of the cavity length. In contrast to solid-state lasers, there is an advantage to the gain medium being long and thin. For a long rod of radius r and length L , the surface-to-active volume ratio is $(2\pi rL)/(\pi r^2L) = 2/r$ [25].

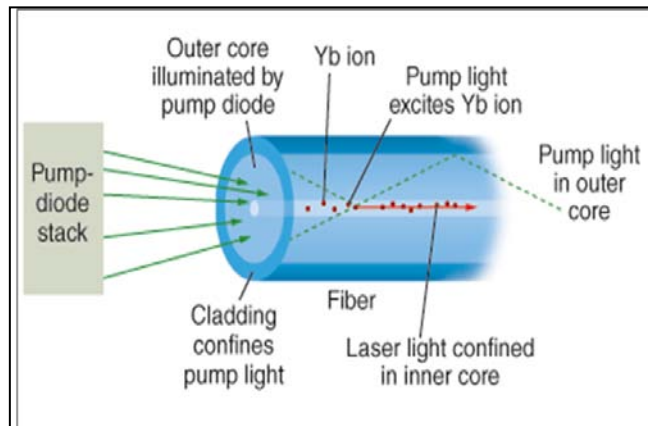


Figure 2.2. Example of a Yb-doped double clad fiber [16].

The radius of the fiber is very small, and the core of the fiber rises in temperature by only a small amount, leading to excellent heat dissipation and distribution of the thermal load over a relatively long length [14]. This is an advantage over solid-state systems, such as the Ti:Sapphire laser, where temperature increases, if not properly cooled, and can generate thermal lensing, limiting the output power, and degrading the beam quality. Therefore, YDF was selected for this experiment in effort to capitalize on its compact structure and efficiency, and also to mitigate thermo-optical problems [25].

A diode pump source was used to pump light into the double-clad fiber, where the cladding confines the pump light and the laser light is confined in the fiber core. The coupling efficiency will be limited by the brightness of the diode laser light, the numerical aperture (NA) of the fiber, and how precisely the pump light is focused into the cladding. The numerical aperture of the fiber is given by,

$$NA = n \sin \theta_{\max} = \sqrt{n_{\text{core}}^2 - n_{\text{cladding}}^2} \quad (2.3.1)$$

where n_{core} and n_{cladding} are the refractive indexes of the core and cladding, respectively. The NA determines the acceptance light cone of the fiber. Both figure 2.3 [26] and equation (2.3.1) show that larger values for NA have larger acceptance angles, and

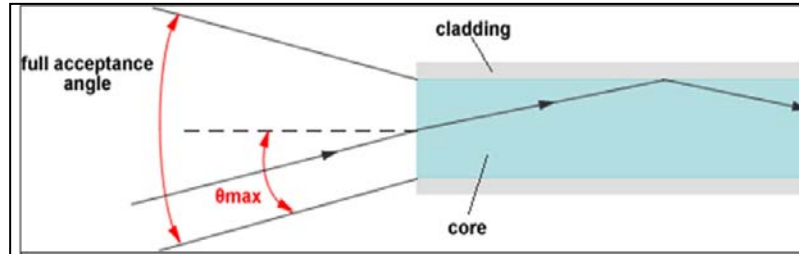


Figure 2.3. Higher Numerical Apertures (NA) in optical fibers lead to lower losses in diode to fiber coupling [26].

therefore less pump light that is wasted. This also helps to mitigate optical damage from the intensity of high power diodes.

From the numerical aperture, the fiber parameter, also known as the V parameter, can be computed for the fiber. This provides information on the number of transverse modes M that will propagate in the fiber. The V parameter for a fiber is given by,

$$V = 2\pi \frac{a}{\lambda} NA \quad (2.3.2)$$

where a is the radius of the fiber core and λ is the wavelength. A fiber will operate in single-mode condition for $V < 2.405$ [27]. As an example calculation, this experiment utilized a fiber with a 20 μm core mode field diameter and NA of 0.12. This yields a V parameter of ~ 14.2 at a wavelength of 1064 nm. Thus, the fiber operates at higher than single mode, which is better for higher power operation, but can also degrade the beam quality.

From the V parameter, the number of modes M in the fiber can be approximated.

$$M \approx \frac{4}{\pi^2} V^2 \quad (2.3.3)$$

Equation (2.3.3) [27] shows the number of modes increases quadratically with V. For the same fiber parameters listed above, the number of modes is approximated to be $M \sim 81$.

High power fiber lasers can be built around the double-clad fiber, where the inner core, which has the highest refractive index, is doped with Yb^{3+} ions, and the outer core (also known as the inner cladding) has an intermediate refractive index between the inner core and outer cladding [16]. The pump light cross-section diameter d can be focused onto the fiber using the relationship found in equation (2.3.4).

$$d = \frac{1.22 f \lambda}{D} \quad (2.3.4)$$

The beam cross-section diameter prior to being focused is given by D , f is the focal length of the lens. It is desired to obtain a value for d as close as possible to the diameter of the fiber's inner cladding. This confines the pump light into the cladding of the fiber and excites the light emitting atoms as the light traverses the core. [16].

Other concerns for optical fibers are the laser induced damage thresholds (LIDT), which are thresholds of energy, intensity, and power propagating through the fiber that can cause damage. For a laser spot size of $10 \mu\text{m}$, (an approximation to the fiber core size of $20 \mu\text{m}$ used in the experiment) the LIDTs of fused-silica at 1064 nm were extrapolated from plots provided by R. M. Wood [28], and are shown in Table 2.1 for pulse sizes on the order of nanoseconds, picoseconds, and femtoseconds.

Table 2.1. LIDT for fused silica of $10 \mu\text{m}$ spot size at 1064 nm [28].

LIDT	ns	ps	fs
J/cm^2	10	1	10
W/cm	10^8	10^9	10^9
W	10^5	10^9	10^{10}

The diode pump powers for this experiment do not exceed 13 Watts, well below the damage threshold for the fibers. However, there are several other factors to consider including stimulated Raman scattering (SRS), stimulated Brillouin scattering (SBS), and surface area quality of the fiber ends. Both SRS and SBS occur when a photon with a particular frequency interacts with a nonlinear material and emerges with either a higher

or lower frequency. In the case of SRS, a photon from the diode pump with a slightly higher frequency than the laser pump light enters the nonlinear medium, such as the Yb-doped fiber, and stimulates the emission of a second signal photon, in which the energy is transferred through the vibrational modes of the medium [27]. SRS is similar to SBS, except that instead of the stimulated scatter of optic phonons, SBS involves the scatter of acoustic phonons when the signal photon enters the fiber. In both cases, the scattering direction is in the reverse direction of the signal and is a third order nonlinear optical process [27].

The SRS and SBS power damage thresholds (P_R and P_B) for an optical fiber are given by [28],

$$P_R = \frac{16A}{g_R L} \quad (2.3.5)$$

$$P_B = \frac{21A}{g_B L} \quad (2.3.6)$$

where A is cross-section area of the fiber, L is the effective interaction length of the fiber and the Raman and Brillouin gain coefficients are given by g_R and g_B , respectively. As a quick approximation relating to this experiment, let the cross-sectional diameter of the fiber be 200 μm , the length of the fiber be 5 m, a Raman gain coefficient of 1×10^{-13} m/W and Brillouin gain coefficient of 6×10^{-11} m/W [29]. The SRS power threshold is approximated at 1.0 MW and the SBS power threshold at 2.2 kW. These equations also reveal a higher threshold power as the length L of the fiber is decreased. However, for a maximum pump power of 13 W used in this experiment, it was assessed the power threshold due to SRS and SBS would not be exceeded.

Additional factors affecting the propagation of light through the optical fiber are the angles at which the fiber is cleaved, the surface quality of the fiber ends, and the bend radius of the fiber. The cleaving angle increases the surface area of the fiber core in which pump light can be focused into the fiber, as well as lowers the stimulated laser light in the gain medium that is reflected back through the fiber from the opposite fiber end. The surface quality of the fiber ends should be polished clean to ensure a smooth surface free of cracks and abrasions. These defects can lead to unwanted scattering of light and melting of the fiber cladding, which can damage the fiber ends when the laser is operating [30].

While transmission of light through an optical fiber is dependent on the fiber length and cross-section diameter, the transmission is also dependent on the bending radius of the fiber. Based on data provided by M. Wood and A. Boechat, a fiber of 400 μm diameter and bend radius of 5 cm, as parameters for one of the fibers used in this experiment, will have a negligible bend loss effect [28].

2.4 Passive Q-Switching

Q-switching a laser results in pulse generation, typically at higher peak powers than would be achieved in continuous wave operation. This is accomplished by increasing the absorption losses in the laser cavity to a level higher than the gain threshold. By preventing the laser from lasing for an interval of time, the loss in the cavity exceeds the gain. During this time, the population inversion ($N=N_2-N_1$) continues to rise such that when lasing is resumed, the loss in the cavity quickly drops below the gain, and this generates a pulse at a higher peak power than in cw operation [31].

This pulse generation technique can be accomplished by active and passive means. A passive Q-switching method using a Cr^{4+} :YAG crystal as a saturable absorber was chosen for this experiment. The reason active Q-switching methods were not explored in this experiment was because they require the use of electro-optical (EO) or acousto-optic (AO) modulators inserted into the cavity. Active Q-switching tends to be an expensive, complex, and bulky solution, since it is achieved through externally driven Pockels cell power supplies, RF oscillators, rotating mirrors and polarizing optics. [32].

In contrast, passive Q-switching using a saturable absorber has attracted interest as a less complex and cheaper alternative to active Q-switching [33]. The Cr^{4+} :YAG crystal was selected as the passive Q-switch enabler because it has excellent optical, thermal, and mechanical properties [34], and has saturable absorption in the range of 0.9 – 1.2 μm , which is ideal for the laser output at 1064 nm for the Yb-doped fiber. Cr^{4+} :YAG crystal has been widely reported in the literature to generate nanosecond and picosecond Q-switched pulses in the near-infrared for a wide range of laser systems, including fiber lasers [35].

2.4.1 Generating a Q-Switched Pulse

This section briefly describes the relationships between gain, loss, and inversion population in the laser cavity that leads to the generation of a Q-switched pulse. This theory was first presented by Wagner and Lengyel using a ruby laser in 1962 [36], and a similar treatment is followed by Saleh [27] and Davis [37]. Let us first define the state of the laser in terms of the photon density Φ as the number of photons, the frequency ν , the

population inversion per volume $N=N_2-N_1$, and the gain and loss coefficients as γ and α , respectively.

For lasing to occur, the gain of the cavity needs to exceed the threshold gain coefficient γ_{th} . For simplicity, the threshold gain is defined as,

$$\gamma_{th} = \alpha - \frac{1}{2L} \ln(R_1 R_2) \quad (2.4.1.1)$$

where L is the cavity length and the R coefficients correspond to the reflectance within the cavity. If the loss coefficient α is increased, the threshold gain increases, and if α exceeds the gain coefficient of the cavity, lasing is stopped. The gain coefficient for a given frequency $\gamma(\nu)$ is shown to be proportional to the population inversion.

$$\gamma(\nu) = \sigma(\nu) \left(N_2 - \frac{g_2}{g_1} N_1 \right) \quad (2.4.1.2)$$

$\sigma(\nu)$ is the stimulated emission cross-section of the gain medium, and the g coefficients relate to the probability for emission from the Einstein coefficients [31]. Therefore, if the population inversion increases, so will the gain in the cavity.

In order to achieve Q-switching, whether using passive or active techniques, the quality factor Q needs to be decreased. The Q-factor of the cavity expresses the amount of energy stored to the rate of energy dissipated, and is given by [27,37],

$$Q = 2\pi \frac{\text{stored energy}}{\text{energy loss per cycle}} = \frac{2\pi\nu_0 L_g}{c(1-R)} = 2\pi\nu_0 \tau_0 \quad (2.4.1.3)$$

$$\tau_0 \approx \frac{1}{c\alpha} \quad (2.4.1.4)$$

where ν_0 is the operating frequency and τ_0 is the photon lifetime of the gain medium with length L_g . It can be seen from equation (2.4.1.3) that the Q-factor can be decreased when

the loss α is increased due to the inverse relationship between the loss and photon lifetime, as shown in equation (2.4.1.4).

From the full derivation carried out by [27,36, 37], and from the concept that increasing the loss will lower the Q-factor and increase the threshold gain coefficient with respect to the gain coefficient, two coupled differential equations are found that relate the change in time of the number of photons $\Phi=qV$ and the population inversion N .

$$\frac{d\Phi}{dt} = \Phi\left(\frac{\gamma}{\gamma_{th}} - 1\right) = \Phi\left(\frac{N}{N_{th}} - 1\right) \quad (2.4.1.5)$$

$$\frac{dN}{dt} = -2\Phi \frac{N}{N_{th}} \quad (2.4.1.6)$$

Equation (2.4.1.5) shows the proportionality between the gain coefficients and the population inversion, while equation (2.4.1.6) shows a decreasing inversion rate with time. These equations can be solved numerically by setting initial conditions for both equations at $t=0$. Initially, $\frac{dN}{dt} \gg \left(\frac{d\Phi}{dt} \approx 0\right)$. Figures 2.4 (a) and 2.4 (b) show a normalized inversion and photon density over a normalized time for two cases. In the first case, figure 2.4 (a), the initial inversion is pumped to 50 times above threshold (similar to the model presented by Davis [37]). Q-switching begins as the initial inversion (Φ) increases above the normalized threshold value ($N=1$ on the y-axis). The peak photon density is observed as N falls below this threshold value with respect to time. The result is a short duration Q-switched pulse in comparison to the longer duration pulse in figure 2.4 (b) where the population N is pumped to just five times above threshold.

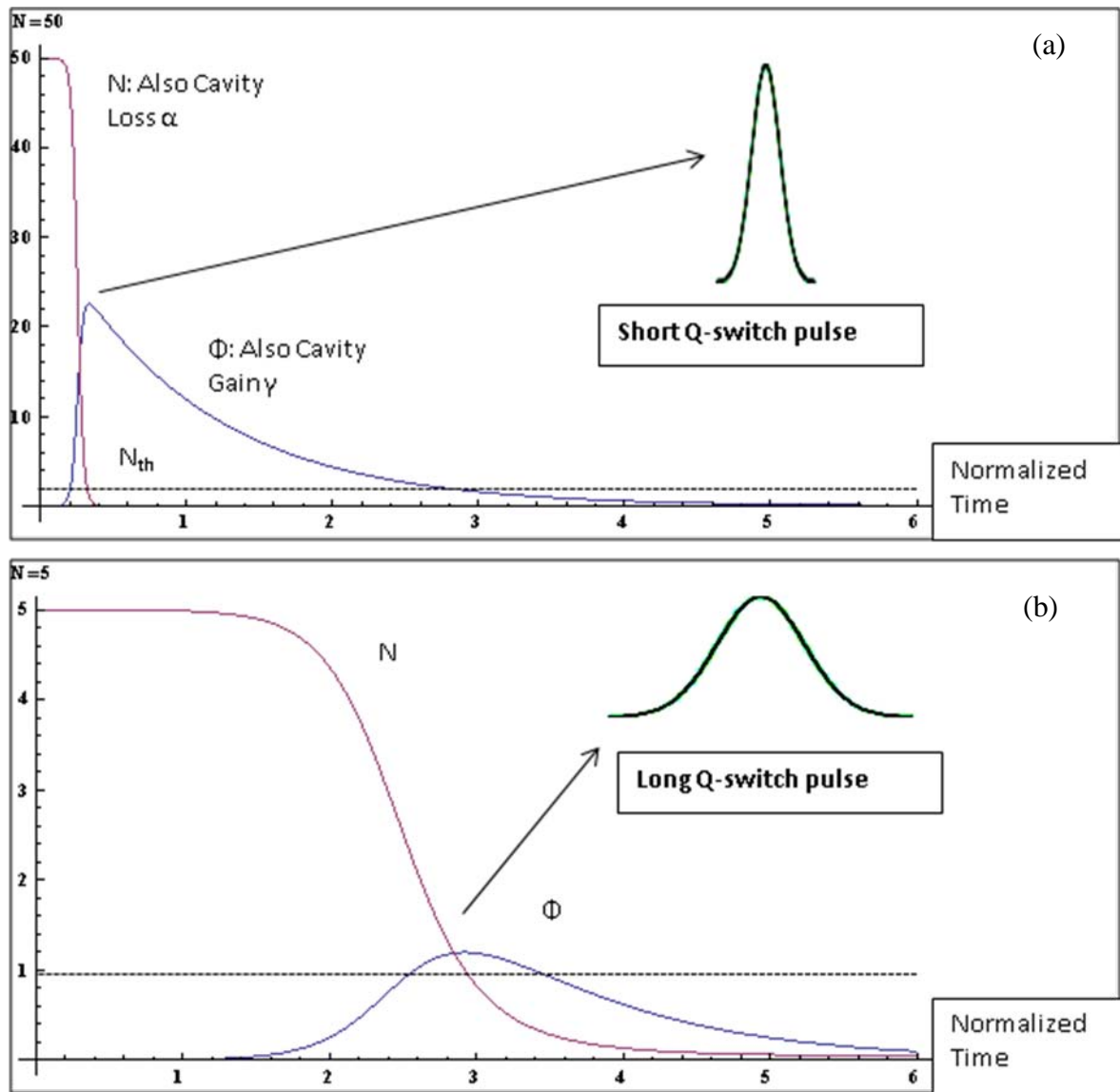


Figure 2.4. Model for Q-switch pulse from numerically solving equations (2.4.1.5) and (2.4.1.6). The population inversion N/N_i in 2.4 (a) is pumped to 50 times above threshold and the inversion in 2.4 (b) is pumped to 5 times above threshold. N and Φ also correspond to losses and gain in the cavity. The intensity profile of the pulse is shown in relation to the initial conditions [37].

2.4.2 Utilizing the Cr⁴⁺:YAG Saturable Absorber

By inserting the Cr⁴⁺:YAG crystal into the cavity, light from the fiber is absorbed by the crystal and the losses increase. Since there is a loss of feedback in the cavity, energy is built up in the gain medium (the fiber), and the population inversion increases as described in section 2.4.1. When the intensity on the crystal reaches a saturation level, the laser light is again transmitted. When transmission occurs, the gain rapidly increases above the threshold for lasing, and the Q-switched pulse is generated in the same manner shown in figures 2.4 (a) and (b).

Experimentally, the average pulse power can be measured directly by a power meter, and the temporal characteristics of the pulse can be measured with an oscilloscope. From the power and time measurements, several of the other variables presented in the theory can be extrapolated or approximated. The power is shown to be dependent on the cavity dimensions, the photon density and transmission of the output coupler. The average pulse power is given by [27],

$$P_{Avg} \approx \frac{Pulse\ Energy}{Pulse\ Period} = \frac{h\nu c}{2L} T \Phi \quad (2.4.2.1)$$

where T is the transmission of the beam from an output coupler, L is the length of the cavity, and Φ is the total number of photons for a given volume. By measuring the average power and the pulse width, the pulse energy can be calculated. Subsequently, by measuring the pulse frequency, the peak pulse power can then be computed from equation (2.4.2.1), and given by [27],

$$P_{Peak} \approx \frac{P_{Avg} (Pulse\ Period)}{\tau_{FWHM}} \quad (2.4.2.2)$$

where τ_{FWHM} is the FWHM of the pulse width measured.

2.5 Passive Mode locking

Light in a mode locked laser can be regarded as a single pulse of photons that reflect within the cavity structure, transmitting a pulse with each reflection off the mirrors [27]. Just as there are active and passive techniques to Q-switching a cw beam, there are also active and passive techniques for mode locking that beam. Primary attempts to passively mode lock the beam were performed in this experiment using a semiconductor saturable-absorber mirror (SESAM) and through nonlinear polarization rotation.

A mode locked pulse train, which is depicted in figure 2.5 [38, 39], will have a frequency spacing, or pulse repetition rate, dependent on twice the cavity length L ,

$$\Delta = \frac{c}{2(n_{air}L_{air} + n_{fiber}L_{fiber})} = \nu_{m+1} - \nu_m \quad (2.5.1)$$

with n being the refractive index, and ν_m is a particular frequency at longitudinal frequency mode m [9]. The repetition rate is inversely dependent on the cavity length such that a long fiber length with a higher refractive index will have a larger effect on this calculation than the part of the cavity in air. Similarly, the inverse of equation (2.5.1) yields the temporal period of the pulse train T_s , which can be experimentally measured with an oscilloscope.

$$T_s = \frac{1}{\Delta} \quad (2.5.2)$$

Finally, the pulse width can be approximated by dividing the pulse separation in equation (2.5.2) by the number of modes m . This can be seen in figure 2.5, and given by,

$$\tau_{pulse} = \frac{T_s}{m} \quad (2.5.3)$$

where pulse width in the time domain decreases for an increased number of modes [27].

It should be noted however that the pulse width calculation in equation 2.5.3 is an ideal case. For ultrashort pulses, the theoretical and experimental treatment of the pulse shape is greatly affected by dispersion and the chirp, or frequency modulation, inherent to medium in which the pulse is propagating. These issues are addressed in section 2.7.

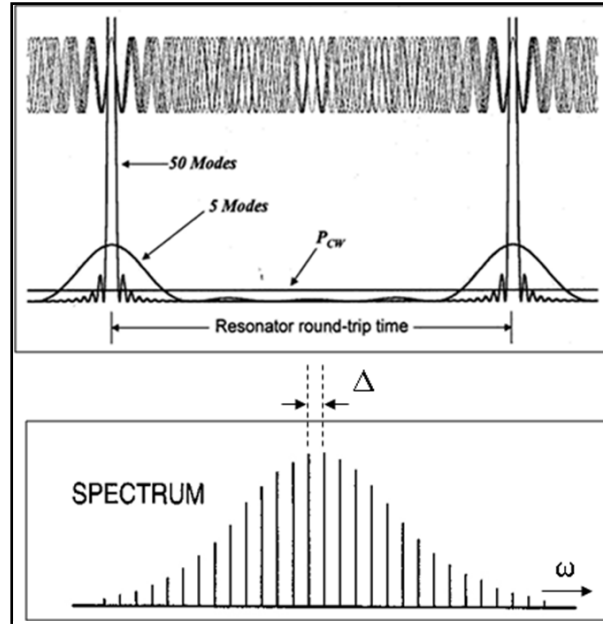


Figure 2.5. Profile of a mode locked pulse in the time and frequency domains [38 (top), 39 (bottom)].

2.5.1 Mode Locking with a Semiconductor Saturable Absorber Mirror (SESAM)

The objective for mode locking the laser using a SESAM is to phase-lock the multiple modes traversing through the fiber using the loss mechanism of the saturable absorber. Since the average power of the mode locked pulse train can be directly

measured with a power meter, the average intensity can be calculated as the power divided by the cross-section area of the beam.

$$Intensity(I) = \frac{P_{Avg}}{A_{Beam}} \quad (2.5.1.1)$$

The SAM, as depicted in figure 2.6, will become saturated at a high enough intensity, permitting the majority of the energy in the cavity to pass through the absorbing material to the mirror, and then reflected back into the cavity [40]. This experiment utilizes a SAM produced by BATOP Optoelectronics, suited for 1060 nm laser output. The SAM is essentially a Bragg-mirror on a Gallium Arsenide (GaAs) semiconductor wafer dependent on parameters of absorption modulation depth, relaxation time, saturation fluence and reflection/absorption bandwidth. These characteristics are more thoroughly explained on the BATOP website [40], but a few of these are emphasized in this section as they directly affect the cavity design in this experiment.

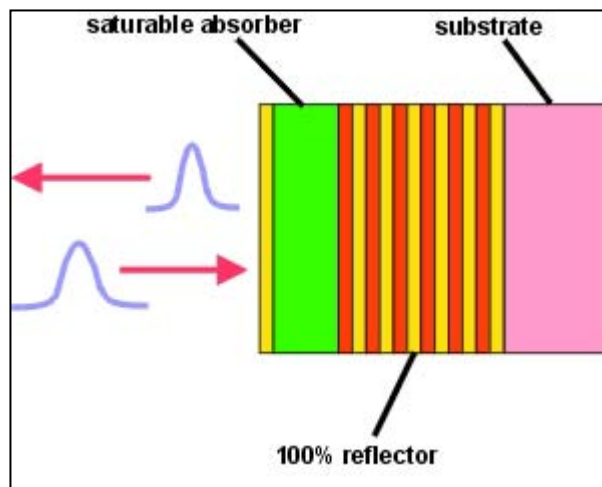


Figure 2.6. Diagram of a Saturable Absorber Mirror (SAM); this diagram was taken from BATOP Optoelectronics [40].

In order for passive mode locking to occur using the SAM, certain conditions need to be satisfied pertaining to the design of the laser cavity. First, the relaxation time of the SAM needs to be less than the roundtrip time for the pulse in the laser cavity [9]. For a roundtrip time found from equation (2.5.2),

$$\tau_{RoundTrip} = \frac{2(n_{air}L_{air} + n_{fiber}L_{fiber})}{c} \quad (2.5.1.2)$$

where L is the cavity length and c is the speed of light, fiber laser cavities are ideally suited for a long enough cavity length to surpass the relaxation time. The saturation intensity on the SAM is given by,

$$I_{Saturation} = \frac{h\nu}{\sigma_A \tau_{relaxation}} \quad (2.5.1.3)$$

where σ_A denotes the absorption cross-section and $\tau_{relaxation}$ is the relaxation time of the SAM [41], while h and ν denote the energy Planck's constant and the frequency, respectively. From the intensity form in equation (2.5.1.1), the saturated energy, also known as the saturation fluence can be calculated [41].

$$E_{Saturation} = \frac{h\nu}{\sigma_A} \quad (2.5.1.4)$$

As a quick calculation, a BATOP SAM with a relaxation time of 500 fs has a saturation fluence of $90 \mu\text{J}/\text{cm}^2$ [42]. For 5 meter long fiber with refractive index of 1.5, and combined laser cavity length (fiber + air) of 6 m, the roundtrip time of the pulse calculated from equation (2.5.1.2) is approximately 57 ns. The inverse of the round trip time yields a repetition rate of about 18 MHz. This roundtrip time exceeds the relaxation time requirement for passive mode locking when using the SAM. The saturation fluence

in J/cm^2 can be converted to units of intensity by multiplying the saturation fluence energy by the pulse repetition rate yielding a $1.6 \text{ kW}/\text{cm}^2$ intensity on the SAM. The focused spot size on the SAM can be calculated using equation (2.3.4), $d = \frac{1.22 f \lambda}{D}$, where the area of the spot size is $A = \pi(d/2)^2$ and the required power intensity to achieve the saturation fluence can be extrapolated for mode locking.

A theoretical model for the focused beam diameter on the SAM that is required to achieve a saturation intensity of $1.6 \text{ kW}/\text{cm}^2$ is shown in figure 2.7. This diameter is plotted over increasing pump power in watts. It will be presented in the experiment setup diagrams in chapter III that the beam is focused onto the SAM with a lens of 88.5-mm

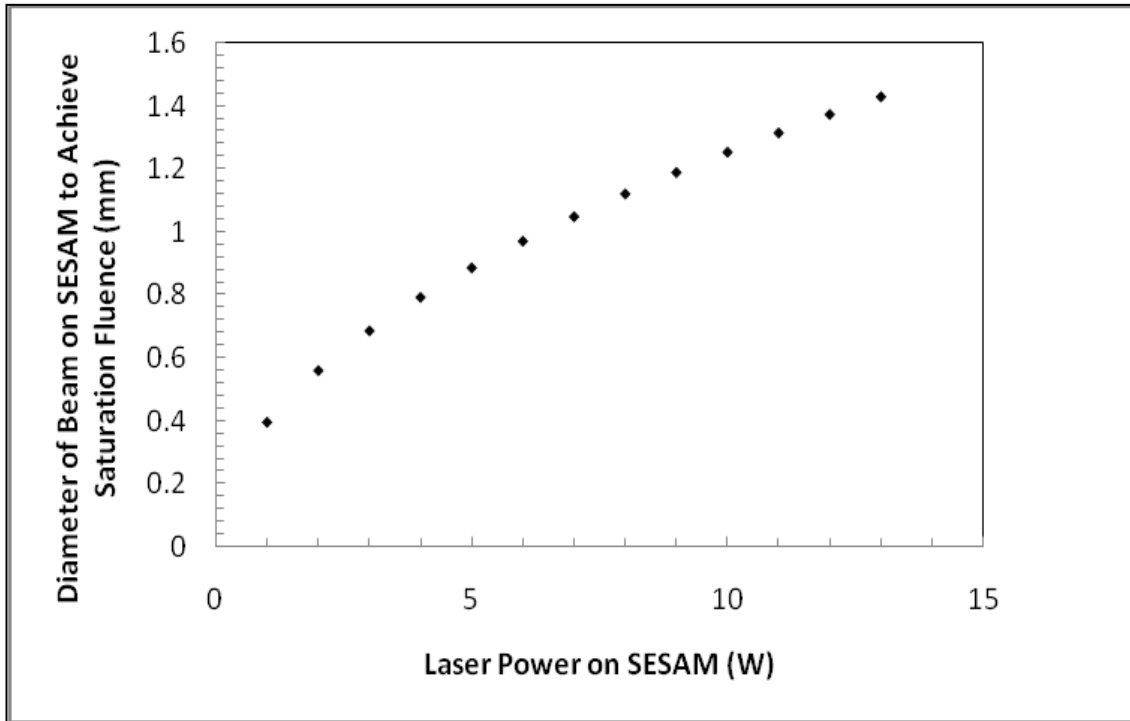


Figure 2.7. Model for spot size diameter on Saturable Absorber Mirror (SESAM) to match the saturation fluence of $90 \mu\text{J}/\text{cm}^2$ (or $1.6 \text{ kW}/\text{cm}^2$) required to initiate passive mode locking. Repetition rate was assumed at 18 MHz for cavity round trip time. Focal length of lens was 88.5mm.

focal length. Using equation (2.3.4), and wavelength $\lambda = 1.06 \mu\text{m}$, the spot size on the lens D can also be calculated. It is shown that as the power of the beam increases, a larger incident spot size on the SAM is required to achieve the saturation intensity. To manipulate the spot size, a translation stage for the SAM can be used to adjust the distance with respect to the lens. This is also explained further in chapter III, section 3.3.

2.5.2 Nonlinear Polarization Rotation

A second method for achieving passive mode locking in this experiment is through nonlinear polarization rotation (NPR). Experimentally, NPR introduces a set of polarizing elements (half wave plates, quarter wave plates, polarized beam splitters, and/or an optical isolator) into the laser cavity, where the polarization wave plates are rotated in order to control the intensity of the beam. Self-started mode locking occurs in a method similar to saturable absorbers because the time-dependent intensity of the pulse is greatest in the center (at $t=0$), and the rotated polarizing plates suppress the outer winglets of the pulse [9]. The theoretical derivation for NPR is rooted in the changes of state of polarization caused by self phase modulation (SPM) and cross phase modulation (XPM) as the orthogonally polarized components of a single pulse propagate through the fiber [22].

To begin simply, an electric field $\epsilon(t)$ is defined with x and y components relative to the fiber cavity and is time dependent [9].

$$\mathbf{E} = \frac{1}{2} (\epsilon_x(t)\hat{x} + \epsilon_y(t)\hat{y}) e^{i(\omega t - kz)} \quad (2.5.2.1)$$

The angular frequency is ω , k is the wave number, and z is the direction of propagation of the wave. If the incident pulse were linearly polarized, then the x- and y-components of $\varepsilon(t)$ would be given by [9],

$$\varepsilon_x(t) = \varepsilon(t) \cos \theta \quad (2.5.2.2)$$

$$\varepsilon_y(t) = \varepsilon(t) \sin \theta \quad (2.5.2.3)$$

with θ being the angle of polarization. Therefore, the linearly polarized beam incident on a half wave plate polarizer at $\theta + 90^\circ$ will rotate the polarization component or reduce the transmission of the incident polarization [9]. The x- and y- components of $\varepsilon(t)$ will have a phase difference $\Delta\phi$, significantly influenced by self phase modulation from propagation inside the fiber, or any nonlinear medium. SPM is a result of the optical Kerr effect where the refractive index $n(I)$ of a third-order nonlinear medium is linearly dependent on the frequency. The optical Kerr effect is given by,

$$n(I) = n + n_2 I \quad (2.5.2.4)$$

where n_2 is the optical Kerr coefficient and is on the order of 10^{-14} to $10^{-7} \text{ cm}^2/\text{W}$ for doped glasses [27]. As the refractive index changes, so too does the phase difference of the electric field wave components as the beam at wavelength λ traverses a medium length L through cross-section area A and at a power P . The time-dependent phase of the wave and phase difference between the components are given by [27],

$$\phi(t) = \frac{2\pi n(I(t))L}{\lambda} = -\frac{2\pi(n + n_2 P(t) / A)L}{\lambda} \quad (2.5.2.5)$$

$$\Delta\phi(t) = -2\pi n_2 \frac{L}{\lambda A} P(t) = -2\pi n_2 \frac{L}{\lambda} I(t) \quad (2.5.2.6)$$

with the intensity of the beam being a measurable quantity as the square of the electric field or the power per unit area.

Specific powers and intensities can be calculated for when the phase difference is known. A simple calculation can be performed when the phase difference is at $-\pi$.

Assume a fiber length of 5 meters, beam cross section diameter of 20 μm (the diameter of the fiber core), and a value for n_2 of $10^{-10} \text{ cm}^2/\text{W}$ [27]. The phase difference of the wave changes by a factor of $-\pi$ at 21.2 mW. Subsequently, phase difference and power relations can be combined with the derivation of J.C. Diels [9] for the time-dependent output intensity as a function of polarization angle,

$$I_{out}(t) = \frac{1}{2} I_{in}(t) [1 - \cos \Delta\phi(t)] \sin^2(2\alpha) \quad (2.5.2.7)$$

where α is the rotation angle of a polarized wave plate. The input intensity $I_{in}(t)$ takes on a Gaussian profile [9],

$$I_{in}(t) = I_0 \exp[-(2(t / \tau_G)^2)] \quad (2.5.2.8)$$

with τ_G being a Gaussian parameter of the pulse width's FWHM equivalent to $\tau_{\text{pulse}}/1.176$ [9]. It is apparent from equation (2.5.2.8) that the maximum intensity occurs at time $t=0$, which is the center of the pulse. This is also where the phase difference $\Delta\Phi(t) = -\pi$ is a maximum, making the output intensity $I_{out}(t=0) = I_0 \sin^2(2\alpha)$. Moving further from the pulse center in the time domain yields a smaller phase difference. The minimum intensity occurs when $\Delta\Phi(t) = 0$. This is when the power and intensity, $P(t)$ and $I(t)$, both equal zero, and laser transmission stops. Near this minimum, there are pulse wings that are elliptically polarized. The ability to suppress these wings by rotating the polarized wave plates makes the NPR technique work similar to a saturable absorber [9].

One of the more thorough mathematical treatments for NPR pertaining specifically to Yb-doped fibers is the 2002 article published by H. Leblond et al. [43]. Follow up analysis of the angular orientations of the polarizers is provided by Ortac et al. [44]. In these articles, regions of cw, mode locked, Q-switched, and unstable operation are mapped as dependent on the rotation angle of two half-wave plates in a NPR cavity, and comparing these results to theoretical master equations that incorporate the birefringence of the fiber, group velocity dispersion, nonlinear gain, and the optical Kerr effect. These results are shown in figure 2.8 to demonstrate the advantage of controlling the pulsed output for a NPR cavity, and showing that pulsed laser operation occurs over a vast range of angle settings.

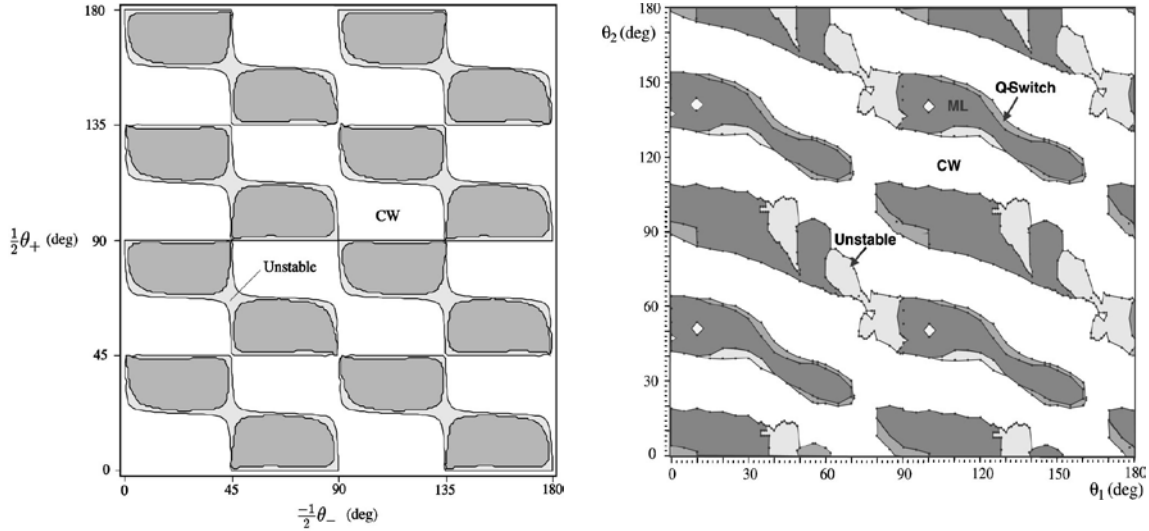


Figure 2.8. Results for theoretical and experimental mapping of regions for cw, mode locked, and Q-switched pulses using NPR with an optical isolator between two half wave plates in a Yb-doped fiber ring cavity [43].

The results of the data presented in chapter IV, section 4.5 were not comprehensive enough to replicate the results in figure 2.8. However, these charts are intended to show a sense of order to the NPR methodology where Q-switched and mode

locked short pulses can be obtained repeatedly and consistently, and also perhaps as a roadmap for future study of NPR at AFIT.

2.6 Compensation of Dispersion with a Grating Pair

One aspect to fiber lasers is the increased group delay dispersion (GDD) induced by the pulse traversing the fiber. GDD, which is the group velocity dispersion (GVD) over a certain length, causes the group velocity of the pulse to be different at different wavelengths. This in turn affects the pulse width and other characteristics of the beam output. One method to compensate for the GDD of the fiber is to insert a diffraction grating into the cavity. This produces negative GDD, which can then cancel out the positive GDD. The discussion below provides a simple method for modeling the GDD of a fused silica fiber at various lengths, and for computing the grating spacing required to compensate for the fiber.

The refractive index of a Yb-doped fiber can be approximated from the Sellmeier equation for fused silica SQ1 [27].

$$n(\lambda) = \sqrt{1 + \left(\frac{0.6962\lambda^2}{\lambda^2 - (0.0684)^2} + \dots + \right)} \quad (2.6.1)$$

The group velocity dispersion is a commonly used equation, and can be derived from the Taylor series expansion of the dispersion relation for $k(\omega)$ [9]. This is given by,

$$\frac{\partial^2 k}{\partial \omega^2} = \frac{\lambda^3}{2\pi c^2} \frac{\partial^2 n}{\partial \lambda^2} \quad (2.6.2)$$

and plotted over the range of 0.8-1.1 μm in figure 2.9. It is observed that the GVD decreases as the wavelength increases.

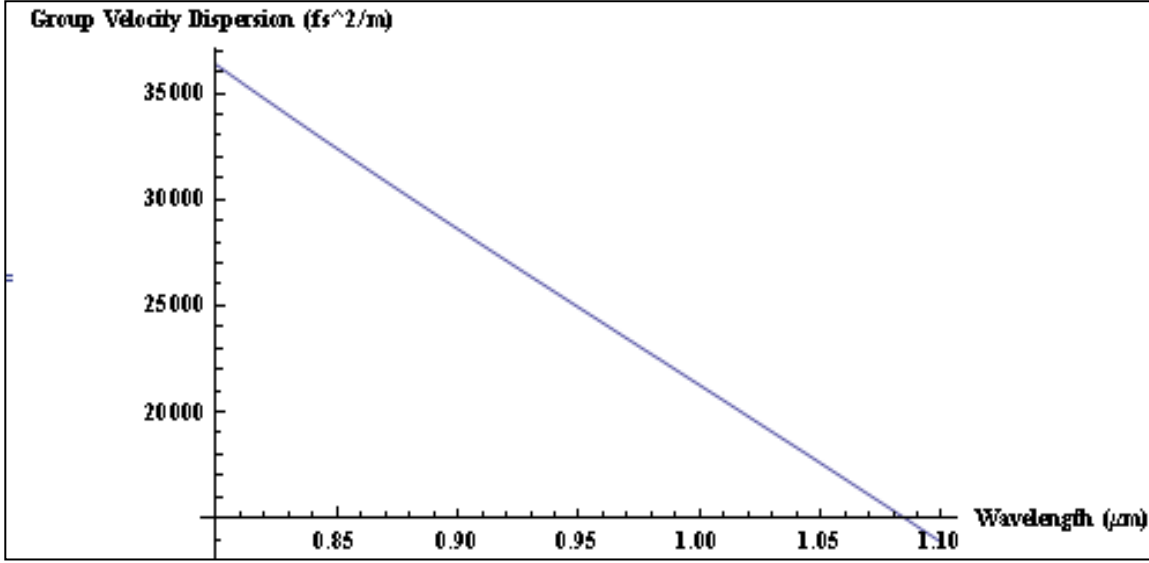


Figure 2.9. Group Velocity Dispersion for silica fiber between wavelengths of 0.8-1.1 μm .

The group delay dispersion is calculated by multiplying the GVD by the length of the fiber (L_{fiber}).

$$GDD = \frac{\partial^2 k}{\partial \omega^2} (L_{\text{fiber}}) \quad (2.6.3)$$

Figure 2.10 shows the GDD dependence on the length of the fiber between wavelengths of 1.0, 1.06, and 1.1 μm , where the expected output for this experiment should be around 1.064 μm . From this relation, we then attempt to determine the optimized separation distance L between the diffraction gratings to compensate for the GDD in the fiber. The GDD of the grating is negative, and is given by [9],

$$\frac{\partial^2 \psi}{\partial \omega^2} = -\frac{b\lambda^3}{2c^2 d^2 \cos(\beta)^3} \quad (2.6.4)$$

where $L = \frac{b}{\cos(\beta')}$ is the separation between the gratings, and d is grating spacing. A

diagram of this relationship is shown in figure 2.11 [38].

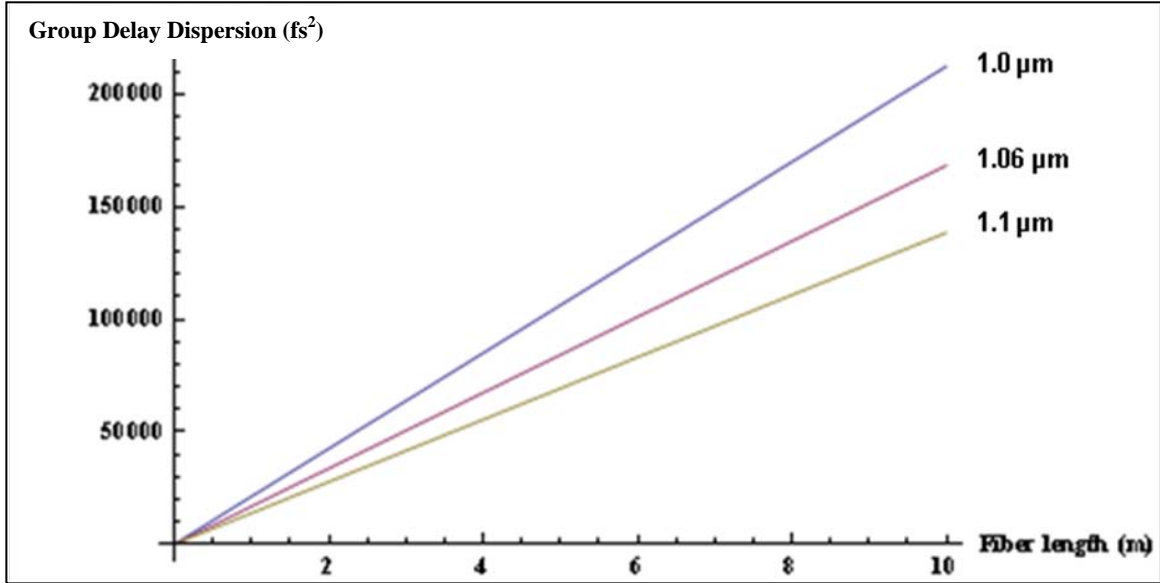


Figure 2.10. Group Delay Dispersion dependence on fiber length for 1.0, 1.06, and 1.1 μm .

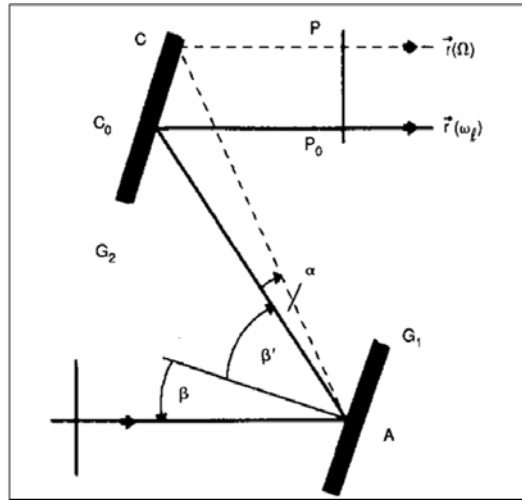


Figure 2.11. Diagram showing the separation distance (L) for a pair of diffraction grating in order to compensate for positive GDD [38].

The angle β' is the reflected angle of the beam off the first grating with respect to the normal. This angle can be determined through the relation with the incident angle β and the grating.

$$\sin(\beta) - \sin(\beta') = \frac{2\pi c}{\omega_0 d} \quad (2.6.5)$$

Figure 2.12 shows the relation between angles β' and β as they relate to the wavelengths of 1.0, 1.06, and 1.1 μm . From these relations, the grating spacing can be selected for a particular emission wavelength, and for a specified fiber length. This is presented in figure 2.13 for 1.0, 1.06, and 1.1 μm at an incidence angle β of 45° .

An additional factor affecting the pulse shape is the third order dispersion term (TOD). This term comes from the derivative of the GVD and is shown in equation (2.6.6) [9]

$$\frac{d^3\Psi}{d\omega^3} = -\frac{3\lambda}{2\pi c \cos^2(\beta')} (\cos^2(\beta') + \frac{\lambda}{d} (\frac{\lambda}{d} + \sin(\beta))) \frac{d^2\Psi}{d\omega^2} \quad (2.6.6)$$

TOD is always a positive value, where d is the grating spacing and $\frac{d^2\Psi}{d\omega^2}$ is shown in equation (2.6.4). The TOD is more difficult to compensate for than the GVD, but a ratio can be taken between the second and third order dispersions, shown as [9],

$$R_{TOD/GVD} \approx \frac{\Delta\omega}{\omega} \left(1 + \frac{\lambda / d (\lambda / d + \sin \beta)}{1 - (\lambda / d - \sin \beta)^2} \right) \quad (2.6.7)$$

where $\Delta\omega$ is the spectral FWHM of the pulse. This ratio is useful in determining the effect that TOD has on the pulse shape, where higher values indicate a larger effect. This ratio can be lowered by adjusting the angles of the gratings, as well as the grating separation distance.

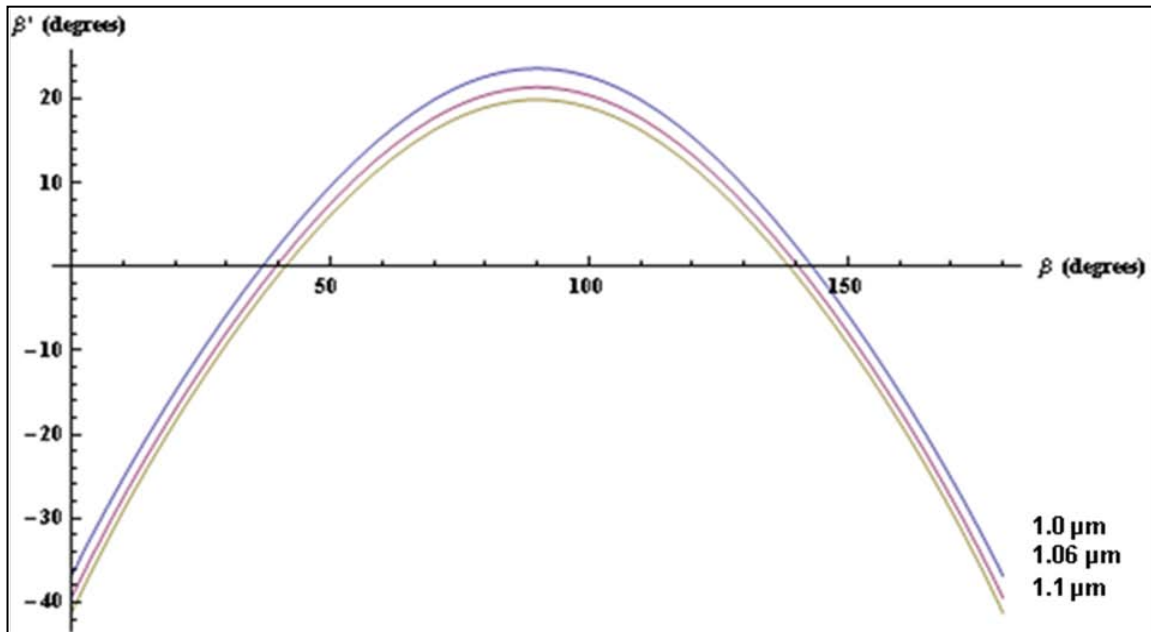


Figure 2.12. Reflected angle β' dependence on incident angle β at specified

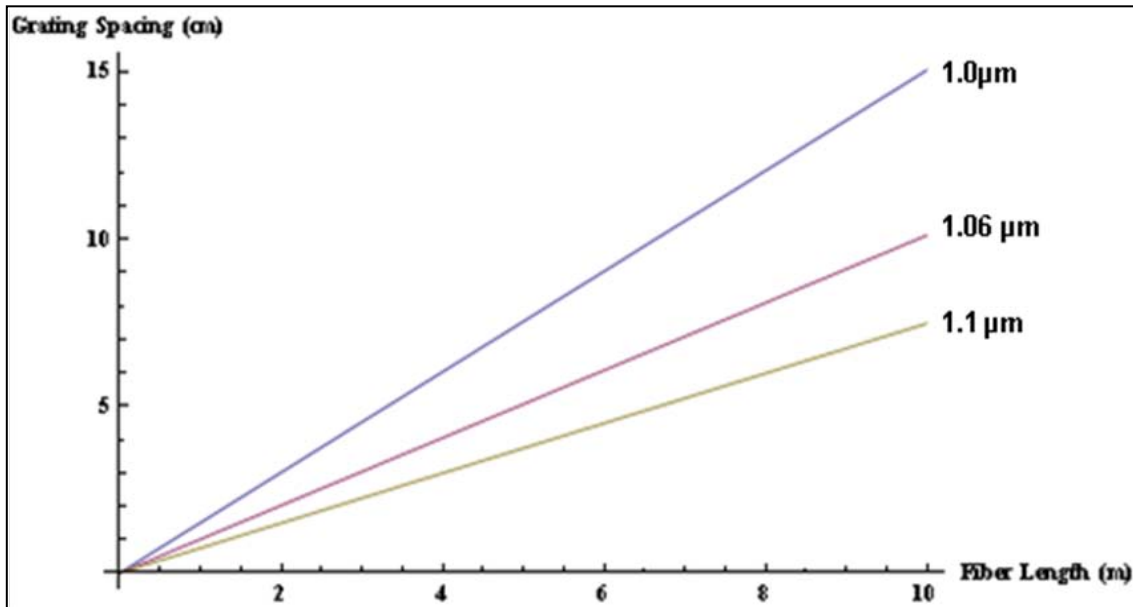


Figure 2.13. Relationship between fiber length and grating separation required to compensate for GDD of the fiber. The optimized angle is near $\beta=40^\circ$.

2.7 Pulse Propagation

The propagation of a Gaussian pulse through a linear dispersive medium is described in equation (2.7.1). In this equation, $\tau_G(z)$ is related to the pulse width as a function of z , while τ_{Go} is related to the minimum (transform limited) pulse width, z is the propagation distance, and k_l'' the dispersion constant [9].

$$\tau_G(z) = \tau_{Go} \sqrt{1 + \left(\frac{2 \cdot z \cdot |k_l''|}{\tau_{Go}^2} \right)^2} \quad (2.7.1)$$

Equation (2.7.1) is non-linear at small values of z , yet as z increases, the second term under the radical becomes much larger than one and the equation can be viewed as linear. For large propagation lengths, this equation can then be reduced to:

$$\tau_G(z) \approx \tau_{Go} \sqrt{\left(\frac{2 \cdot z \cdot |k_l''|}{\tau_{Go}^2} \right)^2} = \frac{2 \cdot z \cdot |k_l''|}{\tau_{Go}} \quad (2.7.2)$$

Equations (2.7.1) and (2.7.2) allow for a linear fit of experimental data and can be used to calculate the GVD and effective GVD of the system under consideration. For instance, the pulse width data can be measured for a configuration without a grating pair, the GVD can be computed, and the spacing of the grating pair can be derived from the computed GVD to determine proper compensation.

τ_G is related to the measured pulse width by $\tau_{Po} = \sqrt{2Ln2} \tau_{Go}$. Substituting this into equation (2.7.1),

$$\tau_P(z) = \tau_{Po} \sqrt{1 + (4Ln2)^2 \frac{(GDD)^2}{\tau_{Po}^4}} \quad (2.7.3)$$

this equation can be used to compare pulse width measurements with the theory and further optimize the laser cavity for passive mode locked operation and the proper grating spacing to compensate for dispersion.

2.8 Summary

This section briefly discussed only a few of the aspects that affected the experiment described in the next section. Background information on previous work conducted on fiber lasers was presented at the beginning of the chapter. The amount of power that can be generated in a fiber laser at cw output has increased exponentially over the past decade, while pulsed output fiber lasers are progressing at a slower pace due to limitations on the damage threshold of optical fibers as well as from linear and nonlinear effects.

This chapter also highlighted some important aspects about light coupling between the pump diode and the fiber, as well as the importance of using a large fiber diameter to accommodate higher power applications. Passive Q-switching and passive mode locking was discussed as they relate to this experiment. Specifically, background information was introduced on the prior successes in using a Cr^{4+} :YAG crystal, saturable absorber mirrors, and nonlinear polarization rotation to achieve passive Q-switched and mode locked pulses. The last part of this chapter discussed the effects of group delay dispersion on a pulse traversing through an optical fiber, and a model was provided showing how to compensate for the GDD using a diffraction grating pair. Figure 2.13 illustrates the grating separation required to compensate for specific lengths of fiber.

Many of the sample calculations performed throughout this section were used to plan the laser cavity designs presented in chapter III.

III. Methodology

3.1 Chapter Overview

This experiment was conducted in phases to facilitate controls on the experiment, and to establish bench marks for progress. The first phase was to set up the fiber laser in a cw operation to measure the power and the spectrum, and to gain familiarity with the equipment and optimization of the system. For the second phase, the Cr^{4+} :YAG crystal was inserted into the cavity in order to achieve passive Q-switching of the laser. Data collected during this phase included the output power, pulse width, pulse separation and spectrum measurements, as well as to identify techniques for optimization and possible mode locking, which has been reported in similar experiments [45].

For the third phase, the SAM was inserted in the cavity without the Cr^{4+} :YAG crystal, with the purpose of passively mode locking the cavity. The same measurements were performed as accomplished in Q-switched operation. The fourth phase involved a nonlinear polarization rotation design with the objective to achieve passive mode locked and passive Q-switched pulses.

3.2 Pump Power Calibration

Prior to setting up the laser cavity, a calibration of the laser diode pump was performed by directing the pump beam into a power meter (Thor Labs 10 Watt). Because the diode pump was controlled in terms of amperes, the purpose of the calibration was to translate the current reading from the LIMO display to a corresponding input pump power into the cavity. Three trials for the calibration were performed and are presented in figure 3.1. The average from these trials was taken, and a linear fit was applied to the

data. The linear fit was used to extrapolate the pump powers that exceeded 10 Watts. Chapter IV will present the figures of the laser's output power in comparison with the diode pump power, which is derived from figure 3.1. The uncertainty of the pump power measurements is approximately ± 5 mW due to fluctuations in the power meter readings.

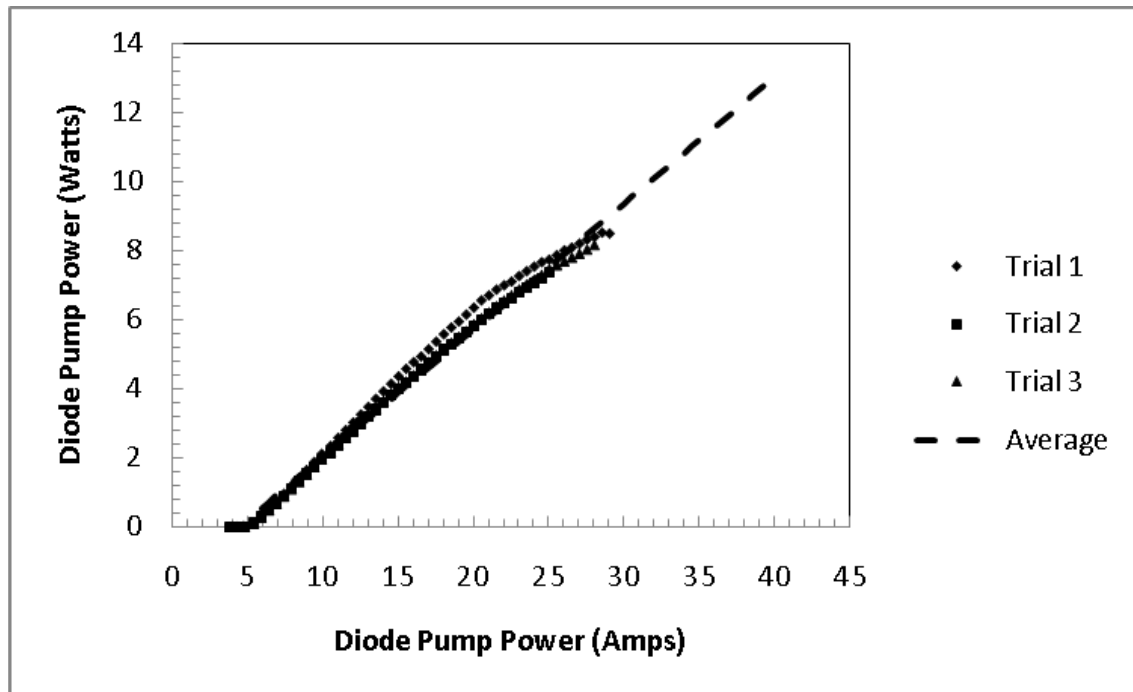


Figure 3.1. Calibration of the diode pump power measured in Amps to corresponding power in Watts.

In the Trial 2 data shown in figure 3.1, it appears the slope of the power is declining as the current is increased. This has to do with the damage threshold of the power meter at 10 W, and slight marking may have occurred on the sensor during these measurements, which likely explains the deviation from Trial 1 and Trial 3 data. A different power meter (also Thor Labs 10 Watt) was used for Trial 3, but the power meter was not exposed to the beam for as long a time period as the first two trials.

3.3 Phase I – CW Operation

A schematic for the continuous wave fiber laser operation is provided in figure 3.2. The setup consisted of a diode pump source, three dichroic mirrors, the Yb-doped double-clad fiber as the gain medium, and additional mirrors and lenses. The diode-pump used was a LIMO Laser Systems (HLU-25F200-975) emitting at 975 nm (measured at 971 nm) focused through a dichroic mirror with high transmission (HT) at 975 nm and a highly reflective (HR) coating at 1064 nm into the Yb-doped fiber. A 20X microscope objective was used to focus the pump beam into the fiber cladding. The light exited the fiber through a second 20X microscope objective, and was reflected at 450 off a second dichroic mirror with HR at 1064 nm through a 100 mm focal length lens, and focused onto a HR mirror. Upon reflection, the light passed back through the lens, was reflected off the dichroic mirror, was focused back through the fiber, and upon exiting,

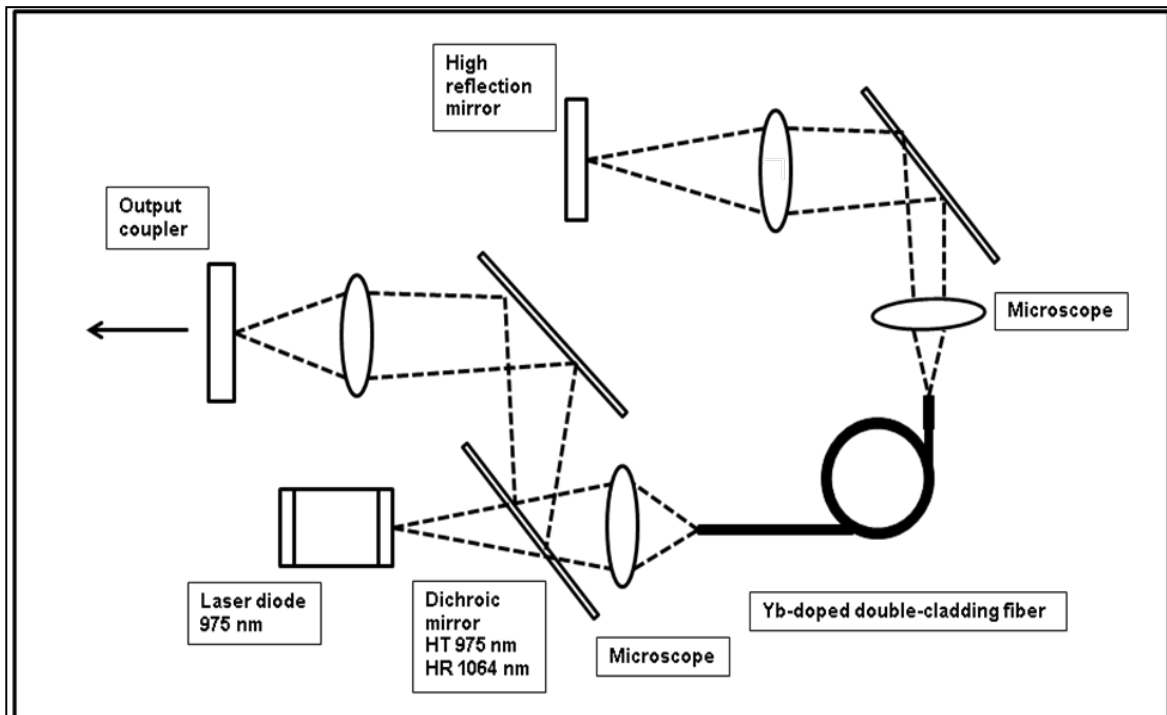


Figure 3.2. Phase I - Continuous Wave fiber laser design concept.

was reflected off the dichroic mirror closest to the pump at an angle of 45^0 . A third dichroic mirror, also angled at 45^0 in the opposite direction, was then used to project the light through a 75.6-mm focal length lens, and focused onto the output coupler (OC).

3.3.1 Ytterbium-doped fiber

Two different fibers were used during phase I of the experiment. The first fiber used was a Nufern ytterbium-doped, large mode area (LMA), double clad fiber that was polarization maintaining (PM) at a length of 8.7 ± 0.1 m. The surface area of the PANDA-style fiber is pictured in figure 3.3 (a) [46]. The core diameter was $20 \mu\text{m}$ and cladding diameter was $400 \mu\text{m}$. Core and cladding numerical apertures were 0.06 and 0.46, respectively, with a cladding absorption of 1.7 dB/m at 975 nm [47]. An OFS Yb-cladding pumped fiber was the second fiber used in the experiment, and subsequently, the primary fiber utilized for the data presented in this paper. At a length of 4.9 ± 0.1 m, the core and cladding diameters were $20 \mu\text{m}$ and $200 \mu\text{m}$ with numerical apertures of 0.12 and 0.45, respectively, and a cladding absorption of 0.15 dB/m [48]. The surface area of this fiber is also presented in figure 3.3 (b) [48].

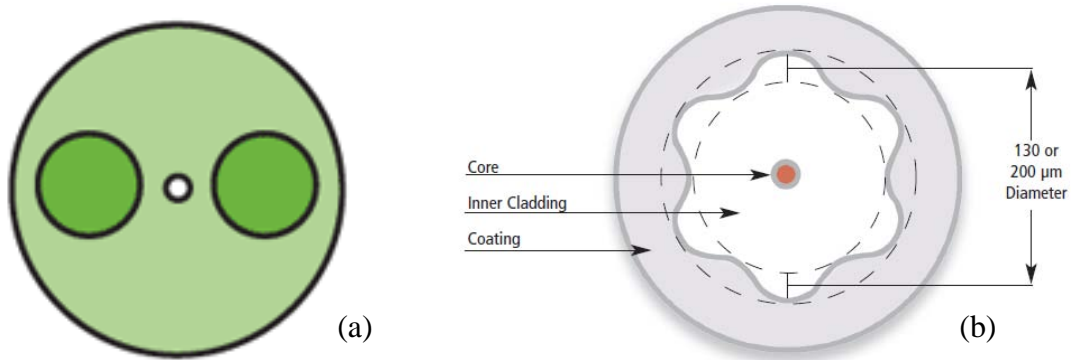


Figure 3.3. Diagrams of the surface areas for the Yb-doped fibers used in the experiment. Figure 3.3 (a) is the Nufern PM fiber and 3.3 (b) is the OFS cladding pumped fiber [46, 48].

3.3.2 Dichroic Mirrors in the Cavity Design

The HR coating for the dichroic mirrors used in the cavity design were optimized for reflection of 1064 nm light when angled at 45° . While this led to some internal losses within the cavity, there were several advantages in the use and placement of these dichroic mirrors. The first mirror placed between the diode pump and the fiber served as a buffer between the pump and the rest of the laser cavity by transmitting the pump light at 975 nm and reflecting the 1064 nm light. The second dichroic mirror, placed at the opposite end of the fiber to the pump, served to filter out the pump light that was not absorbed by the fiber, and to ease the process of aligning the beam in the cavity. Additionally, due to the fractional loss of the dichroic mirror, the light transmitting through the mirror could be detected at both the pump and laser wavelengths, allowing spectral measurements of the output beam to be collected simultaneously with the output power of the laser on opposite ends of the cavity. The third dichroic mirror also generated a fractional loss within the cavity, but no more than 0.5% of the total laser output power. The primary purpose for inserting the third mirror into the cavity was to better facilitate beam alignment.

3.3.3 Beam Alignment in the Cavity

Aligning the beam was performed by placing a chopper wheel in the cavity connected to a lock-in amplifier and a power meter next to the output coupler outside the cavity. Two apertures were placed at opposite ends of the cavity to facilitate visual alignment of the beam reflected off the end mirrors. However, the lock-in amplifier (Stanford Research Systems SR 850 DSP) proved valuable in coupling both the pump

light and reflected light into the fiber on both ends, which were mounted on devices with five position knobs. Once the beam was aligned and a laser output was detected, the chopper wheel was removed from the cavity, and further optimization of the cavity was performed by adjusting the tilt of the end mirror, output coupler, and the focal distances between the fiber ends and the microscope objectives. Translation stages that adjusted the distance between a focusing lens and the end mirror and output coupler were also used to further optimize the laser output power. Some adjustments to the focus of both the 100 mm and 76.5 mm lenses needed to be made as the input pump power was increased.

3.3.4 Diagnostics with the Output Couplers

For this phase, three different output couplers (OC) were placed in the same cavity position as shown on figure 3.2. These OCs had transmissions of 5%, 50%, and 65% respectively. Testing the different OCs allowed for comparison of the output laser power in relation to the diode pump power. Additionally, the motivation for trying different OCs stemmed from repeated burning of the fiber ends when initially using the 5% OC to measure the output power while increasing the pump power.

3.4 Power and Spectrum Measurements

Two power meters (Thor Labs 10 Watt) were used for direct measurements under 10 Watts of the laser output power, both at the primary output coupler location and at the dichroic mirror where the light exited the fiber from the pump side of the cavity. The power from the diode pump was adjusted at incremental steps, and the subsequent output power was measured. For each of the phases I-IV, the output power dependence on the

pump power was plotted and is presented in chapter IV. The power measurements in the cw regime were useful as they provided a baseline for comparison of the inherent power losses that occurred in the Q-switched and mode locked operations.

3.4.1 Diode Pump Temperature Optimization

The chiller temperature for the diode pump affected both the pump power and the laser output power. Figure 3.4 demonstrates this effect as the temperature control was initially set at 25°C at pump power input of $4.78 \text{ W} \pm 10 \text{ mW}$. The temperature was adjusted in one degree increments spanning between 21°C to 29°C, and the end mirrors were adjusted to maximize the laser output. A parabolic trend of the output as it depends on the temperature showed that the optimum pump setting ranged between 23°C to 26°C. For the results presented in chapter IV, the temperature setting of the diode was constant at 25°C.

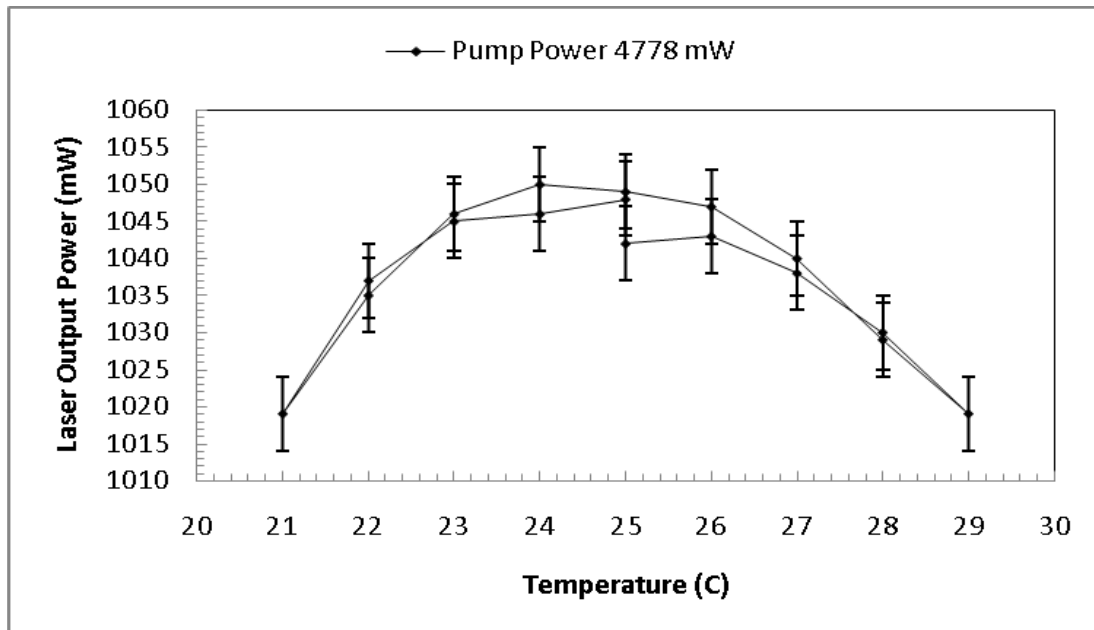


Figure 3.4. Optimization of the temperature setting for the chiller of the diode pump. The vertical axis shows the parabolic fluctuation of the laser output power as the chiller temperature is changed.

3.4.2 Spectrum Characteristics

A spectrum of the output laser beam was measured using an AQ6315A optical spectrum analyzer for the cw, Q-switching, and mode locked regimes in each phase of the experiments at varying laser output power, and for varying pulse profiles. This was performed in order to evaluate the tunability of the laser output, and to draw comparisons between the peak output wavelengths in relation to the different cavity setups. The output beam from the laser was focused into the detector, and a scan of the beam was performed between 900 nm and 1200 nm, with settings at 1 nm resolution and two averages of the sweeps in order to reduce noise in the signal. The spectral profiles collected are presented in chapter IV section 4.2.2.

3.5 Phase II – Passive Q-Switched Operation with Cr⁴⁺:YAG Crystal

Passive Q-switched operation utilized the same cavity design as in the cw operation. The slight modification is that the Cr⁴⁺:YAG crystal was inserted into the cavity close to the output coupler. This setup was similar to the experimental setup demonstrated by J.Y. Huang [45], with some modifications made because the cavity designs are somewhat different. The setup for passive Q-switching is shown in figure 3.5. For passive Q-switching, the Cr⁴⁺:YAG crystal is 4x10 mm² at the cross section perpendicular to the beam and 1 mm thick, and has approximately 92% transmittance in the range of 1064 nm. The crystal was wrapped in indium foil, and mounted without active cooling. Placement of the crystal was chosen to be near the output coupler in order to minimize the beam volume inside the crystal, and to achieve a lower Q-switching threshold, as explained in the theory section of chapter II. Additionally, the mount for the

Cr^{4+} :YAG crystal allowed for adjustment both parallel and perpendicular to the beam to help stabilize pulsing as the pump power was increased.

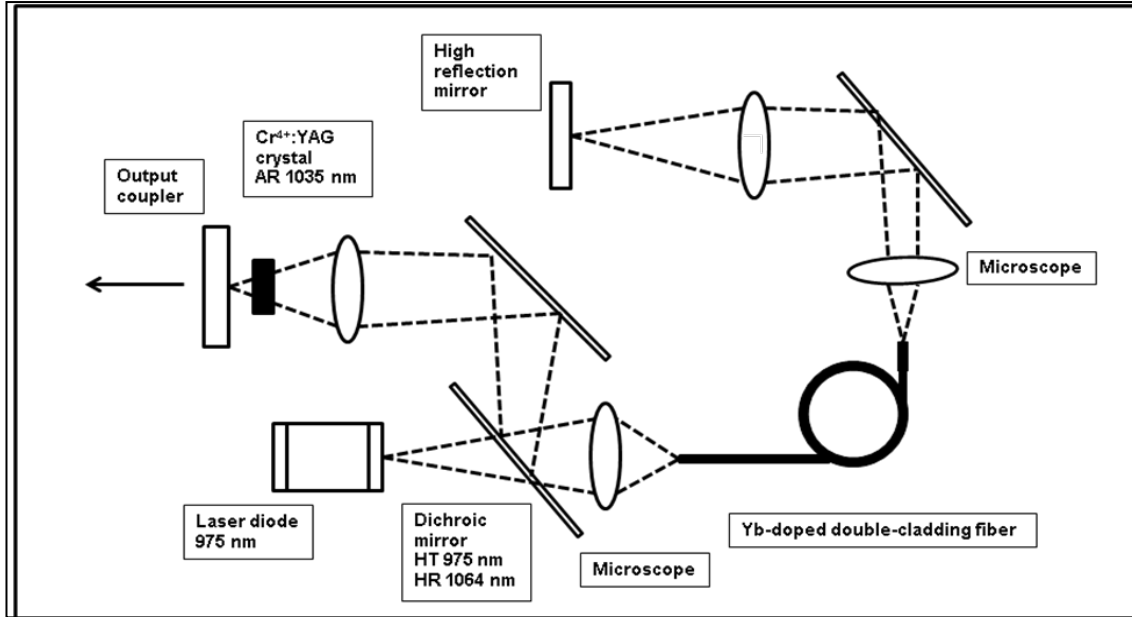


Figure 3.5. Passive Q-switched design concept with insertion of Cr^{4+} :YAG crystal into the cavity.

3.5.1 Q-switch Pulse Measurements

Passive Q-switched pulses were detected and measured using a LeCroy 1GHz oscilloscope connected to a Thor DET 10A high speed silicon detector with spectral range spanning near infrared up to 1100 nm connected to a DC 50 Ω resistive power divider. The primary output beam was focused onto the silicon detector and the signal on the oscilloscope was analyzed. Because the silicon detector had a damage threshold of 100 mW/cm², the beam was passed through an optical density filter in order to reduce the power of the beam's spot size incident on the detector. The Cr^{4+} :YAG crystal was

adjusted inside the cavity such that a periodic and stable Q-switched waveform was apparent.

Measurements of the signal included the FWHM of the pulse width and the period between the pulses. The inverse of the period was calculated as the pulse repetition rate at a particular power setting. The input pump power was then increased, and the same measurements were repeated. The results of the pulse characteristics in relation to pump power are presented in chapter IV, section 4.3.

3.6 Phase III – Passive Mode Locked Operation with a Saturable Absorber Mirror

A few modifications were made to the cavity, as presented in the figure 3.6. For one, the output coupler used was the 50% beam splitter, which was placed on the end mirror position opposite the pump side of the cavity. Second, the SAM (BATOP 1064 nm) was positioned at the end mirror where the output coupler had been for the experiment in phase I. The reason for doing this was because the light was better focused onto the SAM using the 76.5 mm lens as opposed to the 100 mm lens on the other side of the cavity. Attempts to align the laser were much easier with this setup, even though it altered the baseline controls presented in phase I. Additionally, only the 50% beam splitter was used as the output coupler. Attempts were unsuccessful in getting the laser to operate with the 65% transmission OC. That does not mean this was not possible to achieve, it just means this was not achieved in the attempts for this experiment. The 5% transmission was not used during this phase because of the poor performance observed in cw operation. This included both a low power output, and increased risk of burning the fiber as the power was increased.

The design in figure 3.6 demonstrates passive mode locking attempts without the compensation of GVD using a grating pair. Measurements of the power output as the pump power was increased are presented in the next chapter. Similar to phase II, the output beam was focused into the high speed silicon detector and the wave form was studied as the laser cavity was tweaked. The power output, spectrum, and waveforms are presented in chapter IV.

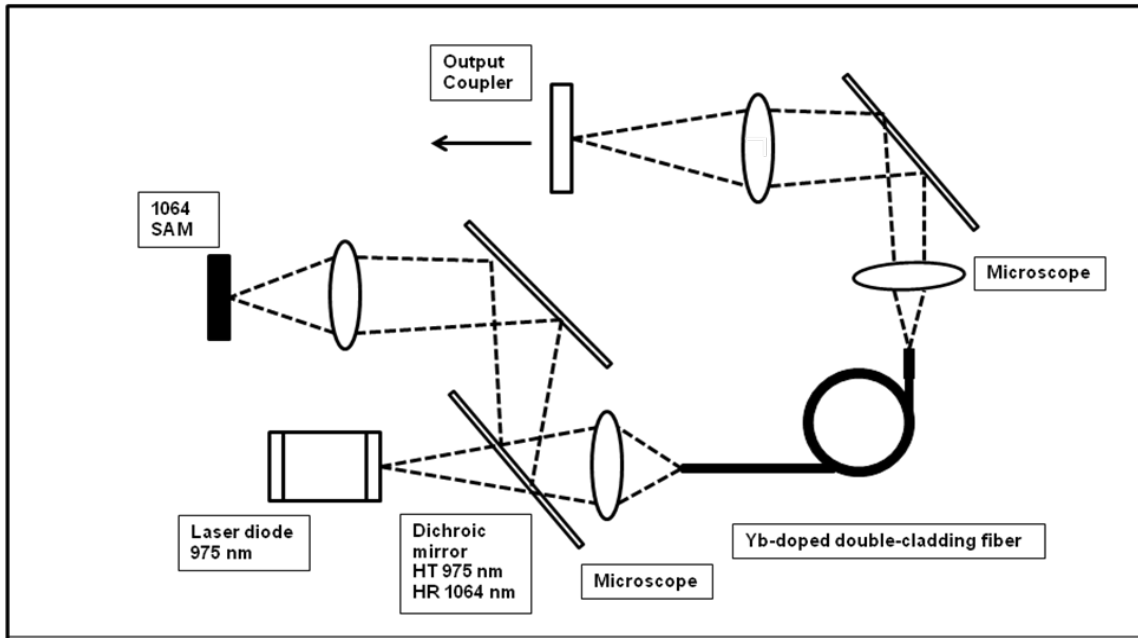


Figure 3.6. Passive mode locking operation using a 1064 saturable absorber mirror.

3.6.1 Measurement of Mode Locked Short Pulses

Mode locking was not achieved using the SAM during this phase of the experiment. A periodic signal was present, such as mode beating, and was observed on the oscilloscope used, but a mode locked profile wasn't realized. Typically, an oscilloscope would be considered too slow to measure the mode locked pulses in the low picoseconds to femtosecond range. Characterization of these pulses would require the use of an autocorrelator. Therefore, the oscilloscope was used to look for mode locking,

but because mode locking didn't occur, an autocorrelator was not used to characterize the short pulses.

3.7 Phase IV – Passive Mode Locking with Nonlinear Polarization Rotation

As presented in section 2.5.2, the second method for achieving passive mode locking was performed through nonlinear polarization rotation. The cavity was similar to the designs presented in phases I-III, but again, with some modifications. Additionally, this design is somewhat similar to the cavity designed by L. Leforte in 2002 [49], with the exception that grating pairs were omitted from the design. Figure 3.7 presents the NPR concept for this experiment. On the cavity end opposite the pump, a lens with focal length of 88.5 mm focused the beam that had propagated through the fiber onto the BATOP 1064 SAM. On the side of the cavity closest to the pump, the light passed through a quarter-wave plate (QWP), a half-wave plate (HWP), then through a polarized beam splitter (PBS) that could be tilted along the x, y, and z axis. As the beam was split on the first pass, part of the beam became the laser output. The part of the beam still in the cavity was then reflected off a HR mirror angled at 45^0 , passed through an optical isolator (OFR IO YAG), and then finally passed through another quarter-wave plate before being focused by a 76.5 mm lens onto another saturable absorber mirror (Del Mar 1040 nm). The purpose for incorporating the SAMs in the cavity was in order to self-start mode locking, and was shown to be successful in Leforte's experiment [49].

As the light reflected off the second SAM passed back through the cavity, a second laser output was emitted at the opposite side of the polarized beam splitter. The second output beam was focused into the high speed silicon detector and analyzed using

the oscilloscope, particularly for changes in the waveform as the polarization plates were rotated.

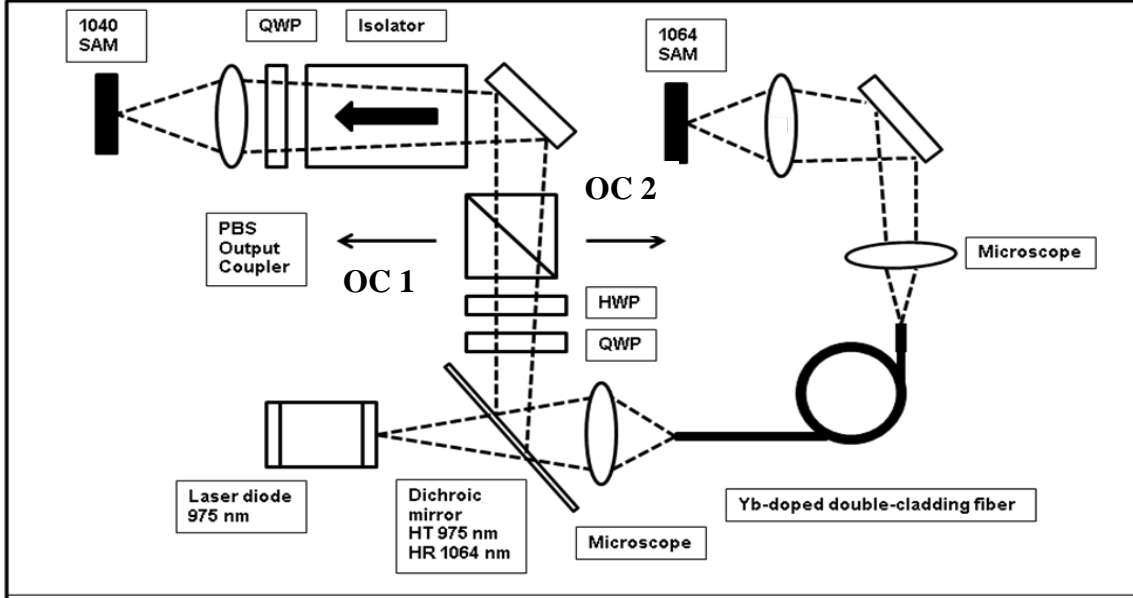


Figure 3.7. Passive mode locking and Q-switching operation using nonlinear polarization rotation. (QWP) Quarter wave plate, (HWP) half wave plate, (OC 1 & 2) are the sides of the (PBS) polarized beam splitter that output power was measured.

3.7.1 Polarization State of the Beam through the Cavity

As discussed in section 2.5.2, the purpose for the polarization controls was to initiate mode locking by isolating the time-dependent intensity, which is strongest in the center where $t=0$. Since the fiber used during this phase was not polarization maintaining, polarization of the beam propagating through the fiber can be attributed to birefringence and the bending of the fiber, as well as random exchanges of power between two polarization components traversing the fiber [27].

Regardless whether the polarization is elliptically polarized or linearly polarized, the purpose of the quarter and half wave plate sequence is to convert the beam to a linearly polarized state, then to rotate it by 45° through the isolator, and then to further

control the polarization of the beam with the quarter wave plate, where it becomes circularly polarized and can pass back through the isolator before passing through the output coupler. This was the intent in order to isolate the central intense part of the beam and then to induce mode locked pulses.

3.8 Summary

This chapter explained the methodology of the experiment setup. The experiment was divided into four phases. The first phase was a cavity design for continuous wave operation. During this phase, primary data collected were power and spectral measurements, while also comparing two types of ytterbium-doped fibers and three different output couplers with the objective of comparing the fiber laser's performance. In phase II, a Cr^{4+} :YAG crystal was placed inside the laser cavity. Data for this phase also included power and spectral measurements, along with pulse characteristics, such as pulse width and repetition rate. The objective of phase III was to passively mode lock the fiber laser using a saturable absorber mirror. The same types of measurements carried out in phase II were performed in phase III with the intent of comparing the passive Q-switched pulses with the passive mode locked pulses. Phase IV involved modifying the cavity design such that a technique known as nonlinear polarization rotation would generate passive short pulses, as well as Q-switched pulses. The power, spectrum and pulse characteristics were measured. In addition, the rotation angles of the polarization wave plates were documented in order to establish the regions of cw, mode locked and Q-switch operation. Table 3.1 further breaks down the methodology and objectives

presented in this chapter in terms of the experiment phase, laser operation, features of the cavity design, and experimental objectives.

Table 3.1. Summary of methodology, experiment features, and research objectives.

Phase	I	II	III	IV
Function	Continuous Wave (CW)	Passive Q-Switch (PQS)	Passive Mode Lock (PML)	Nonlinear Polarization Rotation (PML/PQS)
Feature	Compare Fiber	Cr ⁴⁺ :YAG	1064 nm SAM	Wave Plates
	Compare Output Couplers			Polarized Beam Splitter as Output Coupler
Data	Power			
	Spectrum			
		Pulse Shape Characteristics		
GVD Compensation		Grating (intended, but not accomplished)		
Objectives	Present Results			
	Quantify Advantages and Disadvantages			
	Propose future research objectives			

IV. Analysis and Results

4.1 Chapter Overview

This chapter presents the results of the four laser designs described in the methodology section of chapter III. For continuous wave operation (section 4.2), results of the output power are shown in comparison to the two fibers used, and the 95%, 50%, 35% reflectance output couplers. The spectrum for one of the designs is graphically presented as constant with respect to input power and diode pump chiller temperature. The spectrum for the other designs is summarized for the other designs.

Due to the higher output powers and efficiencies observed with the OFS fiber (NA=0.12) in conjunction with the 50% and 35% reflectance OC's, these elements were used in the diagnostics performed in phases II-IV. In phase II, where the Cr⁴⁺:YAG was inserted into the cavity, results of the output power, pulse width, and repetition rate are presented in section 4.3 with analysis on why the pulses were measured larger than was expected. Phase III (section 4.4) shows the resulting waveforms collected while attempting to passively mode lock the laser using the SESAM. However, since mode locking was not achieved in this phase, more focus is given to analysis on why this was not achieved. Section 4.5 presents the results from phase IV. Power measurements were taken as the polarization wave plates were rotated, demonstrating increased control of the output power for a constant input power. Oscilloscope data of the output indicate mode locking was possibly achieved. Q-switching was also observed. To further the analysis of these results, a Fast Fourier transform (FFT) was performed on the signals, which were collected for both phases III and IV.

4.2 Continuous Wave Operation

4.2.1 Output Power

With regards to continuous wave operation, and the setup according to figure 3.2, the output power of the laser was measured as the input power was increased at 1.0 Amp increments. The calibration presented in figure 3.1 was used to determine the corresponding diode pump input power. The results of the increased output power as the pump power increased is shown in figure 4.1. For this particular setup, two different Yb-doped fibers were used while the 50% output coupler remained the constant in both cavity designs. The length of the Nufern PM fiber (NA=0.06 for the core and NA=0.46 for the cladding) was 8.7 m +/- 5 cm. The cavity length outside the fiber was 84.1 cm, for the cladding) was 8.7 m +/- 5 cm. The cavity length outside the fiber was 84.1 cm,

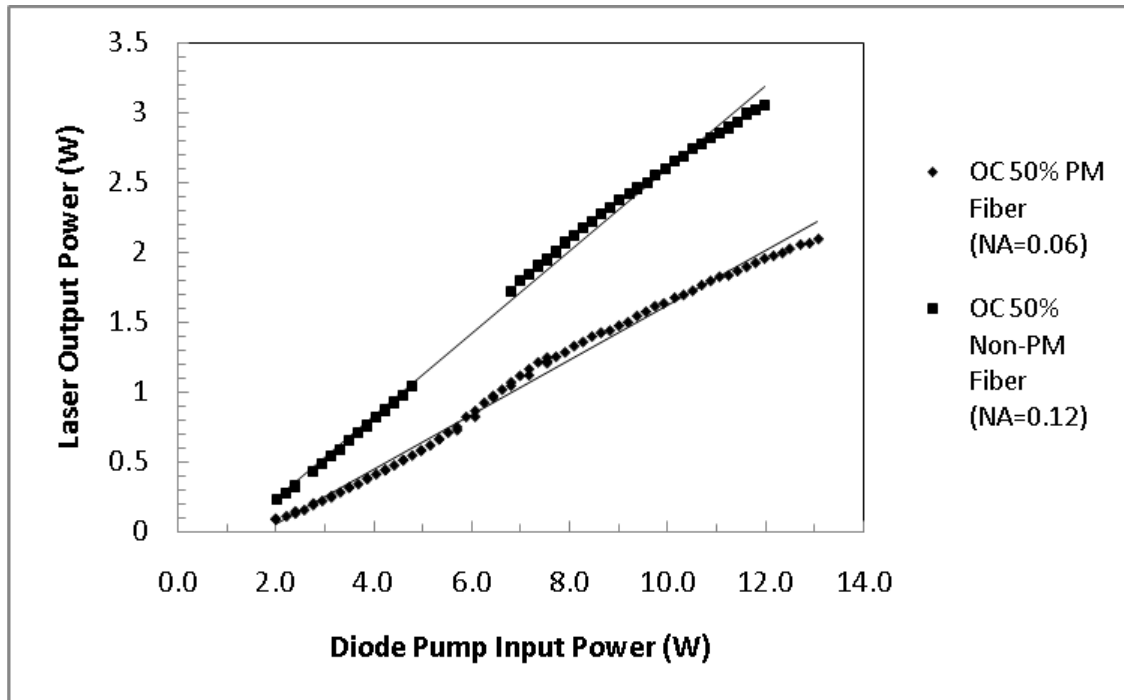


Figure 4.1. Continuous wave operation showing the output power of the laser when comparing two fibers of different length and numerical apertures using a 50% output coupler. The gap for the Non-PM data was due to measurements collected on separate days, where a linear relationship was assumed.

yielding a total cavity length of 9.5 m +/- 0.1 m. The length of the OFS non-PM fiber (NA=0.12 for the core and NA=0.45 for the cladding) was 4.9 m +/- 5 cm and total cavity length was 5.8 m +/- 0.1 m. The discrepancy of 8 cm for the air cavity length in the design when comparing the two fibers was a result of aligning the laser during each setup, and using translation stages to optimally focus the beam at various points in the cavity.

Based on the similarities of the design for the results in figure 4.1, the discrepancies between the power outputs can be described by the fiber length and numerical aperture of the fiber core, as was previously explained in section 2.3. The higher NA of the non-PM fiber allowed more of the pump light into the cladding, and subsequently more pump light to be absorbed in the core.

Figure 4.2 shows the efficiencies of the output power as a ratio of the diode pump input power.

$$Efficiency(\%) = \frac{Output\ Power}{Input\ Power} \times 100 \quad (4.2.1.1)$$

The significance of figure 4.2 is that it shows the efficiency of the laser increasing with increased pump power to a certain point, then leveling off, and finally rolling off. Subsequent figures in this section of the slope efficiency show this same trend. This is because the gain and population inversion of the medium become clamped at threshold values; the rolling off of the efficiency curve indicates saturation effects. At increased pump powers approaching 12-13 Watts, precise output power measurements became increasingly more tedious to acquire. Thus, the roll off and saturation effects observed in figure 4.2 are at the beginning stages, but would likely continue to roll off at increased

pump powers. Self focusing of the beam at increased pump powers was mostly mitigated by adjusting the distances between lenses and mirrors in order to optimize the output power, however, nonlinear processes such as Raman and Brillouin scattering and self phase modulation have not been explored in this analysis of the data to further explain the efficiencies achieved.

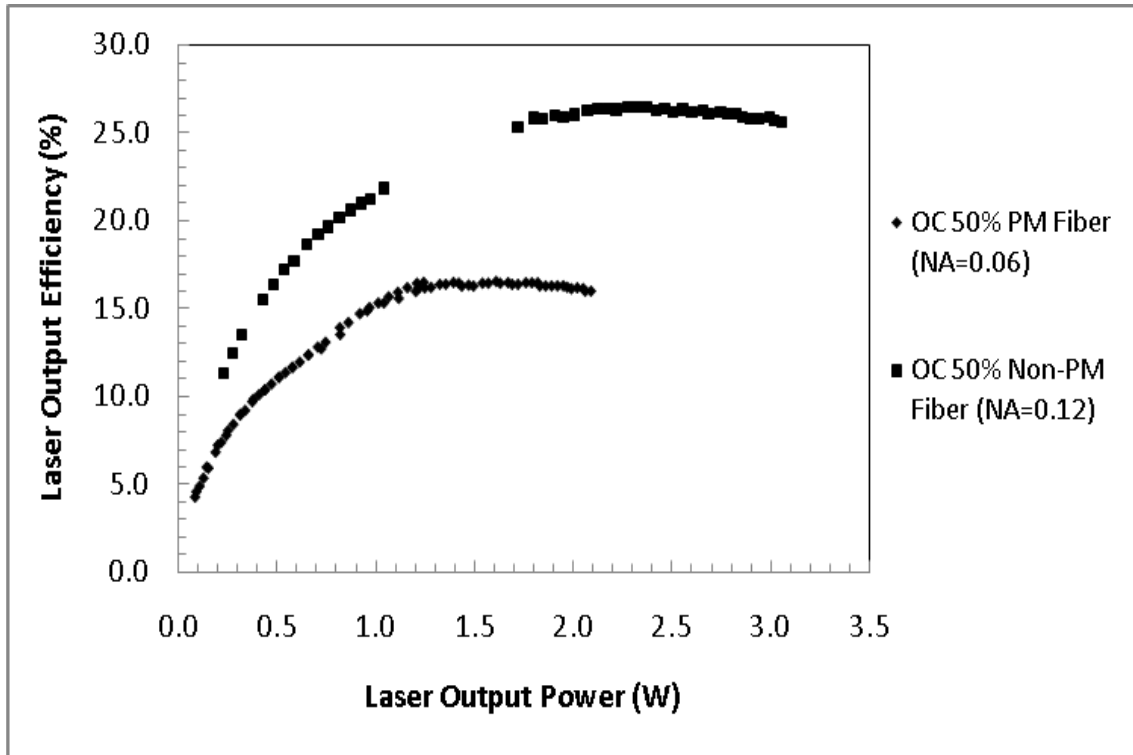


Figure 4.2. Laser output efficiencies when comparing the laser output to input pump power for two different fibers and a 50% output coupler. The gap for the Non-PM data was due to measurements collected on separate days, where a linear relationship was assumed.

As was also mentioned in section 3.3.2 for the setup design, there was a dichroic mirror on each side of the fiber in which some of the laser output power could also be measured. This was done in order to allow for simultaneous measurements of the

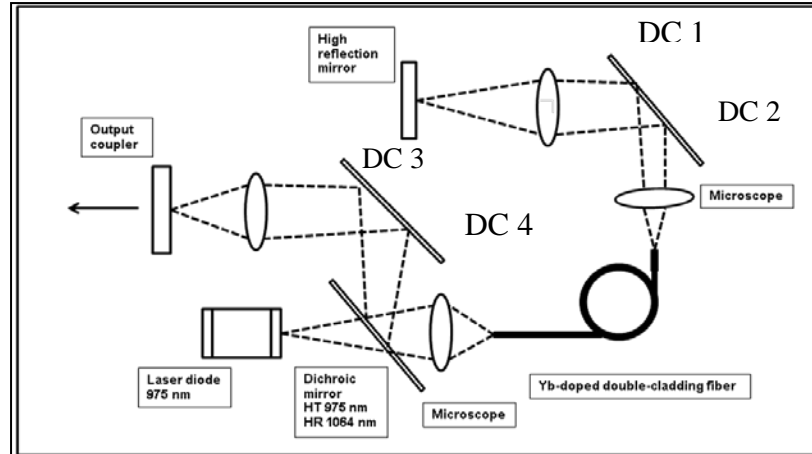


Figure 4.3. Diagram from figure 3.1 showing locations of output power from dichroic mirrors (DC).

spectrum, as well as to isolate the laser light from the pump light within the cavity. Power meters were setup at these locations, as depicted in figure 4.3, and the output power from the dichroic mirrors was measured simultaneously with the output power from the output coupler. Figure 4.4 depicts these power measurements when using the PM fiber and 50% output coupler. The output power is plotted on a logarithmic scale in order to better resolve the data in comparison to the power measured at the output coupler.

The power measurements of the dichroic mirrors are small compared to the output power measured at the 50% OC. However the most significant output measured was at DC 1. This is where the light is first emitted from the opposite side of the fiber and reflects off the dichroic mirror. Most of this light that propagates through the mirror is pump light at 971 nm as the laser light is reflected inside the cavity. However, by symmetry, DC 2 indicates the amount of laser light that does propagate through the mirror, and represents a cavity loss of less than 1% of the output power measured at the

output coupler. In addition, DC 3 and DC 4 have nearly equivalent power readings, with DC 4 slightly less due to an additional reflection off the output coupler before propagating through the mirror. The losses at DC 3 and DC 4 account for less than 0.01% of the total power loss in comparison to the power measured at the output coupler.

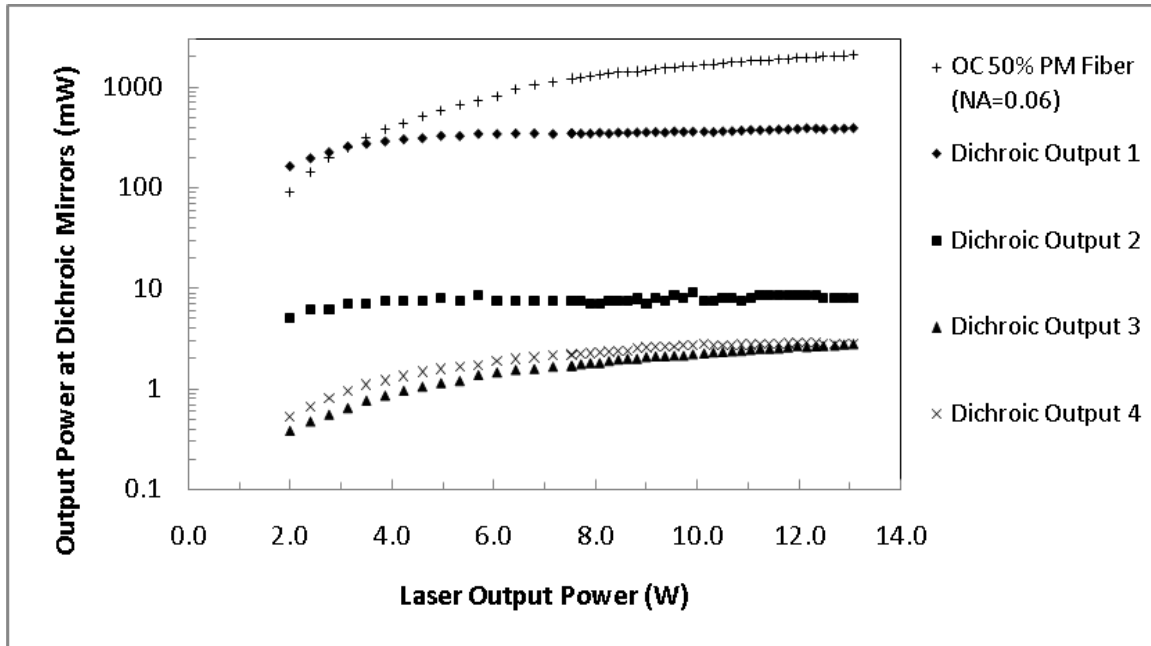


Figure 4.4. Power measurements taken at the dichroic mirrors of the laser cavity shown in figure 4.3. The logarithmic scale of the power measured show cavity losses due these mirrors is less than 1% of the output, where output at DC1 is primarily pump light.

Since the non-PM fiber with higher NA was a better choice for this experiment, a comparison of the output power in relation to output couplers of different transmittances was also performed. Figure 4.5 shows the output power measured when using OCs of 65%, 50% and 5% transmittance, where the placement of the OC is shown in figures 3.2 and 4.3. The corresponding efficiencies, computed from equation (4.2.1.1) are shown in figure 4.6. The output power was highest for the OC at 65% transmittance, followed by the 50% OC. Using the 65% OC, an output power of $5.0 \text{ W} \pm 10 \text{ mW}$ was achieved at an input pump power of $8.3 \text{ W} \pm 10 \text{ mW}$, yielding a slope efficiency of 60%. For the 50%

OC, $3.05 \text{ W} \pm 10 \text{ mW}$ of power was measured at a pump input of $11.9 \text{ W} \pm 10 \text{ mW}$, for an efficiency of 26%. Power measurements using the 5% transmittance OC are also presented, however the number of data points are limited because the fiber was burned repeatedly due to overloading the power in the cavity while using this output coupler.

It can be observed in figures 4.1, 4.2, 4.4, and 4.5 that there is a gap in the data for the Non-PM fiber using a 50% output coupler. This occurred because the data was taken on separate days, and no data was taken where the gap exists. Attempts were made in this experiment to maintain a certain schedule devoted to cw, Q-switching, and mode locking, and by making the assumption that the output power increases linearly with the input power, no attempt was made to collect data to fill this gap.

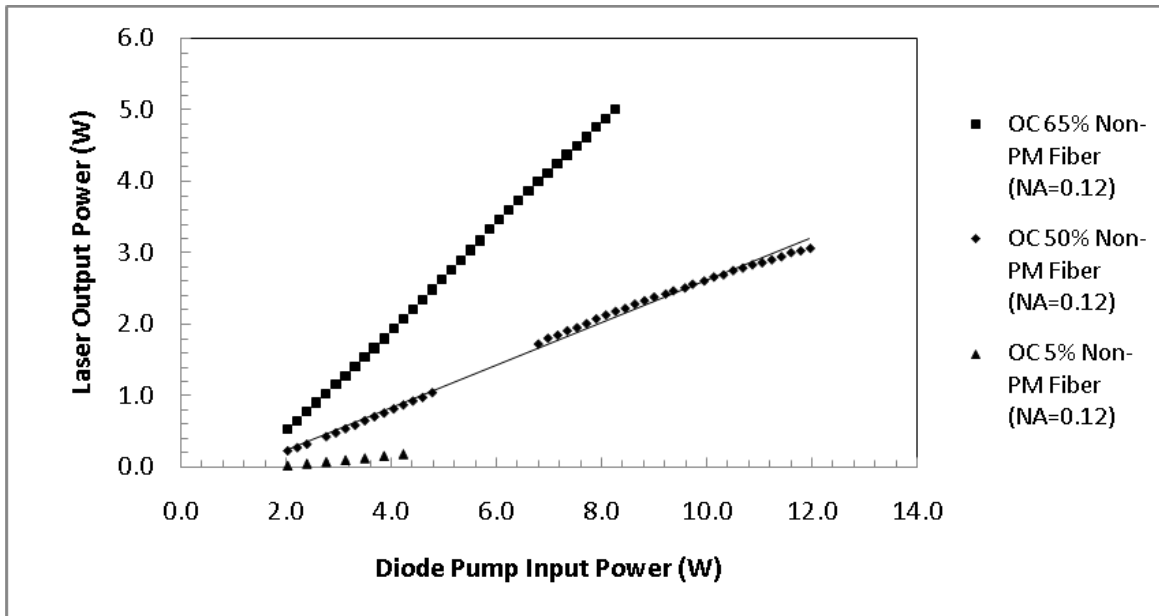


Figure 4.5. Output power of the cavity using different output couplers for the non-PM fiber with $\text{NA}=0.12$. The gap for the Non-PM data was due to measurements collected on separate days, where a linear relationship was assumed.

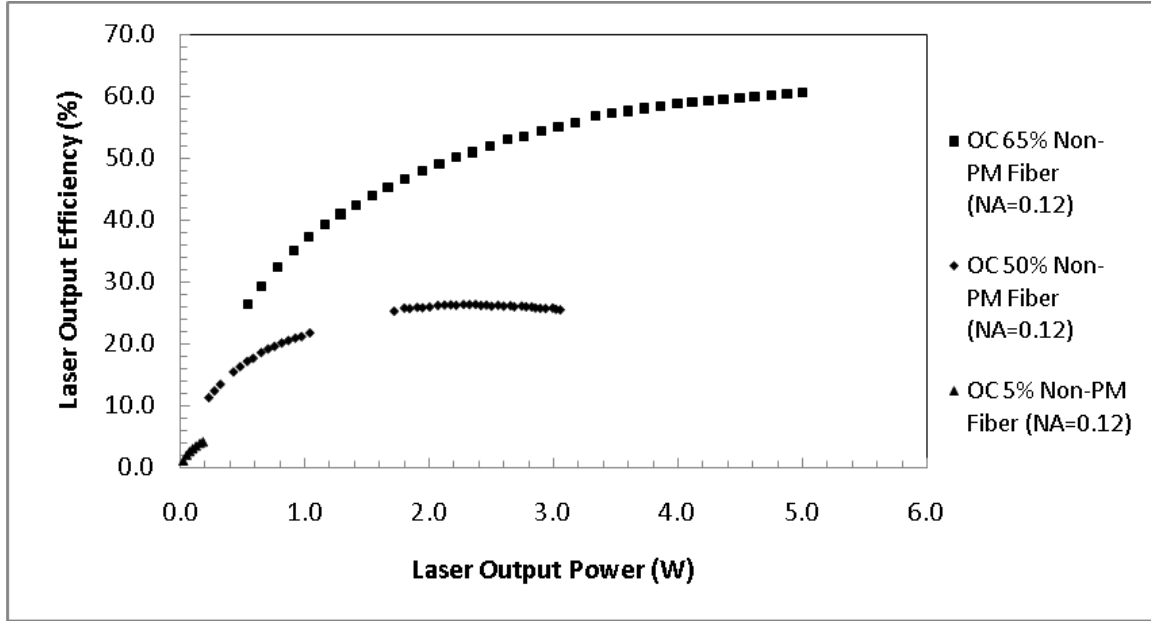


Figure 4.6. Efficiency of the output power when comparing different output couplers.

The power measurements collected using the different output couplers were done in order to identify an ideal output coupler for the cavity. In order to further explore this, both the 50% and 65% OC's were placed at opposite ends of the cavity, in which a laser output power for each OC was measured. This acted as a single OC with a reflectance of 17.5%. Only a few data points of the power were collected for this setup, and they are presented in figure 4.7 as part of a crude rigrod analysis for optimizing the output coupling of the laser.

It can be seen in figure 4.7 that the output power becomes optimal for output coupling reflectance between 15% to 35%, or rather transmittances between 65% to 85%. This trend is somewhat consistent with theory for optimum coupling of high gain and high loss where the net integrated gain is approximated by [31],

$$Net\ Integrated\ Gain = \frac{T_2}{1-T_2} + Ln \frac{1}{1-T_2} = L_g (\gamma_o - \alpha_{int}) \quad (4.2.1.2)$$

where T_2 is the transmittance of the output coupler, L_g is the length of the gain medium, γ_0 is small-signal gain and α_{int} represents the internal losses of the cavity. When the transmittance is less than 1.0 and with the length of the gain medium as a known quantity, the difference between γ_0 and a constant α_{int} will increase logarithmically with the transmittance.

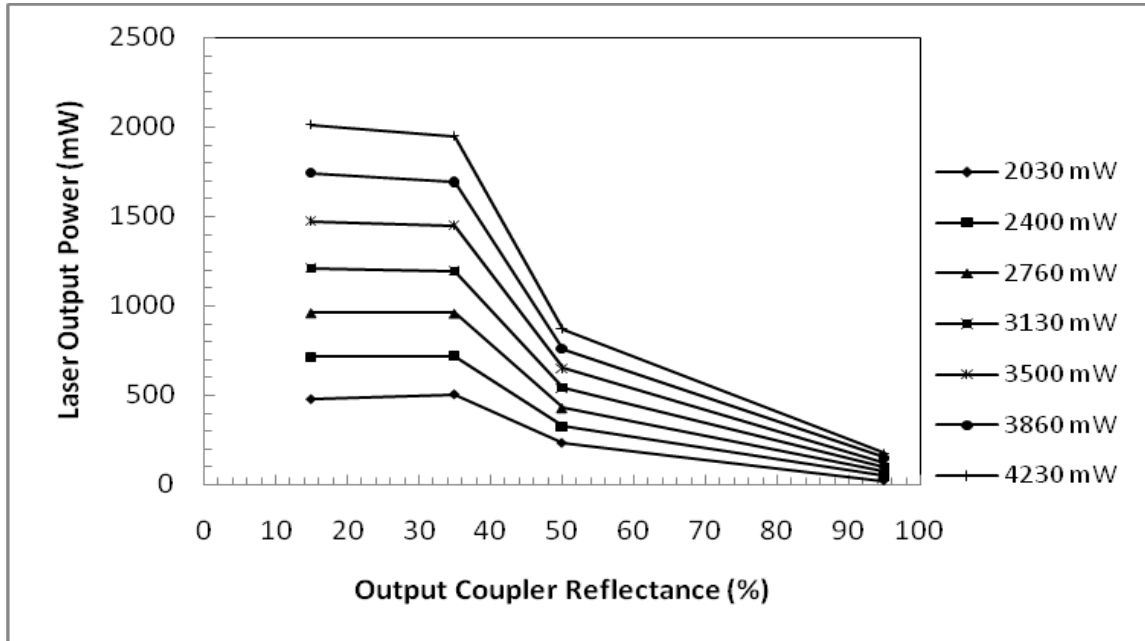


Figure 4.7. Laser output power in relation to reflectance of the output coupler used. The legend shows the corresponding diode pump input power.

4.2.2 Spectrum Measurements

A spectrum of the output beam was taken for the two fibers and three OCs were tested. The results are presented in Table 4.1. The cavity designs presented in chapter III did not incorporate many mechanisms for tuning the laser other than adjusting the end mirrors, OCs, and microscope to fiber coupling distance. These adjustments did not have a noticeable effect on the spectrum. For this reason, the spectrum for a particular design

remained mostly constant with increased power, and also when varying the diode pump chiller temperature.

Table 4.1. Results of spectrum measurements in relation to the fiber and output coupler.

Fiber	Output Coupler	Wavelength (nm)
PM (8.7 m)	50%	1098-1108
Non-PM (4.9 m)	50%	1091-1094
Non-PM (4.9 m)	65%	1087-1093

The wavelength ranges presented in Table 4.1 are in the higher end of the tunable range for Yb-doped fibers. This is indicative of a high gain and low loss cavity. The Yb-doped fiber acts as a quasi three-level system, where the Yb^{3+} produces stimulated emission between the $^2F_{5/2}$ and $^2F_{7/2}$ energy levels. The emission wavelengths between the sub-energy levels of $^2F_{5/2}$ and $^2F_{7/2}$ are higher when the threshold gain is low because less pumping is required for the population inversion. Similarly, for laser wavelengths above 1080 nm, this quasi three-level system acts similar to a four level system [50]. This is advantageous in terms laser operation because four-level systems have lower gain thresholds than three-level systems.

Figure 4.8 shows a sample spectrum for the Non-PM fiber (NA=0.12) and 50% OC when the sensor was placed inside the cavity. The resolution of the spectrum when the data was taken was 1.0 nm. The peak in the figure is the pump source at 971 nm. This output compares well with theory of the tuning range of the gain medium. Figure 4.9 shows how the spectrum remains constant for both the central peak of the spectrum,

and the mean peak based on the FWHM to within about 5 nm over multiple spectral measurements as the diode pump power is increased. The data in figure 4.9 also represents the PM fiber with a 50% output coupler. Similar spectral measurements were also taken with respect to the diode pump chiller temperature, and also remained relatively constant. These results are presented in figure 4.10, where the chiller temperature was varied between 19-28° C.

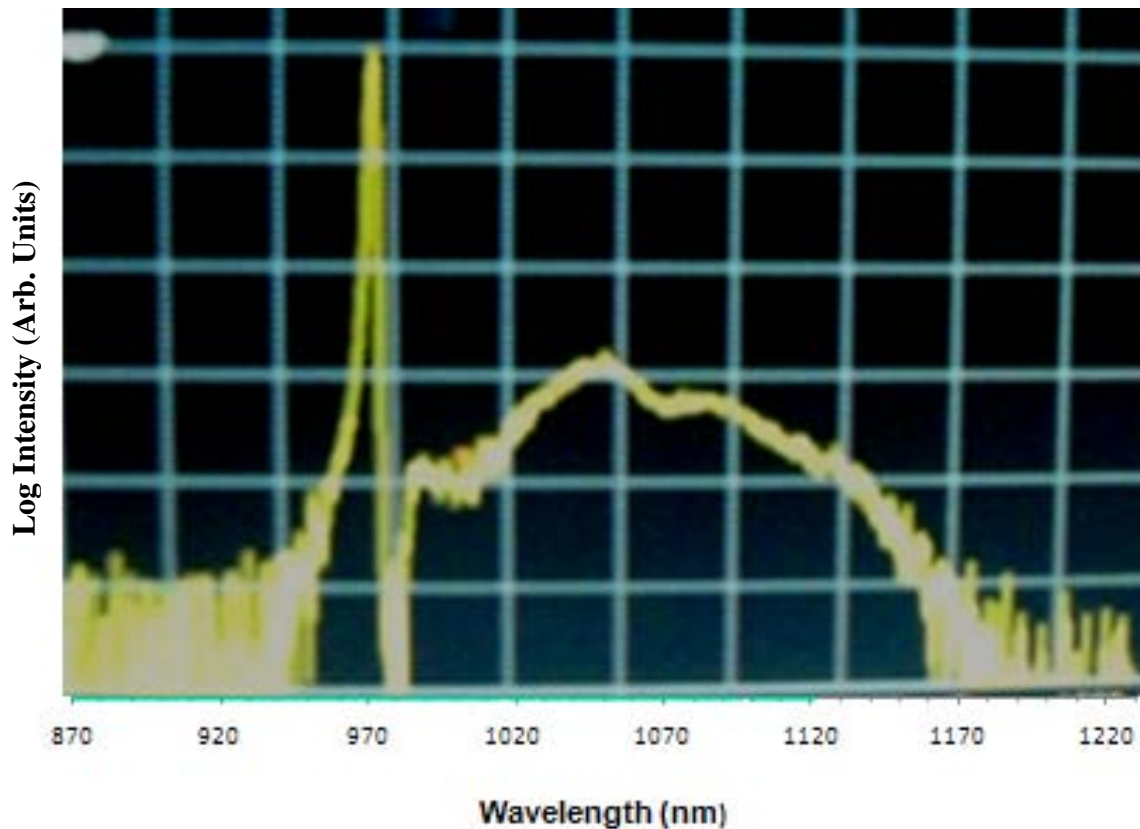


Figure 4.8. Sample spectrum where the sensor was placed inside the cavity as light exited the fiber. The peak is the pump light at 971 nm. Emission observed ranging from 980-1160 nm.

In summary for the spectrum, emission for the laser output beam ranged from 1087-1108 nm where the spectral resolution was about 1 nm. For multiple spectra taken at increased pump power and varying diode chiller temperatures, the peak laser

wavelength remained relatively constant within a 5 nm range. As a quasi-three level system, the wavelength of operation for this laser was more indicative of a four level system.

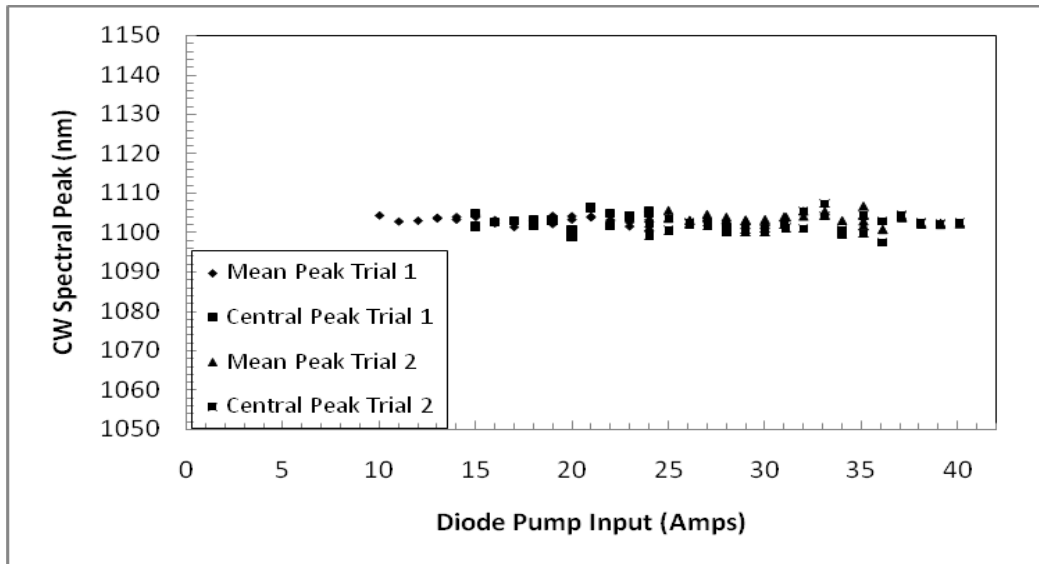


Figure 4.9. Spectrum measured with respect to increased diode pump power.

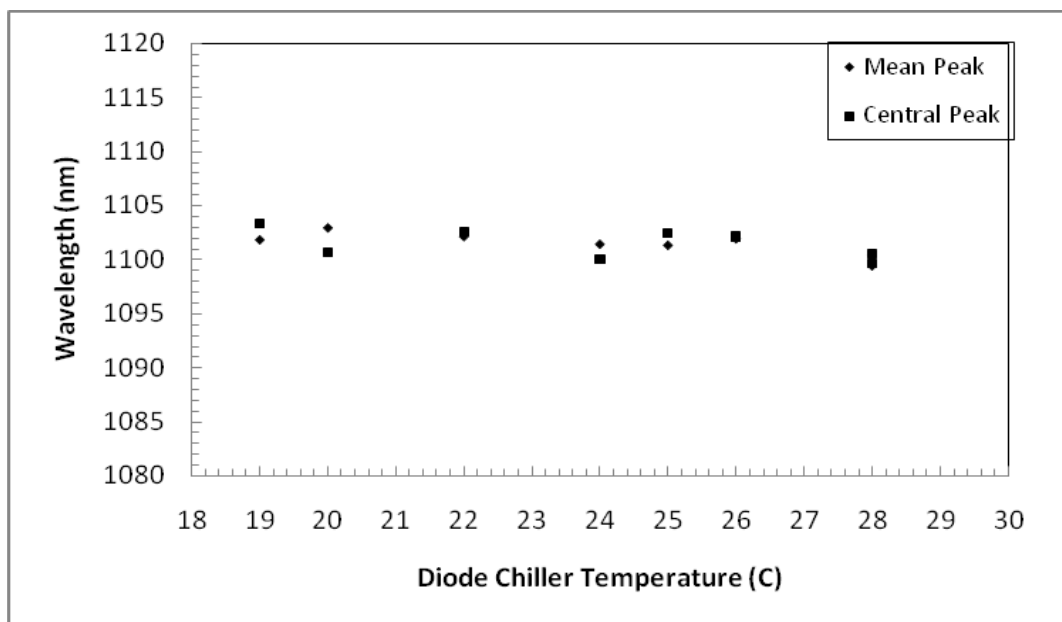


Figure 4.10. Spectrum measured with respect to varying diode pump chiller temperature.

4.3 Q-Switched Operation

As described in section 3.5, passive Q-switching was achieved by inserting a Cr^{4+} :YAG crystal into the cavity as depicted in figure 3.5. For this experiment, both the 50% and 65% transmittance output couplers were used. The output power was measured as the input power was increased in order to compare this power with that of the continuous wave operation. The signal of the pulse was analyzed with an oscilloscope in order to measure the pulse width, pulse separation, and pulse repetition rate.

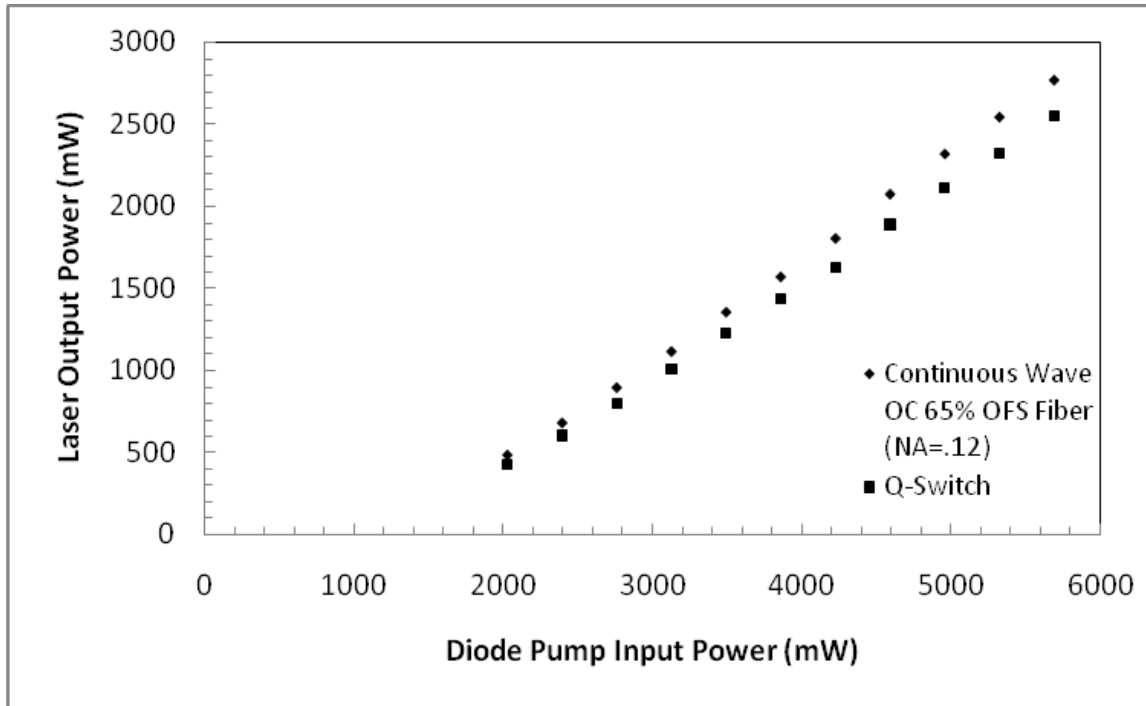


Figure 4.11. Comparison of the output power in Q-switched operation with the output power in cw operation using a 65% transmittance output coupler.

Figure 4.11 shows the output power for Q-switched operation in comparison to continuous wave operation when using the 65% transmittance output coupler. It can be seen from this plot that there is a degradation of the power measured when the Cr^{4+} :YAG crystal was inserted, which is primarily attributed to the 8% loss of the crystal. This loss

is observed in figure 4.12 where two plots are shown. The bottom plot is the efficiency of the laser operating in cw operation, which increases as the pump power is increased. The plot at the top of the graph is the Q-switched power divided by the cw power, which is shown to be constant at about $90\% \pm 2\%$.

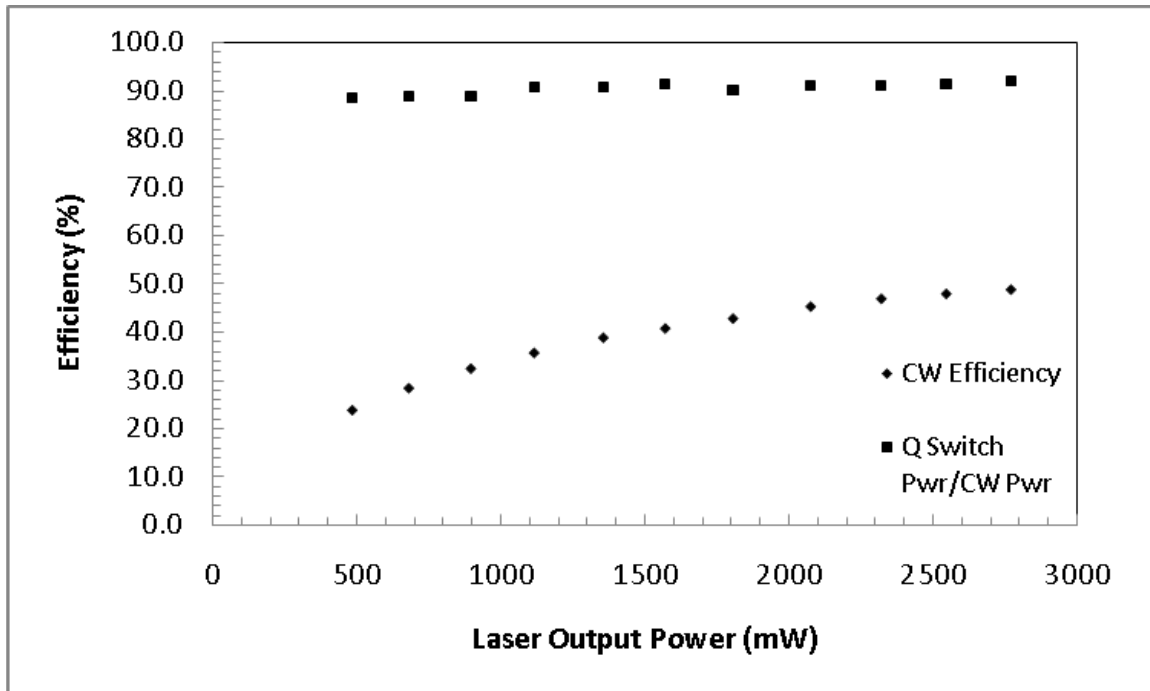


Figure 4.12. Output power efficiency of the Q-switched operation in relation to the cw operation. The efficiency for Q-switched operation was 90% that of cw efficiency.

A sample of the Q-switched signal is shown in figure 4.13. One notable observation during this experiment is that the output observed on the oscilloscope varied significantly in terms of stability. As the Cr^{4+} :YAG crystal was in one position and yielding a stable pulsed signal at a particular pump power, the stability would diminish as the pump power increased. Thus, in order to regain stability, the crystal had to be slightly repositioned within the cavity. Additionally, Q-switched pulse measurement was limited by increased pump power and a critical point where the crystal may have become

bleached by too high a power in the cavity. The requirement for repositioning the Cr^{4+} :YAG crystal at increased pump powers may have been the result of nonlinear effects of the beam inside the cavity, such as self focusing. The cross-section area of the beam can change at increased powers, thereby affecting the absorption of the crystal and the Q-switched output as presented earlier in chapter II with the beam's cross-section area dependence for the equations presented in section 2.4 [27].

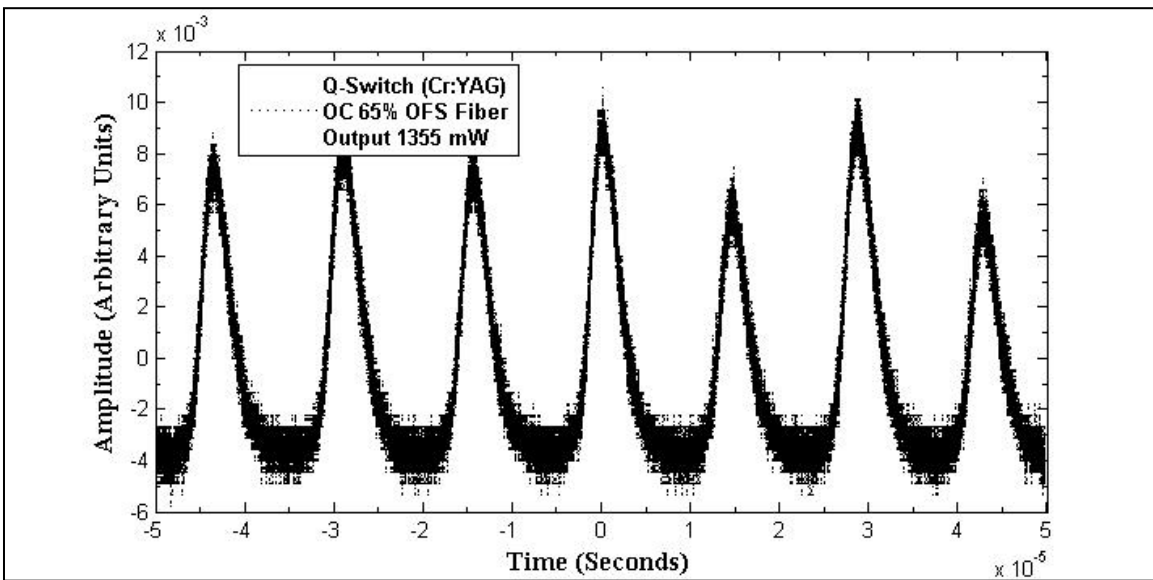


Figure 4.13. Sample wave form for passive Q-switched operation using 65% output coupler and non-PM fiber.

Figure 4.14 and figure 4.15 show the measured pulse width, pulse separation, and subsequent repetition rate. Figure 4.14 shows a pulse width that is increasing slightly with the laser output power. However, there is a degree of uncertainty in concluding the pulse was getting longer with increased pump power because there was significant jitter in the wave forms observed. Uncertainties in the pulse width measurements were approximately $\pm 0.5 \mu\text{s}$. Uncertainty of the period was $\pm 1.0 \mu\text{s}$. From equation (2.4.2.2),

the Q-switched pulse width is proportional to the ratio of the pulse energy over the peak power, and defined as [27],

$$\tau_{pulse} \propto \frac{(Pulse\ Energy)}{(Peak\ Power)} = \tau_0 \frac{(\frac{N_i - N_f}{N_i})}{(N_i / N_{th}) - \ln(N_i / N_{th}) - 1} \quad (4.3.1)$$

where $\tau_0 = 1/\alpha$ is the photon lifetime, discussed earlier in equation (2.4.2.1). N_i , N_f , and N_{th} are the initial, final, and threshold population densities, respectively, that were introduced in equations (2.4.1.5) and (2.4.1.6). When the initial population density is much larger than the threshold population density, then $\tau_{pulse} \approx \tau_0$. Therefore, the inverse relationship between the photon lifetime and the loss α becomes significant when the gain of the cavity is very high.

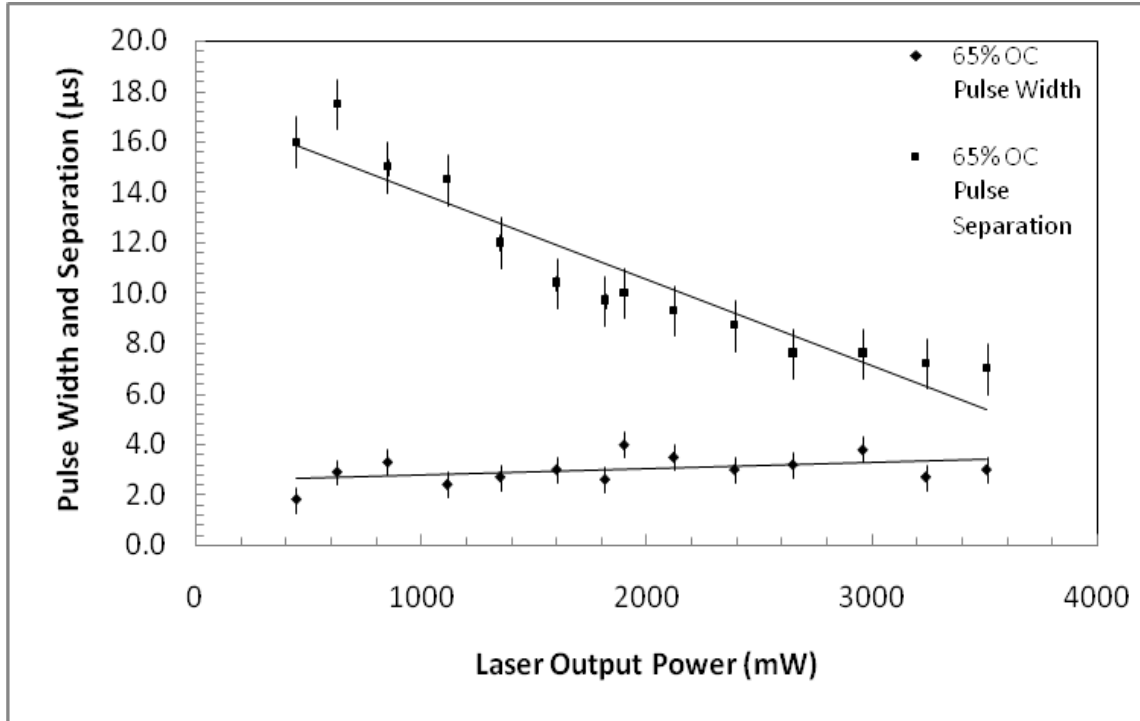


Figure 4.14. Oscilloscope measurements of stabilized Q-switched wave forms for pulse width and pulse separation as diode pump input power was increased.

From figure 4.14, the slight increase in the Q-switched pulse length can be attributed to increased pulse energy, or alternatively, a decrease in the loss within the cavity relative to the increased pump power and gain. The Q-switched pulse lengths were measured at a mean of $2.9 \mu\text{s} \pm 0.5 \mu\text{s}$. This is a rather large length compared to results found in the literature reporting pulse lengths on the order of nanoseconds and picoseconds [1,3,6,8,24,25,26,27,31]. From equation (4.3.1) and the theory presented in section 2.4, the reason the pulse widths measured for this experiment were on the order of μs is because there was not enough loss in the cavity with the Cr^{4+} :YAG crystal. The loss of the crystal was about 8%, and it is likely that if the losses were significantly higher, pulses on the order of nanoseconds or shorter could have been achieved.

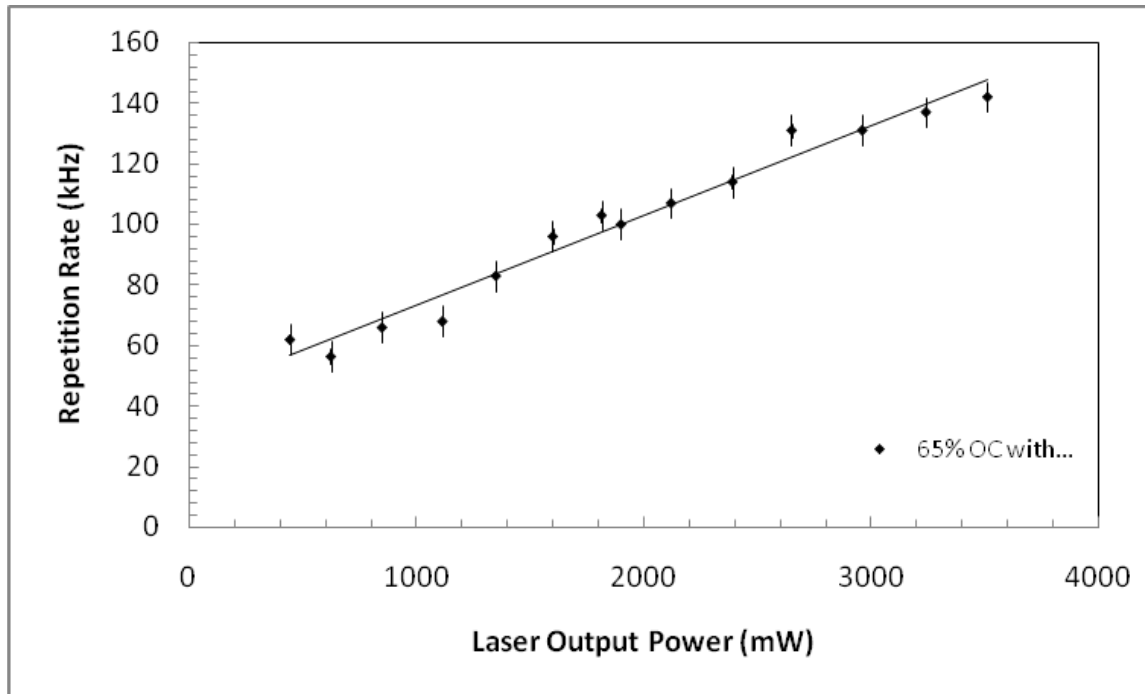


Figure 4.15. Repetition rate for Q-switched pulses calculated as the inverse of the pulse period, and plotted over the laser output power with the Cr^{4+} :YAG crystal in the cavity.

From the pulse separation measurements in figure 4.14, the repetition rates were calculated as the inverse of this pulse separation and presented in figure 4.15. While the increasing trend of the repetition rate is an obvious result of the decreasing period measurements, these repetition rates on the order of kHz are consistent with repetition rates reported in the literature and consistent with the relaxation time of the Cr^{4+} :YAG crystal between 3.4 to 4.6 μs [32].

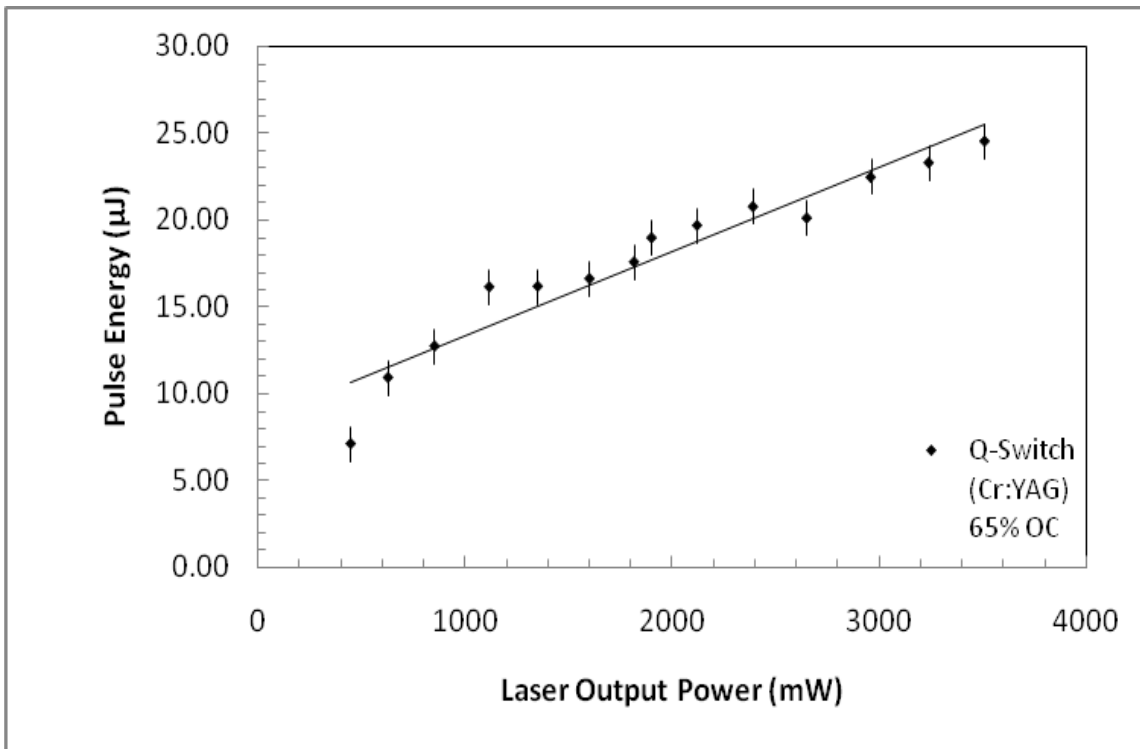


Figure 4.16. Calculated Q-switched pulse energies plotted over laser output power.

Using equations (2.4.2.1) and (2.4.2.2), the pulse energy and peak powers were computed, and are presented in figures 4.16 and 4.17. The energy and peak powers are shown to increase with the output power, as expected. For figure 4.16, the uncertainty in the energy calculations is approximately $\pm 1 \mu\text{J}$, based on the measured uncertainties of

the output power and pulse separation. In figure 4.17, the peak power is presented in comparison to the output power as the diode pump power is increased. There is a large margin of error attributed to the peak power calculations of ± 1 W attributed to the uncertainties of the pulse width and pulse period measurements. The peak power is higher than the average power, but not as high as intended. Peak powers on the orders of kW and MW can be achieved with the Cr^{4+} :YAG crystal and results presented in this experiment are on the order of Watts. This is attributed to the long pulse width on the μs scale. If the pulse widths were ns or ps long, the peak powers would likely be on the order of kW and MW, respectively. As mentioned, the long pulse widths result from low losses in the cavity to generate the pulses.

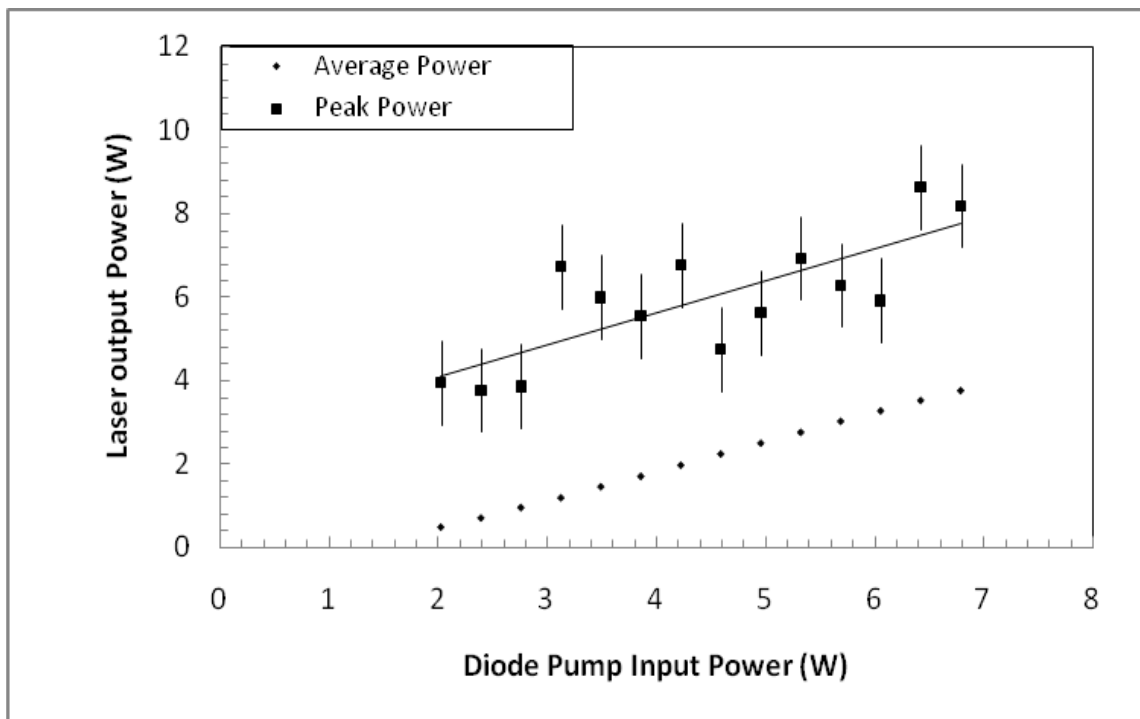


Figure 4.17. Calculated Q-switched pulse peak power in comparison with the measured average power. The output coupler had a transmittance of 65%.

4.4 Passive Mode Locking - Mode Beating

Passive mode locking was not achieved when placing the BATOP 1064 SESAM in the cavity. Instead, a form of mode beating was observed on the oscilloscope. This section will present the pulse width measurements obtained during the experiment, an example of the wave form observed on the oscilloscope and the Fourier transform of the mode beating observations. For the data presented in this section, the non-PM fiber of length $4.86 \text{ m} \pm 5 \text{ cm}$ with an additional air cavity length of $78.5 \text{ cm} \pm 2.5 \text{ cm}$ was utilized in conjunction with the 50% transmittance output coupler.

Figure 4.18 presents the beat width, beat separation, and the repetition rate of the signal measured on the oscilloscope as the diode pump power was increased. The data is plotted over laser output power measured, with the beat width and separation measurements in ns, and the repetition rate in MHz. A slight increase in the beat width was observed over increased pump power ranging between $4.6 \pm 1 \text{ ns}$ and $8.5 \pm 1 \text{ ns}$. The beat separation measured was constant at a mean value of $56 \pm 2 \text{ ns}$. Likewise, the repetition rate was constant at $17.7 \pm 2 \text{ MHz}$. The measurements for the beat separation and repetition rate correlate with the theory presented in section 2.5 for computing the free spectral range or repetition rate, Δ , in equation (2.5.1). Theoretical calculations for Δ of 18.5 MHz closely match the experimental mean of $17.7 \pm 2 \text{ MHz}$ to within 4%. Part of this error can be attributed to the uncertainty in the beat separation measurements due to jitter.

The mode beating data presented in figure 4.19 was measured from the oscilloscope and is characterized by a strong central peak and subsequent beats on both

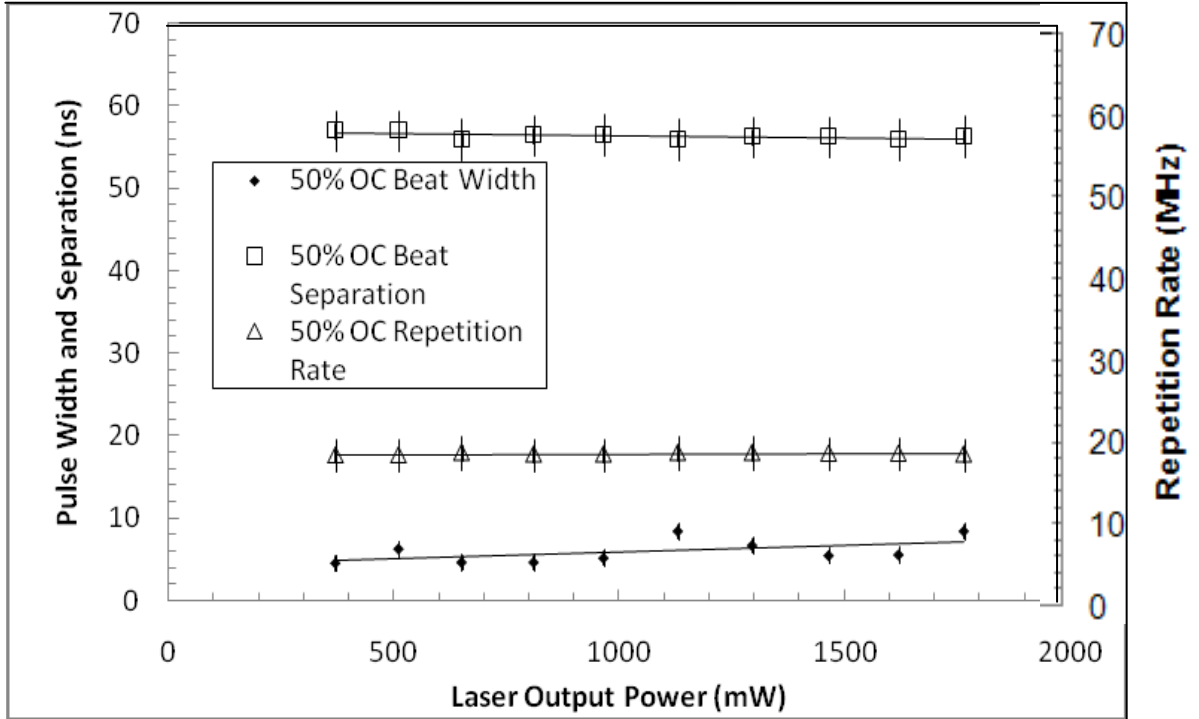


Figure 4.18. Beat width, beat separation, and repetition rate plotted over laser output power when using a Saturable Absorber Mirror. This data is not mode locked, but rather displays mode beating.

sides. Using a Fast Fourier Transform (FFT) routine in MATLAB, the frequency spectrum in figure 4.20 shows the resonant frequencies evenly spaced at 18 ± 0.5 MHz and spectral widths of 5 ± 0.5 MHz. The resonant frequency spacing closely matches the 17.7 MHz repetition rate measured on the time scale and is within the uncertainty of that measurement. The inverse of the spectral width in figure 4.20 is approximately equal to the time span of the data shown in figure 4.19 and is not very significant to this analysis. Jitter from the oscilloscope signal indicated that phases of the modes were not locked and that the periodic signal was likely mode beating. Also, if the laser was mode locked, the FFT in figure 4.20 would more closely resemble the frequency comb profile shown in figure 2.5.

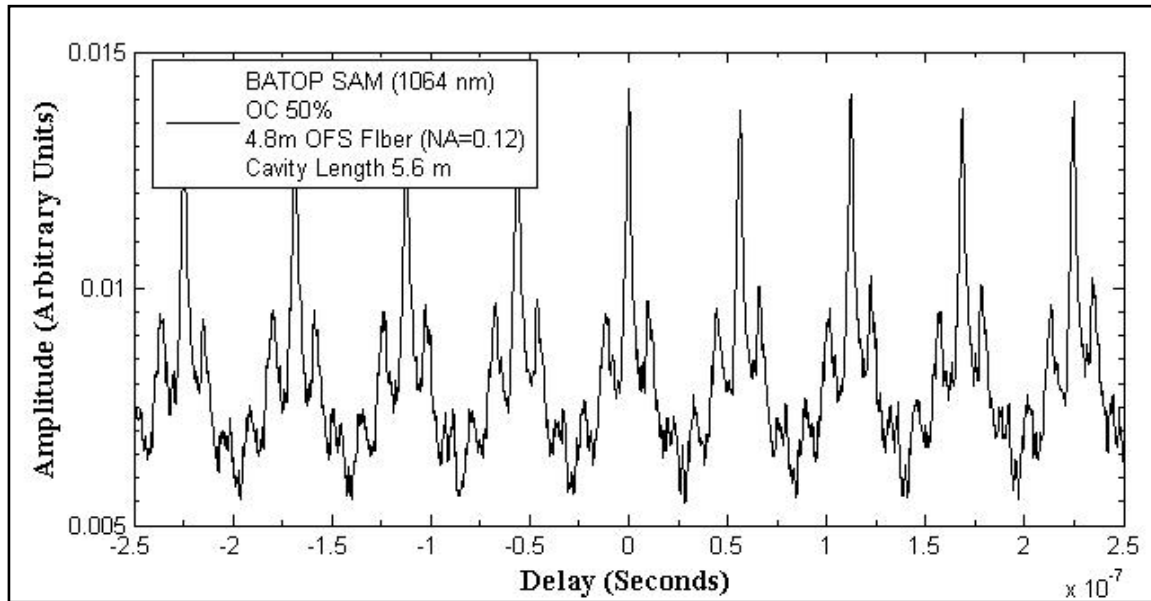


Figure 4.19. Mode beating signal observed in attempting to passively mode lock the laser using a saturable absorber mirror. The output power was 1130 mW.

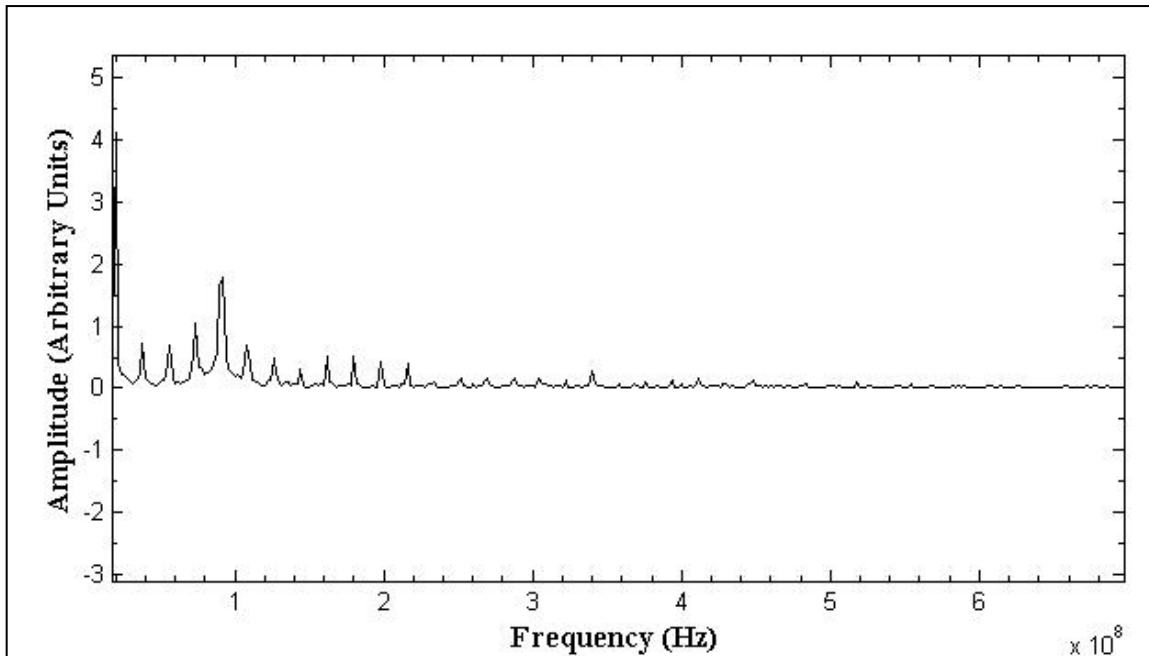


Figure 4.20. Fast Fourier Transform of the oscilloscope signal presented in figure 4.19. The frequency peaks are evenly spaced at 18 MHz with FWHM of 0.5 MHz.

4.4.1 Gratings

Because mode locking was not achieved for this part of the experiment, the grating pair was not incorporated into the cavity to compensate for dispersion. Had mode locking been observed, the theory presented in section 2.6 may have been applied to the laser design in terms of grating spacing. From the cavity design and the calculations presented in figures 2.12 and 2.13, a space between the gratings of about 4.0 cm would be needed for adequate compensation with the first grating the beam encounters angled near 45° with respect to that beam.

4.4.2 Reasons Mode Locking was not Achieved

There are two reasons proposed as to why passive mode locking was not achieved. As discussed in section 2.5.1 and shown in figure 2.7, there was a saturation fluence of $90 \mu\text{J}/\text{cm}^2$ needed for mode locking. This was calculated as being achievable. To accommodate this issue, the SESAM was placed on a translation stage, such that the focused spot size of the beam could be adjusted by positioning the SESAM at different distances from the lens. However, mode locking was still not observed after repeated tweaking of the SESAM mount, as well as the other mirrors and optics in the cavity. The second reason mode locking did not occur may have to do with the SESAM being defective. An example of this would be a lack of sufficient modulation depth of the saturable absorber of the SESAM. However, further analysis in this claim has not been fully explored other than the observation that mode locking was not achieved while using this device.

4.5 Nonlinear Polarization Rotation (NPR)

Between the two methods to achieve passive mode locking, NPR proved to be the most promising in terms of controllability of the output power and generating cw, Q-switched, and mode locked pulses. The results in this section demonstrate the degree to which the output power could be controlled by rotating the polarization plates, and a few sample oscilloscope signals that indicate possible mode locking and Q-switched operation. By possible mode locking, it is meant that the signal observed on the oscilloscope displayed a partial mode locked profile that was mostly stable, and part of a profile that resembled mode beating or Q-switching. A stable Q-switched signal was also easily attained, and the results were comparable to those achieved using the Cr^{4+} :YAG crystal.

Figure 4.21 shows the measured laser output power as the diode pump input power was increased incrementally from 2.03 W to 4.23 W. The output power was measured on both sides of the polarized beam splitter (PBS), labeled OC 1 and OC 2 in figure 3.7. The combined output power in figure 4.21 is the sum output power measured from both OC 1 and OC 2. At the maximum pump power of $4.23 \text{ W} \pm 10 \text{ mW}$, a combined output power of $1.0 \text{ W} \pm 10 \text{ mW}$ was measured, yielding a power output to input efficiency near 24%. However, the data in figure 4.21 only shows the power measured when the two quarter wave plates (QWP) and half wave plate (HWP) were held at a constant angle setting, which was experimentally determined as the maximum power angle settings.

Figure 4.22 (a) and figure 4.22 (b) show the output power measured from OC1 and OC 2, respectively, as each of the three wave plates was rotated through 360° , while keeping the other two wave plates at a constant angle. The input pump power for both of these figures was $4.23 \text{ W} \pm 10 \text{ mW}$. The significance of figures 4.22 (a) and 4.22 (b) is that the total output power remains mostly constant while the output from OC1 and OC2 can be varied significantly. This allows for manipulation of the phase difference, as discussed in section 2.5.2. Further analysis of the output power and wave plate angle relationship in correlation with cw, mode locked, and Q-switched operation could have led to mapping the pulsed operation similar to Leblond's work in figure 2.8 [43].

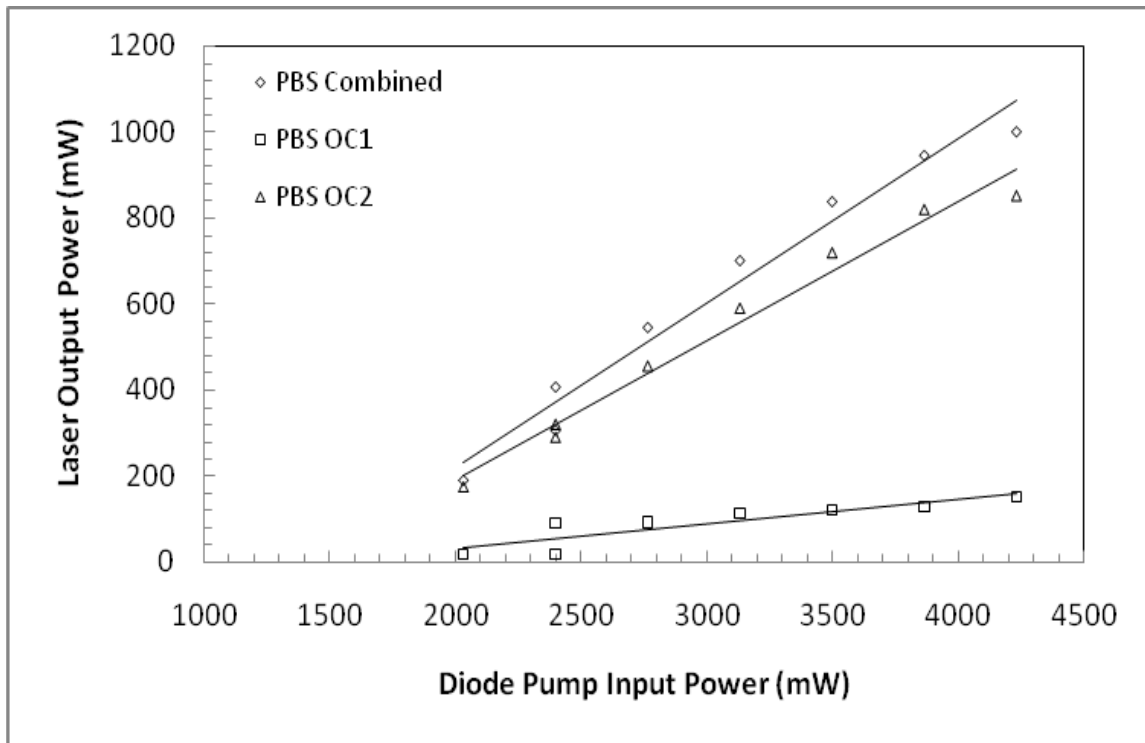


Figure 4.21. Measured output power vs. diode pump input power for nonlinear polarization rotation (NPR). The data depicted as OC1 and OC2 are the output powers measured from opposite ends of the polarized beam splitter (PBS), shown in figure 3.7. The data labeled PBS combined is the sum output of OC1 and OC2.

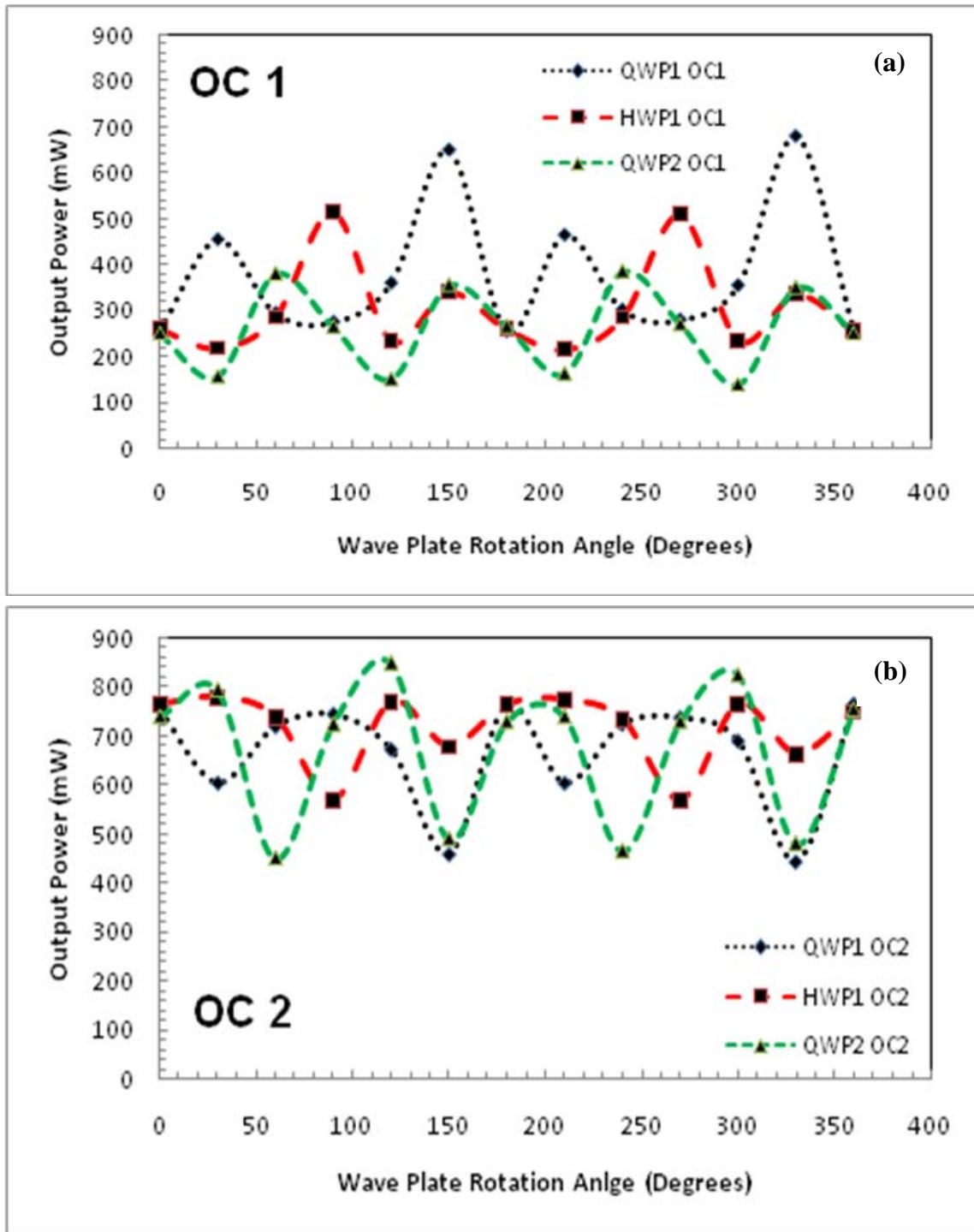


Figure 4.22. (a) Output power from OC 1 of the polarized beam splitter for NPR operation as dependent on the rotation of the three polarized waved plates used in the cavity. Figure (b) shows the output power measured from OC 2. For both figures, the diode pump input power was 4.23 W.

Passive mode locking may have been achieved using NPR from the signal shown in figures 4.23 (a) and (b). "Possible" mode locking and not definitive mode locking is used to describe this signal because a mode locked profile looks very distinct in figure 4.23 (a) on the time delay scale between 0-1 μ s, but the bulge before the mode locked signal is indicative of either mode beating or a Q-switched pulse. This signal remained stable with a little jitter, and was easily attained by rotating the three polarizers.

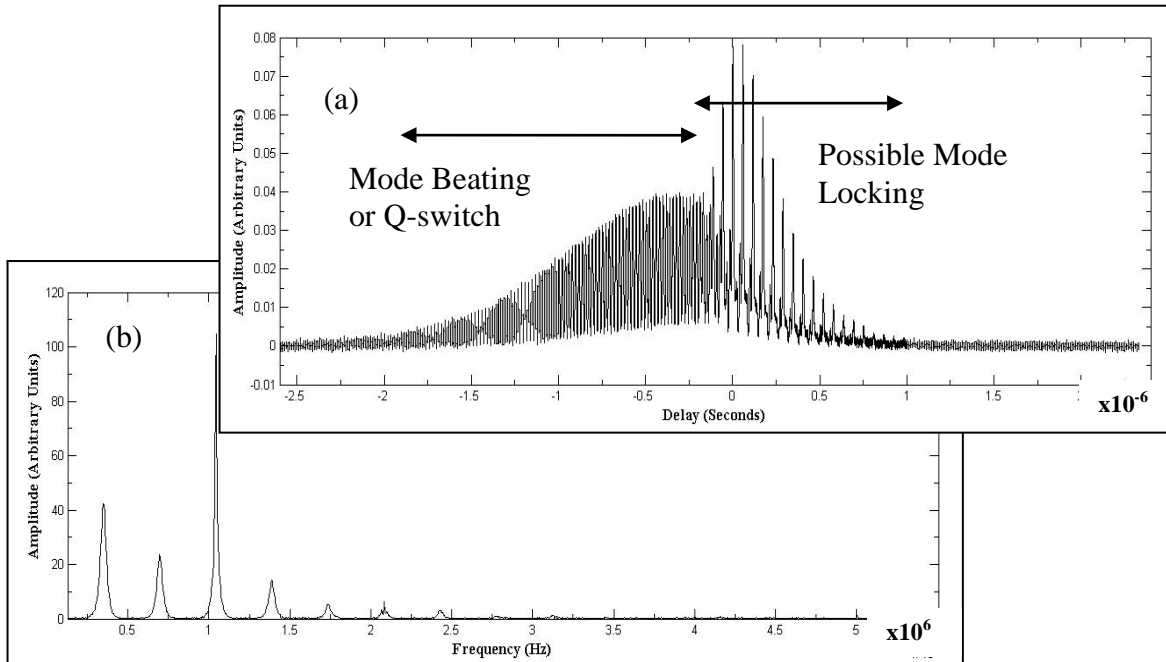


Figure 4.23. (a) Possible mode locking and mode beating or Q-switched signal and 4.23 (b) subsequent FFT.

The peaks of the possible mode locked signal in figure 4.23 (a) have a FWHM of approximately $10.5 \text{ ns} \pm 0.5 \text{ ns}$ and a period of $58.0 \text{ ns} \pm 0.5 \text{ ns}$, which corresponded to a repetition rate of 17.2 MHz. Unfortunately, the mode locked profile could not be isolated from the larger pulse preceding it, as the signal would revert back to mode beating, cw, or Q-switching.

In contrast to the claim that mode locking was achieved in figure 4.23 (a), the FFT in figure 4.23 (b) reveals little in terms of a mode locked spectral profile. Aside from the consistent spacing of the frequency peaks, it more resembles the profile of figure 4.20, which resembled that of mode beating.

Figures 4.24 and 4.25 depict sample Q-switched signals obtained with the NPR configuration. In figure 4.24, input pump power was 2.4 W, the output power measured at OC 1 was 175 ± 5 mW. The pulse width at FWHM was 2.8 ± 0.2 μ s, and the repetition rate was 28.8 kHz. This corresponded to a peak power of 3.4 W using equation (2.4.2.2). The input pump power in figure 4.25 was 3.5 W, and the output power measured at OC 1 was 675 ± 5 mW. The FWHM was measured at 1.8 ± 0.2 μ s with a repetition rate of 72.2 kHz. From this, the peak power was calculated to be 5.2 W.

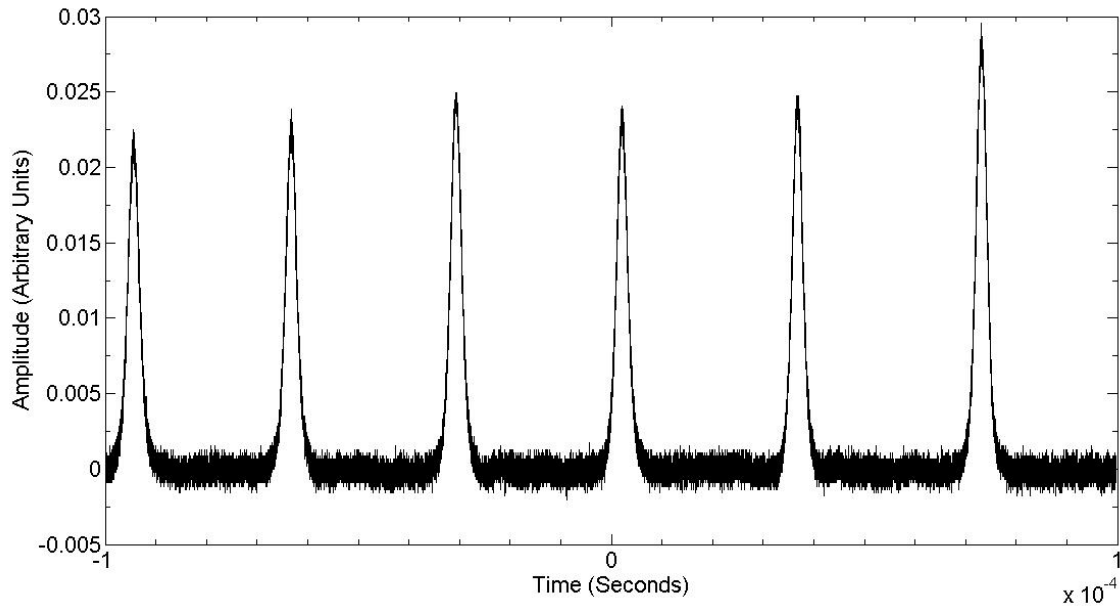


Figure 4.24. Q-switched signal from the oscilloscope at a pump input power of 2.4 W. The pulse FWHM was 2.8 μ s with a repetition rate of 28.8 kHz.

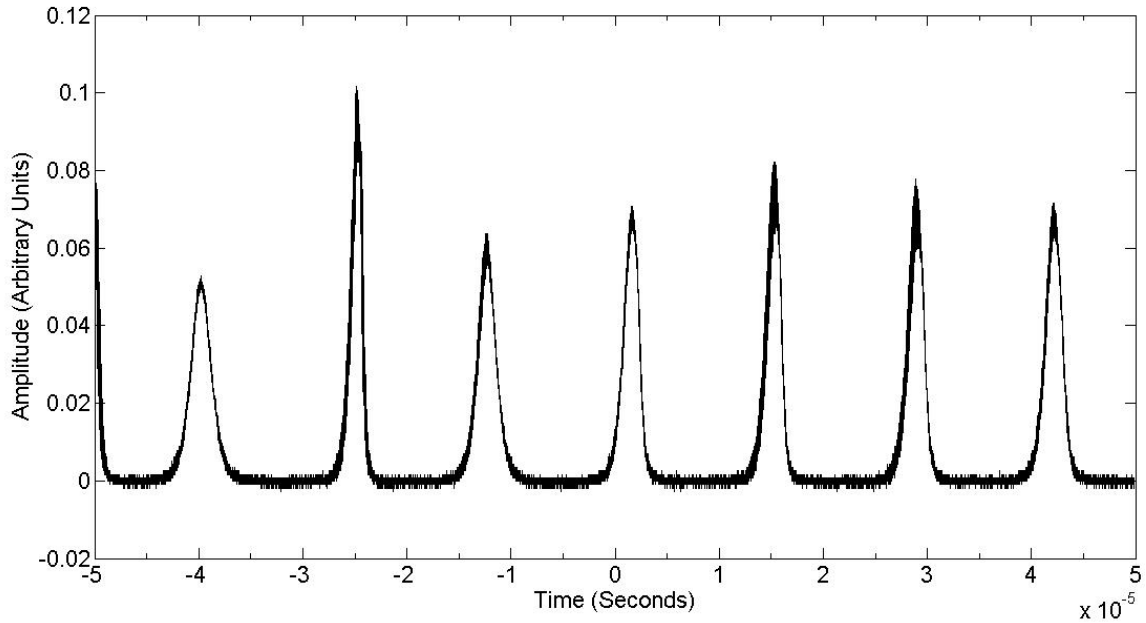


Figure 4.25. Q-switched signal from the oscilloscope at a pump input power of 3.5 W. The pulse FWHM was 1.8 μ s with a repetition rate of 72.2 kHz.

Q-switched operation using NPR showed similar characteristics to Q-switched operation using the Cr^{4+} :YAG crystal. As the pump power was increased, the pulse width was observed to decrease and the repetition rate increased. The uncertainty of the pulse width and pulse period measured also increased, and the Q-switched signal appeared increasingly unstable as the pump increased. The signal shown in figure 4.25 was somewhat unstable, and therefore, the uncertainty in the peak power calculation of 5.2 W may be as high as ± 0.5 W. Nevertheless, the calculated peak powers using NPR were much higher in relation to the average power, when compared to the Q-switch results using the Cr^{4+} :YAG crystal. From the Q-switch results in section 4.3, the peak power was about twice as high as the average power. Using NPR, the peak powers ranged from seven to nineteen times higher than the average power.

Further analysis for the NPR experiment was limited due to damaging the fiber. The fiber was damaged in NPR operation at a diode pump input power of approximately 4.5 W while rotating the polarized wave plates. This may have been attributed to poor coupling of the power into the fiber or a pulsed intensity inside the cavity that exceeded the damage threshold of the fiber. There were intentions to map out the regions of the polarization rotation where cw, Q-switched, and mode locked operation took place, as exemplified in figure 2.8 [43]. However, this was not accomplished during the course of this experiment. Chapter V will go into more discussion on recommended future research, mostly focusing on the NPR operation.

4.6 Summary

This chapter presented the results for the experiments performed in continuous wave, passive Q-switched, passive mode locked, and nonlinear polarization rotation operations as proposed in chapter III. For continuous wave operation, two different fibers were used and three output couplers were tested in order to compare the output power of the laser. It was shown that the fiber with a higher numerical aperture and shorter length yielded a higher output power relative to the diode pump input power. The best efficiency result was with a 4.9 m fiber with core NA of 0.12, using a 65% transmittance output coupler, and measuring a laser output of 5 W for an input power of 8.3 W. This yielded an output to input efficiency of 60%.

Spectra were taken of the laser in cw operation. The spectral peak for the PM fiber was between 1098-1108 nm. Spectral peaks for the non-PM fiber using a 50% and 65% transmittance OC ranged between 1087-1094 nm, respectively. Additionally,

spectra were taken for increased diode pump input power, and while varying the diode chiller temperature. These spectral results were shown to remain consistent within these wavelength ranges. While stimulated emission for Yb^{3+} is a quasi-three-level system, it was discussed that at peak wavelengths above 1080 nm, the gain medium is acting more like a four-level system. This is advantageous from the stand point that a four-level system has a lower threshold gain than a three-level system.

In phase II, the Cr^{4+} :YAG crystal was placed inside the cavity to act as a saturable absorber and to generate passive Q-switched pulses. Q-switching was achieved with a mean pulse width of 2.9 μs spanning an output power range of 400 mW to 3.5 W. However the pulse width may have been increasing slightly with increased power. Pulse repetition rates increased with increased power, ranging from 60-150 kHz. Pulse energies were computed between 7-24 μJ and peak powers were calculated at twice the average power. The passive Q-switching results yielded relatively long pulses with lower than desired pulse energies and peak powers compared to results in the literature. Reasons for these shortcomings are likely due to the Cr^{4+} :YAG crystal not having enough loss to improve the results obtained.

A semiconducting saturable absorber mirror was used in phase III to generate passive mode locked pulses. Passive mode locking was not achieved, and the results presented were likely the result of mode beating effects on the detector. However, the periodic signals measured were consistent with the round trip cavity time, and the experimental repetition rate of the mode beats was 17.7 MHz, which was consistent with the mode locking theory. Reasons presented as to why mode locking was not achieved

include the inability to focus a high enough intensity to saturate the absorber mirror, and a possibility that the SAM was not working according to factory specifications. While dispersion compensation had been presented in the theory using a grating pair, these gratings were not used in this experiment as planned because mode locking was not achieved without them.

The nonlinear polarization rotation experiment demonstrated the ability to operate the fiber laser in cw, possible mode locked and Q-switched operation. The polarization wave plates allowed the output power to be varied significantly while maintaining a constant input power. Possible mode locked pulses 10.5 ns in length with a repetition rate of 17.2 MHz were observed, but the signal was complicated by either a mode beating or Q-switched pulse profile preceding it. This indicates some discrepancy with regards to phase locking the modes within the cavity, and was irresolvable. In Q-switched operation, pulses were measured between 1.8-2.8 μ s and repetition rates between 28.8-72.2 kHz. The peak power to average power ratio for NPR was seven to nineteen times higher compared to the results for Q-switching with the Cr^{4+} :YAG crystal. This primarily has to do with the length of the Q-switched pulse measured and the ability to vary the losses within the cavity.

V. Conclusions and Recommendations

5.1 Chapter Overview

This chapter has three objectives. First is to briefly highlight the key points from chapters I-IV in terms of the goals initially stated for this research, the methodology derived to perform the experiments, the results obtained, and reasons for error. The second objective is to expound upon the advantages and disadvantages of the fiber laser system based on the results from this experiment in comparison to results found in the literature. The third part of this chapter is a proposal for future research in fiber lasers and pulsed operation at the Air Force Institute of Technology.

5.2 Research Objectives and Results Obtained

The objective of this experiment and thesis was to design a Yb-doped fiber laser cavity and to generate passively Q-switched and mode locked short pulses. Because there was no prior fiber laser cavity in place to begin immediate work on Q-switching and mode locking the laser, considerable attention was dedicated to diagnostics of the laser in continuous wave operation, in terms of output power, efficiency, and operating wavelength. The course of this experiment led to several different methods and techniques to explore the cw, Q-switched, and mode locked operation of fiber lasers.

In cw operation, the best output power achieved was 5 W at a diode pump input power of 8.3 W yielding a slope efficiency of 60%. This was achieved using a 65% transmission output coupler and a non-PM fiber of 4.9 m length with NA of 0.12. The spectral measurements of the various laser cavities tested ranged from 1087-1108 nm. Passively Q-switched pulses were generated when a Cr^{4+} :YAG crystal was inserted into

the laser cavity. Measurements of the pulse width may have increased slightly with increased pump power, but were within a mean measured value of $2.9 \mu\text{s} \pm 1 \mu\text{s}$. The pulsed repetition rate, pulse energy, and peak powers were shown to increase linearly with increased pump power and average output power. In the Q-switched regime, the experiment was limited by the inability to resolve a stable pulsed wave form at progressively higher pump powers. The long pulse length in μs , and low pulse energies and peak powers compared to results found in the literature are likely due to not enough loss in the Cr^{4+} :YAG crystal.

To initiate passive mode locking, two methods were used. The first method was with a saturable absorber mirror and the second was through nonlinear polarization rotation. Instead of mode locking with the SESAM, a mode beating signal was observed. Possible mode locking was achieved using NPR, but the signal seems to be combined with a form of mode beating or a Q-switched pulse. If mode locking was achieved, the pulses were measured at 10.5 ns and a repetition rate of 17.2 MHz. Because dispersion and GVD affect the width of a mode locked pulse, it was intended to incorporate a grating pair into the mode locking experiments in order to compensate for this dispersion. However, the gratings were not incorporated with the SESAM because mode locking was not achieved, and they were not used for NPR due to time constraints of the experiment.

Q-switching was also achieved using NPR. Short pulses with FWHM ranging from 1.8-2.8 μs and repetition rates between 28.8-72.2 kHz repetition rates were measured. The peak powers for the NPR Q-switched pulses were significantly higher

than the peak power for the Q-switched pulses generated using the Cr^{4+} :YAG crystal. This was attributed to the ability to control the losses within the cavity better using NPR.

5.3 Advantages and Disadvantages of Fiber Lasers

There are several points to address regarding the advantages and disadvantage of fiber lasers as a simpler, more compact, and less costly solution to current laser applications where bulk solid-state lasers are the current industry standard. This section addresses the issues of simplicity, cavity size, and economy of fiber laser systems in the context of how they can benefit the Department of Defense in the development of future weapons systems. The results from this particular fiber laser experiment, which was developed mostly from equipment available at AFIT at very little additional cost, help to weigh in on several advantages that are unachievable with solid-state lasers. These advantages include higher efficiencies, lower maintenance requirements, and smaller cavity size. As future research in fiber lasers leads to power levels and short pulse operation that are competitive with solid-state lasers, there will be less speculation on the future of fiber lasers, and more of a motivation to acquire and implement them.

However, there are distinct disadvantages to fiber lasers that should be addressed in the context of potential applications for DOD weapon systems. Results obtained in this experiment reflect several disadvantages of fiber laser systems that may not be as prominent in solid-state lasers. These issues include burning the fiber ends under trivial circumstance, sensitivities to misalignment and subsequent degraded performance, inconsistent performance of the fiber laser on a day-to-day basis leading to greater

uncertainty in precise measurements, as well as deleterious nonlinear effects specific to fiber laser operation.

With regards to the advantages of fiber lasers, it is fairly straight forward to show from this experiment that the laser can be simple, compact, and less costly. In terms of simplicity, the cavity designed for this experiment was quite simple, requiring at minimum a diode-pump source, the fiber as the gain medium, a few dichroic mirrors, lenses, HR mirrors and output couplers that are suitable for 1064 nm applications. The methods for passively Q-switching and mode locking the laser were simple. They merely required inserting a Cr^{4+} :YAG crystal, saturable absorber mirror, or polarizers into the laser cavity and pulsed operation was generated with minor adjustments of the cavity.

The overall size of the laser cavity can be greatly reduced with a fiber laser due to the ability to coil the gain medium. The lengths of the cavity designs in this experiment ranged from 5.8 m to 9.5 m, but were confined to an overall area of 61 cm^2 (2ft^2), not including the diode pump control, which has an area smaller than the laser cavity in this case. Unlike several solid state laser systems where the gain medium requires external cooling equipment, the Yb doped fiber did not require cooling for this experiment. Only for much higher power operations would the fiber require water cooling [51]. Additionally, gratings used to compensate for GVD require spacing on the order of cm, compared to meters of space required by prisms, commonly used for compensation in solid state lasers.

While claiming that a fiber laser is less costly than a bulk solid-state laser can be somewhat relative or misleading, the fiber laser designed for this experiment was

economical. As mentioned, all parts to this laser, the diode, fiber, lenses, and mirrors were available at AFIT. However, Yb-doped fiber is a relatively cheap gain medium in comparison to some solid-state crystals (not including the equipment required to cool them). The saturable absorbers (Cr^{4+} :YAG crystal and SESAM), which were procured for this experiment, are lighter weight and around the same cost or cheaper than the equipment needed to actively generate Q-switched and mode locked pulses, such as Pockels Cells and EO/AO modulators.

A definitive advantage of fiber laser systems over solid-state lasers is the efficiency of operation. This experiment demonstrated a 60% efficiency of output power compared to the diode pump input power, an efficiency that has yet to be achieved with a solid-state laser such as the Ti:Sapphire. This primarily has to do with the means of pumping the laser. While Ti:Sapphire lasers require a 4-stage means of pumping from the laser diode to Nd:YVO and then through second harmonic generation (SHG) before being pumped into the crystal, the Yb-doped fibers can be directly pumped with conversion efficiencies greater than 50% [52]. Therefore, not only is the power output efficiency higher with a fiber laser, but the cooling requirements, maintenance, and ultimately, operating costs are far less, and bring full circle the advantages of simplicity, smaller size, and less cost.

Despite the advantages presented, there are distinct disadvantages to fiber lasers that significantly hindered the progression of this experiment. The primary drawback was sensitivity of the fiber to poor coupling with the pump light or reflected beam, and sudden adjustments of the fiber cavity that could lead to pulsed reflections exceeding the

damage threshold of the fiber. While this was discussed more in depth in the theory section of chapter II, facet damage of the fiber occurred quite frequently throughout the experiment.

Additionally, inserting an IR card or any object into the cavity for pump powers above 4-5 Watts posed a risk of facet damage. This posed a problem during the passive Q-switch experiments where the Cr^{4+} :YAG crystal required slight adjustments in order to stabilize the pulsed waveform. The fiber was also burned while operating in cw mode with the 95% reflectance output coupler where the energy density inside the cavity may have exceeded the damage threshold of the fiber at a pump power of about 5 Watts. For NPR operation, the fiber end was damaged while rotating one of the polarizing wave plates, again at around 5 Watt pump input. On the other hand, cw operation was successfully carried out while using a 50% output coupler at pump powers exceeding 12 Watts. Therefore, this trend of damaging the fiber when a modification is made to the cavity too quickly or when the pump light is not effectively focused into the fiber core can lead to a disruption of the beam in the cavity, or rather a large enough pulse that exceeds the damage threshold of the fiber.

Damage to the fiber ends is avoidable, and better methods could have been utilized to couple the pump power into the fiber than the method used for this experiment. In particular, the use of wavelength division multiplexers (WDMs), different microscope objectives to focus the pump light into the fiber, or better beam collimation may have resolved the difficulties experienced in this experiment with regards to fiber damage. Nevertheless, the sensitivity of the fiber is significant in terms of military applications.

Whether fiber lasers can be applied to high power weapons or communications systems, military weapons systems require a moderate degree of durability depending on the operating environment in which they are used. While a fiber laser could prove useful for weapons systems that do not require additional cooling systems and bulky equipment, the pump-to-fiber mechanism is still a delicate process, and may limit fiber laser applications to mostly laboratory, industry, and other stationary environments.

A second disadvantage observed during the course of the experiment was the difficulty in optimizing the laser to achieve repeatable results. For the cavity designs presented in chapter III, there were four primary locations where the cavity mirrors could be adjusted to improve the output power measured. The first two locations were where the light was coupled between the microscope and the fiber. The other two locations that could be adjusted were at the end mirror and at the output coupler. Typically, adjustments to the cavity needed to be made each time the pump power was increased. This was due to nonlinear processes inherent to the fibers, and this affected the focusing of the beam in the cavity. Such slight adjustments of the end mirrors could lead to output power increases on the order of 10's of mW improvement, while proper coupling of the pump light to the fiber core could improve the output power by 100's of mW.

5.4 Recommendations for Future Research

There are many avenues of research currently being performed in the area of fiber lasers, and in particular, Yb-doped fibers, in effort to achieve higher output powers as well as high peak power Q-switched and mode locked pulses. Several laser systems of interest to the DOD emphasize the need for high performance and broad applications, but

need to impose restrictions regarding cost, space, durability, and maintenance in order to make the weapon system effective. A few of these examples include the Airborne Laser (ABL) [53], the recent unveiling of the FIRESTRIKE solid-state laser weapons system [54], and High Energy Liquid Laser Air Defense System (HELLADS). In January 2008, the Air Force announced funding for fiber laser research [55] specifically to address the issues of performance, space, and cost. This is a very good time for fiber laser research in terms of developing fiber lasers that are competitive with their solid-state or other type of laser counterparts, and to extrapolate the benefits fiber lasers offer in these areas, as well as to overcome their disadvantages. Combining this with research efforts in passive Q-switching and mode locking even further reduces the complexities and bulk of these types of lasers.

Of the fiber laser designs and techniques presented from this experiment, the method of nonlinear polarization rotation showed the most promise as a multipurpose laser that could operate in cw, Q-switched, mode locked, and Q-switched/mode locked operation simply by adjusting polarization controllers. Unfortunately, this part of the experiment was devoted the least amount of time due to the progression of diagnostics performed in phases I-III, and the limited amount of time to perform all of these experiments. Nevertheless, the NPR fiber laser cavity described in this experiment displayed many of the attributes that were sought, including high output power, simple design, compact cavity, low cost, and simple generation of passive Q-switched and mode locked short pulses. The drawback to the NPR design, as mentioned in the previous

section, was that the fiber end was burned while rotating one of the polarizers at a pump power above 5 Watts.

An additional recommendation for future research would be for AFIT to explore fiber lasers using doped-photonic crystal fibers (PCFs). As mentioned briefly in chapter II, the advantages of PCFs are that they possess a much larger numerical aperture than the double-clad fiber used in this experiment, allowing for improved pump light coupling, and therefore improved output power potential of the laser. As PCFs were developed in the mid-1990's, their widespread use has yet to fully take off in the realm of fiber laser research, but some of the highest output powers achieved to date for fiber lasers, as discussed in chapter II, have been using PCFs [5656].

5.5 Summary

In conclusion to this thesis, a Yb-doped fiber laser oscillator was successfully developed. Results of the output power demonstrate a higher level of efficiency than most solid state laser systems. Attempts to generate passively Q-switched and passively mode locked short pulses were successful. However, measurements of the generated pulse widths were much larger than desired and not competitive with the results found in the literature using the same means to passively generate these pulses.

The theory developed in chapter II was intended to identify concepts and design issues that were specific to fiber lasers, Q-switching, and mode locking. While the topics presented in the theory are not as thorough as one might find in textbooks on the same subjects, there were no issues identified in prior research or in the limitations of the materials and instruments used that indicated Q-switched and mode locked pulses could

not be generated at shorter time scales than μs and ns , respectively. Efforts to address these shortcomings were addressed in chapter IV.

The methodology presented in chapter III describes in detail the design, procedure, and research objectives for each of the four phases in the development of this laser system. With regards to the idea of fiber lasers being a simpler, more efficient, and economical alternative to the current industry standards, the designs presented were kept simple, and the means to generate pulses were kept simple. While the higher efficiencies were inherent to the Yb-fiber, the cost to perform this research was relatively low because all the materials are readily available at many laser laboratories.

Several results were discussed in chapter IV pertaining to the laser output power, spectrum, and the pulse characteristics in Q-switched and mode locked operations. The trends of the data were consistent for the most part with the theory, except that the results obtained in Q-switched and mode locked operation showed long pulses, low peak powers, and mode beating. Reasons for measurement uncertainty and error were discussed along with reasons why better results were not achieved for each phase in the experiment.

Finally, chapter V incorporates a discussion of the advantages and disadvantages of fiber lasers. This thesis was not intended to be a marketing document making the pitch that fiber lasers are the solution to all problems in the field of laser research. Fiber lasers are obviously not the only solution, and the progression of this experiment was hindered on several occasions by issues that may or may not be experienced when working with solid state laser systems, such as fiber damage.

Nevertheless, as this experiment demonstrated successful cw, Q-switched, and possible mode locked operation, there are still many ways in which fiber laser research at AFIT can move forward with regards to high power scaling and pulsed generation. There are several military applications that could benefit from the advantages that fiber lasers and passive pulse generation can offer. Additional research using nonlinear polarization rotation and experimenting with photonic crystal fibers is recommended.

Appendix A - Component Specifics

Table A.1. Equipment list for continuous wave, Q-switched, and mode locked operation.

#	Description	Manufacturer	Model Number
1	Diode Pump (975 nm)	LIMO Laser Systems	HLU-25F200-975
1	8.7 meter Yb-doped fiber, 20 μ m core, 400 μ m diameter	Nufern	PLMA-YDF-20-400
1	4.9 meter Yb-doped fiber, 20 μ m core, 200 μ m diameter	OFS	Yb050406
3	Dichroic mirrors HR @ 45 ⁰	UNK	5104 1064 nm
2	20X microscope objectives	Optics For Research	LLO-8-8-1064
1	40X microscope objective	Newport	UNK
1	10X microscope objective	Newport	UNK
1	75.6 mm lens @ 1064 nm	Newport	KBX-058
1	100.00 mm lens @ 1064 nm	Newport	KBX-064
1	88.5 mm lens @ 1064 nm	Newport	KBX-061
1	95% reflectance output coupler	CVI	PRI-1047-95-0512
1	50% reflectance output coupler	CVI	BS1-1064-50-2025
1	35% reflectance output coupler	UNK	UNK
1	HR mirror @ 0 ⁰ (1064 nm)	New Focus	
2	HR mirrors @ 45 ⁰ (1064 nm)	New Focus	5104 1064 nm
1	Cr ⁴⁺ YAG crystal 4x10x1 mm ³ (T=92% @ 1035 nm)	EKSPLA	
2	1064 SESAM (A=1%)	BATOP	1VA-30
1	1040 SESAM (A=1%)	Del Mar	SAM-1040-2-25AS
2	X-Y-Z translation stages for fiber	Newport	561/562 Series UltraAlign
2	10 W power meters	Thor Labs	D10MM
1	10 W power meter	Coherent	Field Max
1	Lock-In Amplifier	Stanford Research Systems	SR 850 DSP
1	Optical Isolator IO YAG @ 1064 nm	Optics For Research	18182-2
2	$\lambda/2$ polarizing wave plates	CVI	
2	$\lambda/4$ polarizing wave plates	CVI	
1	1 GHz Oscilloscope	LeCroy	Wave Pro 7100
1	High speed silicon detector	Thor Labs	DET 10A
1	Optical Spectrum Analyzer	Yokogawa	AQ-6315A
2	X-translation stages for HR mirrors	Oriel	116132/16031
2	Polarized Beam Splitters	CVI	
1	Chopper wheel	Stanford Research Systems	SR540
2	600 line/mm gratings	Thor Labs	GR25--0610

Bibliography

1. Y. Wang, A.M. Rios, H. Po, "Analysis of a Q-switched ytterbium-doped double-clad fiber laser with simultaneous mode locking", *Optics Communications* Vol. 224 (2003) 113-123.
2. K. Sumimura, H. Yoshida, F. Hisanori, M. Nakatsuka, "Yb fiber mode locked laser with a wide tuning range for chirped pulse amplification systems," *IEICE Electronics Express*, Vol. 3, No. 11, (2006) 233-237.
3. L. Zhang, D. Li, Q. Zhang, C. Li, Z. Wei, B. Feng, P. Fu, Z. Zhang, "Diode-pumped passive Q-switched and mode locked 946 nm Nd:YAG laser with a Nd, Cr:YAG saturable absorber" *Optics Communications* Vol. 250 (2005) 174-177.
4. J. Limpert, T. Schreiber, T. Clausnitzer, K. Zollner, H.-J. Fuchs, E.-B. Kley, H. Zellmer, A. Tunnermann, "High-power femtosecond Yb-doped fiber amplifier", *Optics Express* Vol. 10, No.14, 15 July 2002 pgs (628-638).
5. C.J. Koester, E. Snitzer, "Amplification in a fiber laser", *Applied Optics* Vol. 3 No. 10,(1964) pgs 1182-1186. Also available at W. T. Silfvast, "Selected papers on fundamentals of lasers," *SPIE Milestone Series*, Vol. MS 70, 1993 pgs (430-434).
6. L.E. Hargrove, R.L. Fork, M.A. Pollack, "Locking of He-Ne laser modes induced by synchronizing intracavity modulation," *Applied Physics Letters*, Vol. 5(1) July 1, (1964). Pgs 4-5.
7. A. J. DeMaria, W. H. Glenn, M. J. Brienza, M. E. Mack, "Picosecond laser pulses," *IEEE*, Vol. 57(1), January (1969) pgs 2-25.
8. C.V. Shank, E. P. Ippen, "Subpicosecond kilowatt pulses from a mode locked cw dye laser," *Applied Physics Letters*, Vol. 24(8), April 15 (1974) pgs 373-375. Also available at W. T. Silfvast, "Selected papers on fundamentals of lasers," *SPIE Milestone Series*, Vol. MS 70, 1993 pgs (509-511).
9. J.C. Diels, W. Rudolph, "Ultrashort Laser Pulse Phenomena," Academic Press, USA, (2006). Pp 361, 278, 32, 119,315, 318-319.
10. M.T. Asaki, C. P. Huang, D. Garvey, J. Zhou, H. Kapteyn, M. M. Murnane, "Generation of 11 fs pulses from a self-mode locked Ti:Sapphire laser," *Optics Letters*, 18 (1993) pgs 977-979.
11. A. Stingl, C. Spielmann, F. Krausz, R. Szipocs, "Generation of 11 fs pulses from a Ti:Sapphire laser without the use of prisms," *Optics Letters*, 19 (1994) pgs 204-206.

12. J. Dawson, M. Messerly, J. An; Fiber Laser Replacement for Short Pulse Ti:Sapphire Oscillators – Scalable Mode Locking to Record Pulse Energies”, Lawrence Livermore National Laboratories UCRL-TR-220157, 27 March 2006.
13. B. Shiner, “High-power fiber lasers gain market share,” Article posted to Industrial Laser Solutions, http://www.industrial-lasers.com/display_article/247670/39/none/none/Feat/High-power-fiber-lasers-gain-market-share 1 Feb (2006).
14. Institute of Applied Physics, “Fiber Based High Power Laser Systems,” <http://www.iap.uni-jena.de/laser/r-and-d.html>, (2006).
15. S. Christensen, G. Frith, B. Samson, "Developments in thulium-doped fiber lasers offer higher powers", SPIE, 11 July (2008), available at <http://spie.org/x26003.xml?ArticleID=x26003>.
16. J. Hecht “Photonic Frontiers: High-Power Fiber Lasers: Pumping up the Power,” Laser Focus World, http://www.laserfocusworld.com/articles/article_display.html?id=234077, (2005).
17. F. Roser, J. Limpert, A. Tunnermann, “High-Power Fiber Lasers: Ultrafast fiber laser reaches gigawatt peak powers,” Laser Focus World, http://www.laserfocusworld.com/display_article/328528/12/none/none/Feat/High-power-fiber-lasers:-Ultrafast-fiber-laser-reaches-gigawatt-peak-power 1 May (2008).
18. F. Röser, J. Rothhard, B. Ortac, A. Liem, O. Schmidt, T. Schreiber, J. Limpert, A. Tünnermann, “131 W 220 fs fiber laser system,” Optics Letters 30 (2005) 2754–2756.
19. Polar Onyx, Fiber laser products http://www.polaronyx.com/Uranus_introduction.htm.
20. Business Wire Press Release, “SPI Lasers 30W pulsed fiber laser competes with traditional marking lasers,” <http://www.forbes.com/businesswire/feeds/businesswire/2008/08/22/businesswire20080822005401r1.html> August 22, (1008).
21. SPI Lasers, Fiber laser products http://www.spilasers.com/Fiber_Laser_Products_and_Applications/Pulsed.aspx.
22. G. P. Agrawal, "Nonlinear Fiber Optics", 2nd edition, Academic Press, New York, (1995), pg 18,562.

23. J. Buckley, A. Chong, S. Zhou, W. Renninger, F. Wise, "Stabilization of high-energy femtosecond ytterbium fiber lasers by use of a frequency filter", Optics Society of America, Vol. 24, No. 8 August (2007), pp 1803-1806.
24. F.D. Teodoro, C.D. Brooks, "Fiber sources reach multimewatt peak power in ns pulses," Laser Focus World, November (2006) pp 94-98.
25. R. S. Quimby, "An Introduction to Photonics and Lasers," Wiley and Sons, New Jersey, 2006.
26. Diagram from website, <http://www.fiberoptics4sale.com/Merchant2/optical-fiber.php>.
27. B.E.A. Saleh, M.C. Teich, "Fundamentals of Photonics," John Wiley & Sons, Inc, New Jersey, (2007). Pp 376-377, 613-615, 615-620, 895-896, 341.
28. R. M. Wood, "The power-and energy-handling capability of optical materials, components, and systems," SPIE, (2003), pp 48-49.
29. Y. Jeong, J. Nilsson, J. K. Sahu, D. B. S. Soh, P. Dupriez, C. A. Codemard, S. Baek, D. N. Payne, R. Horley, J. A. Alvarez-Chavez, and P. W. Turner, "Single-mode plane-polarized ytterbium-doped large-core fiber laser with 633-W continuous-wave output power," Opt. Lett. 30, 955-957 (2005).
30. J. M. Jacobs, "Suggested guidelines for the handling of optical fiber -White Paper", Corning Incorporated, (2001), pgs 1-8.
31. J. T. Verdeyen, "Laser Electronics," Prentice Hall, 3rd Ed. (1995).
32. Y. Kalinsky, "Cr⁴⁺-doped crystals: their use as lasers and passive Q-switches," Progress in Quantum Electronics. 28 (2004) pgs 249-303.
33. S. Wang, Q. Li, S. Du, Q. Zhang, Y. Shi, J. Xing, D. Zhang, B. Feng, Z. Zhang, S. Zhang, "Self-Q-switched and mode locked Nd,Cr:YAG laser with 6.52 W average output power", Optics Communications 277 (2007) pg 130-133.
34. Y.L. Chen, S.W. Tsai, S.C. Wang, "High-power diode-pumped Q-switched and mode locked Nd:YVO₄ laser with a Cr⁴⁺:YAG saturable absorber," Optics Letters Vol. 25, Issue 19 (2000) pp 1442-1444.
35. S. Zhang, E. Wu, H. Zeng, "Q-switched mode locking by Cr⁴⁺:YAG in a laser-diode-pumped c-cut Nd:GdVO₄ laser," Optics Communications 231 (2004) pg 365-369.
36. W. G. Wagner, B. A. Lengyel, "Evolution of the giant pulse in a laser", Journal of Applied Physics, Vol. 34 No. 7, July 1963, pgs 2040-2046.

37. C. C. Davis, "Lasers and electro-optics; fundamentals and engineering", Cambridge University Press (1996), pgs 179-182.
38. R. Trebino, "The Generation of Ultrashort Laser Pulses," Power Point presentation, Frequency Resolved Optical Grating Lectures, <http://www.physics.gatech.edu/gcuo/lectures/>.
39. M. Bohn, "Mode locked lasers," Power Point presentation, Lecture Notes.
40. BATOP Optoelectronics, Inc. "How does a SAM work?". Available at http://www.batop.de/informations/SAM_infos.html.
41. D.A. Jones, "Portable diode pumped femtosecond lasers", thesis, Air Force Institute of Technology, March (2007), pg 24.
42. BATOP Optoelectronics, Inc. "SAM DataSheet SAM-1064-1-x-500fs=1064 nm". Available at http://www.batop.de/products/saturable_absorber/SAM/pdf_sheets/1064nm/sam-1064-1-500fs.pdf.
43. H. Leblond, M. Salhi, A. Hideur, T. Chartier, M. Brunel, F. Sanchez, "Experimental and theoretical study of the passively mode locked ytterbium-doped double-clad fiber laser", Physical Review A, Vol. 65 063811 (2002) pp 1-9.
44. B. Ortac, A. Hideur, M. Brunel, T. Chartier, M. Salhi, H. Leblond, F. Sanchez, "Characterization of an ytterbium-doped double-clad fiber laser passively mode locked by nonlinear polarization rotation", Applied Physics B, 77 (2003), pp 589-594.
45. J. Y. Huang, H. C. Liang, K. W. Su, Y. F. Chen, "High power passively Q-switched ytterbium fiber laser with Cr^{4+} :YAG as a saturable absorber," Optics Express. Vol. 15, No. 2, 473-479 (2007).
46. Nufern, "Polarization maintaining fibers". Available at <http://www.nufern.com/polarization-maintaining-fibers.php>.
47. Nufern, "Part #: PLMA-YDF-20/400". Available at http://www.nufern.com/fiber_detail.php/57.
48. Optical Fiber Solutions (OFS), "Cladding pumped fibers specifications sheet: Ytterbium cladding pumped fibers". Available at <http://www.specialtyphotronics.com/pdf/products/fibers/rareearth/Ytterbium%20Cladding%20Fibers.pdf>.

49. L. Lefort, J. H. V. Price, D. J. Richardson, G. J. Spuhler, R. Paschotta, U. Keller, A. R. Fry, J. Weston, "Practical low-noise stretched-pulse Yb³⁺-doped fiber laser", Optics Letters, March (2002) pp 291-293.
50. Encyclopedia of Laser Physics and Technology, "Ytterbium-doped Gain Media", available at http://www.rp-photonics.com/ytterbium_doped_gain_media.html.
51. IPG, "Frequently asked questions about fiber lasers," available at <http://www.ipgphotonics.com/faqs.htm>.
52. H. Endert, G.S. Galvanauskas, R. Patel, M. Stock, "Novel ultrashort pulse fiber lasers for micromachining applications", RIKEN Review, No. 43, Focus on 2nd International Symposium on Laser Precision Microfabrication (LPM2001), January, (2002) pp 23-27.
53. Boeing, "Integrated Defense Systems, Airborne Laser", available at <http://www.boeing.com/defense-space/military/abl/index.html>.
54. Laser Focus World, "Northrop Grumman releases FIRESTRIKE laser weapon", November 13 (2008), available at http://www.laserfocusworld.com/display_article/345272/12/none/none/PRODH/Northrop-Grumman-releases-FIRESTRIKE-solid-state-laser-weapo.
55. M. Callier, "Air Force announces funding for fiber laser research, considers applications", Air Force Office of Scientific Research Public Affairs, Air Force Material Command, January 4, (2008), available at <http://www.afmc.af.mil/news/story.asp?id=123081143>.
56. Crystal Fibre, "Technology Tutorial - Introduction", available at http://www.crystal-fibre.com/technology/technology_tutorial.shtm.

REPORT DOCUMENTATION PAGE				Form Approved OMB No. 074-0188	
<p>The public reporting burden for this collection of information is estimated to average 1 hour per response, including the time for reviewing instructions, searching existing data sources, gathering and maintaining the data needed, and completing and reviewing the collection of information. Send comments regarding this burden estimate or any other aspect of the collection of information, including suggestions for reducing this burden to Department of Defense, Washington Headquarters Services, Directorate for Information Operations and Reports (0704-0188), 1215 Jefferson Davis Highway, Suite 1204, Arlington, VA 22202-4302. Respondents should be aware that notwithstanding any other provision of law, no person shall be subject to a penalty for failing to comply with a collection of information if it does not display a currently valid OMB control number.</p> <p>PLEASE DO NOT RETURN YOUR FORM TO THE ABOVE ADDRESS.</p>					
1. REPORT DATE (DD-MM-YYYY) 26-03-2009		2. REPORT TYPE Master's Thesis		3. DATES COVERED (From – To) June 2008 – March 2009	
4. TITLE AND SUBTITLE Q-Switched and Mode Locked Short Pulses from a Diode Pumped, Yb-Doped Fiber Laser				5a. CONTRACT NUMBER	
				5b. GRANT NUMBER	
				5c. PROGRAM ELEMENT NUMBER	
6. AUTHOR(S) Swift, Seth, M., Captain, USAF				5d. PROJECT NUMBER N/A	
				5e. TASK NUMBER	
				5f. WORK UNIT NUMBER	
7. PERFORMING ORGANIZATION NAMES(S) AND ADDRESS(S) Air Force Institute of Technology Graduate School of Engineering and Management (AFIT/EN) 2950 Hobson Way, Building 640 WPAFB OH 45433-7765				8. PERFORMING ORGANIZATION REPORT NUMBER AFIT/GAP/ENP/09-M10	
9. SPONSORING/MONITORING AGENCY NAME(S) AND ADDRESS(ES) Left Blank Intentionally				10. SPONSOR/MONITOR'S ACRONYM(S)	
				11. SPONSOR/MONITOR'S REPORT NUMBER(S)	
12. DISTRIBUTION/AVAILABILITY STATEMENT APPROVED FOR PUBLIC RELEASE; DISTRIBUTION UNLIMITED.					
13. SUPPLEMENTARY NOTES					
14. ABSTRACT A diode-pumped, ytterbium (Yb)-doped fiber laser system was designed and demonstrated to operate in continuous wave (cw), passively Q-switched and possibly passively mode locked operation. To our knowledge, this was the first fiber laser oscillator built at the Air Force Institute of Technology. A Cr ⁴⁺ :YAG (Chromium: Ytterbium Aluminum Garnett) crystal was used as a saturable absorber to generate Q-switched pulses. Attempts to mode lock the laser were performed using a semiconductor saturable absorber mirror (SESAM) and through nonlinear polarization rotation (NPR). The best output power result was 5 Watt (W) while pumping at 8.3 W, yielding 60% efficiency and peak spectral outputs between 1087-1108 nm. Passive Q-switched pulses were generated using the Cr ⁴⁺ :YAG crystal with a mean width of 2.9 μs and repetition rates between 60-150 kHz. This corresponded to pulse energies of 7-24 μJ and peak powers twice as high as the average power. Q-switched and possible mode locked pulses were generated using NPR. Q-switched pulse widths ranged between 1.8-2.8 μs with repetition rates between 29-72 kHz. Mode locked pulse widths were 10.5 ns with a repletion rate of 17.2 MHz. Mode locking was not achieved using the SESAM, but the results that resemble mode beating are presented, and causes for error were analyzed.					
15. SUBJECT TERMS Yb-doped fiber, Passive Q-Switch, Cr ⁴⁺ :YAG, Passive Mode Locking, Nonlinear Polarization Rotation					
16. SECURITY CLASSIFICATION OF:			17. LIMITATION OF OF ABSTRACT	18. NUMBER OF PAGES	19a. NAME OF RESPONSIBLE PERSON
a. REPORT	b. ABSTRACT	c. THIS PAGE			Matthew J. Bohn, Lt Col, USAF (ENP)
U	U	U	UU	115	19b. TELEPHONE NUMBER (Include area code) (937) 255-3636, ext 4573 Matthew.Bohn@afit.edu